

(P. Nachtkorn)

NASA CR-152297

(NASA-CR-152297) DEVELOPMENT OF AN IMPROVED
TOUGHNESS HYPERPURE SILICA REFLECTIVE HEAT
SHIELD Contractor Report, 3 Jul. 1978 - 3
Jul. 1979 (McDonnell-Douglas Astronautics
Co.) 93 p HC A05/MF A01

N81-18095

Unclas

CSSL 11D G3/24 16384

DEVELOPMENT OF AN IMPROVED TOUGHNESS HYPERPURE SILICA REFLECTIVE HEAT SHIELD

By E. L. Rusert, T. L. Hackett and D. N. Drennan

Prepared by

MCDONNELL DOUGLAS ASTRONAUTICS COMPANY-ST. LOUIS DIVISION
St. Louis, Missouri

*for Ames Research Center
Moffett Field, California 94035*



1. Report No. CR152297		2. Government Accession No.		3. Recipient's Catalog No.	
4. Title and Subtitle DEVELOPMENT OF AN IMPROVED TOUGHNESS HYPERPURE SILICA REFLECTIVE HEAT SHIELD				5. Report Date Aug 1979	
				6. Performing Organization Code	
7. Author(s) E. L. Rusert, T. L. Hackett and D. N. Drennan				8. Performing Organization Report No.	
9. Performing Organization Name and Address MCDONNELL DOUGLAS ASTRONAUTICS COMPANY-ST. LOUIS P. O. BOX 516 ST. LOUIS, MISSOURI 63166				10. Work Unit No.	
				11. Contract or Grant No. NAS 2-10003	
12. Sponsoring Agency Name and Address NATIONAL AERONAUTICS AND SPACE ADMINISTRATION AMES RESEARCH CENTER MOFFETT FIELD, CALIFORNIA 94035				13. Type of Report and Period Covered Contractor Report 3 July 1978-3 July 1979	
				14. Sponsoring Agency Code	
15. Supplementary Notes					
16. Abstract High purity (hyperpure silica <25 ppm and Astroquartz <500 ppm) three dimensionally woven silica-silica materials were evaluated for use as a tough reflective heat shield (H/S) for planetary entry probes. A special weave design was selected to minimize light piping effects through the heat shield thickness. Various weave spacings were evaluated for densification efficiency with an 0.7 μ m particle size high purity silica (1 ppm total metallic impurities). An 0.23 cm spacing was selected as the optimum Y-yarn spacing for densification. Spectral hemispherical reflectance was measured from 0.2 to 2.5 microns at room temperature. Reflectance increases due to densification and purity of material were measured. Reflectance of 3D hyperpure silica was higher than 3D Astroquartz silica for all wavelengths. Mechanical properties were measured in beam flexure and beam shear tests. Results indicated strengths lower than reported for slip cast fused silica (NASA-152118). Low strengths were attributed to low densities achieved through vacuum impregnation.					
17. Key Words (Suggested by Author(s)) SILICA REFLECTIVE HEAT SHIELD ENTRY TECHNOLOGY JUPITER ENTRY PROBE PROJECT GALILEO				18. Distribution Statement	
19. Security Classif. (of this report) UNCLASSIFIED		20. Security Classif. (of this page) UNCLASSIFIED		21. No. of Pages	
				22. Price*	

FOREWORD

This final report was prepared by McDonnell Douglas Astronautics Company-St. Louis under NASA Contract NAS 2-10003 and covers work performed during the period July 1978 to July 1979. This work was administered under the direction of NASA Ames Research Center with Dr. Philip R. Nachtsheim as the Technical Manager.

The authors wish to acknowledge the efforts of the following personnel who contributed to the successful completion of this program: A. H. Bay, A. R. Brown, J. C. Conti, and N. L. Crump--Supervision; J. H. Detjen--Silica Machining; R. J. Schmitt--Reflectance Measurements; D. F. Beilman and M. S. Biggs--Strength Analysis; J. E. Lenz and R. L. Hillman--Thermal Conductivity Measurements; Y. Harada and J. L. Sievert--IIT Research Institute--Mechanical Property Measurements.

TABLE OF CONTENTS

<u>NUMBER</u>	<u>TITLE</u>	<u>PAGE</u>
1.0	Introduction.	1
2.0	Program Summary	3
3.0	Fabrication, Densification and Machining of 3D Woven Silica Preforms	5
3.1	Weave Pattern Design	5
3.2	Fiber Spacing	7
3.3	Silica Fibers	7
3.4	Preform Cleaning	11
3.5	Effects of Cleaning Processes on Fiber Strength	12
3.6	Densification	15
	3.6.1 Binder Preparation.	15
	3.6.2 Densification Technique	15
	3.6.3 Discussion of Densification Results	16
3.7	Specimen Machining	20
	3.7.1 Specimen Layout	20
	3.7.2 Machining	20
4.0	Density Gradient Measurements	27
4.1	Specimen Description	27
4.2	Measurement Results	27
4.3	Discussion of Density Gradient Results	30
5.0	Thermal Conductivity Measurements	32
5.1	Test Description	32
5.2	Thermal Conductivity Test Results.	34
6.0	Optical Property Measurements	36
6.1	Test Description and Rationale	36
6.2	Optical Property Measurement Test Results.	39
	6.2.1 "As Woven" Reflectance	39
	6.2.2 "As Densified" Reflectance	39
	6.2.3 "As Machined" Reflectance	39
	6.2.4 "As Machined" Transmittance	44
	6.2.5 Scattering and Absorption Coefficients.	49
7.0	Mechanical Property Measurements.	58
7.1	Test Plan.	58
	7.1.1 Test Specimen Definition	58
	7.1.2 Specimen Testing	60
7.2	Mechanical Property Test Results	64
	7.2.1 Firing Temperature Study.	64
	7.2.2 Room Temperature Flexure Tests.	64
	7.2.3 Elevated Temperature Flexure Tests.	70
	7.2.4 Short Beam Shear Tests	73
7.3	Discussion of Mechanical Property Test Results	76
	7.3.1 Physical Properties	76
	7.3.2 Mechanical Properties	76
	7.3.2.1 Room Temperature Flexure Data	76
	7.3.2.2 Elevated Temperature Flexure Data	76
	7.3.2.3 Short Beam Shear Data	77
	7.3.2.4 Mechanical Property Summary Data	77
7.4	Conclusions	77

TABLE OF CONTENTS

<u>NUMBER</u>	<u>TITLE</u>	<u>PAGE</u>
8.0	Full Scale Prototype 3D Silica Heat Shield Cost Analysis	79
9.0	Conclusions and Recommendations for Future Work	83
9.1	Conclusions	83
9.2	Recommendations for Future Work	84
	References	85

LIST OF FIGURES

<u>NUMBER</u>	<u>TITLE</u>	<u>PAGE</u>
3-1	Light Piping Proportional to Concentration of Fibers Parallel to Light Rays	6
3-2	Selected Layer-to-Layer Interlock Design	6
3-3	3D Jupiter Heat Shield Weave Pattern	7
3-4	Woven Preform Characteristics	8
3-5	Astroquartz Preform--"As Received" - 0.15 cm Spacing	9
3-6	Astroquartz Preform--"As Received" - 0.23 cm Spacing	9
3-7	Astroquartz Preform--"As Received" - 0.32 cm Spacing	10
3-8	Hyperpure Preform--"As Received" - 0.23 cm Spacing	10
3-9	Preform Cleaning Sequence	12
3-10	Reflectance of Hyperpure Preform Heat Cleaned at 200°C and 540°C Compared to Astroquartz Heat Cleaned at 540°C	13
3-11	Effect on Preform Cleaning Processes on Fiber Strength	14
3-12	Apparatus for Vacuum Impregnation with Hyperpure Silica Binder.	16
3-13	Densification Histogram for Astroquartz Preforms	17
3-14	Densification Histogram for Hyperpure Preform	19
3-15	Test Specimen Layout for Astroquartz Preforms	21
3-16	Test Specimen Layout for Hyperpure Silica Preform	22
3-17	Test Specimens Identification	23
3-18	Typical Specimens Machined from the 0.23 cm Y-yarn Spacing Astroquartz Preform	25
3-19	Typical Specimens Machined from the 0.23 cm Y-yarn Spacing Hyperpure Preform	26
4-1	Density Gradient for the 0.15 cm Spacing Densified Astroquartz	28
4-2	Density Gradient for the 0.23 cm Spacing Densified Astroquartz	29
4-3	Density Gradient for the 0.32 cm Spacing Densified Astroquartz	29
4-4	Density Gradient for the 0.23 cm Spacing Densified Hyperpure Preform (Specimen Core Drilled From the Center)	31
4-5	Density Gradient for the 0.23 cm Spacing Densified Hyperpure Preform (Specimen Core Drilled From the Corner)	31
5-1	Thermal Comparator Equipment for Determining Thermal Conductivity	33
5-2	Thermal Comparator Apparatus Schematic.	33
5-3	Thermal Conductivity of 3D Woven Hyperpure Silica	35
6-1	Optical Property Test Matrix	37
6-2	Optical Property Specimen Orientation and Designation	38
6-3	Room Temperature Reflectance of 3D Woven Astroquartz and Hyperpure Composites in the "As Cleaned" Condition Measured on the Surface	40
6-4	Comparison of "As Cleaned" and "Densified" Reflectance for 0.15 cm Astroquartz Preform of the Y Surface	41
6-5	Comparison of "As Cleaned" and "Densified" Reflectance for 0.23 cm Astroquartz Preform Measured on the Y Surface Direction	41
6-6	Comparison of "As Cleaned" and "Densified" Reflectance for the 0.32 cm Astroquartz Preform Measured on the Y Surface	42

LIST OF FIGURES

<u>NUMBER</u>	<u>TITLE</u>	<u>PAGE</u>
6-7	Comparison of "As Cleaned" and "Densified" Reflectance for the 0.23 cm Hyperpure Preform Measured on the Y Surface	42
6-8	Z Direction Reflectance of 0.5 cm Thick Silica (3D Woven Densified)	43
6-9	Effects of Purity on Reflectance	45
6-10	Light Piping in Astroquartz 3D Silica Woven Composite	46
6-11	Light Piping in Hyperpure 3D Silica Woven Composite	47
6-12	Effect of Thickness on Reflectance of 0.23 cm Y-yarn Spacing Astroquartz (Z Direction)	48
6-13	Scattering and Absorption Coefficients for 0.50 cm (0.20 in.) Thick 0.15 cm Y-yarn Spacing Astroquartz (Y Direction)	50
6-14	Thickness Effects on Scattering and Absorption Coefficients for 0.15 cm Y-yarn Spacing Astroquartz (Z Direction)	51
6-15	Scattering and Absorption Coefficients for 0.50 cm (0.10 in.) Thick 0.23 cm Y-yarn Spacing Astroquartz (Y Direction)	52
6-16	Thickness Effects on Scattering and Absorption Coefficients for 0.23 cm Y-yarn Spacing Astroquartz (Z Direction)	53
6-17	Scattering and Absorption Coefficients for 0.50 cm (0.20 in.) Thick 0.32 cm Y-yarn Spacing Astroquartz (Y Direction)	54
6-18	Scattering and Absorption Coefficients for 0.50 cm (0.20 in.) Thick 0.32 cm Y-yarn Spacing Astroquartz (Z Direction)	55
6-19	Scattering and Absorption Coefficients for 0.50 cm (0.20 in.) Thick 0.23 cm Y-yarn Spacing Hyperpure (Y Direction)	56
6-20	Scattering and Absorption Coefficients for 0.50 cm (0.20 in.) Thick 0.23 cm Y-yarn Spacing Hyperpure (Z Direction)	57
7-1	Mechanical Properties Test Matrix	59
7-2	Schematic of Short Beam Shear Test Setup	61
7-3	Schematic of Beam Flexure Test Setup	62
7-4	Photograph of Long Beam Flexure Test Setup	63
7-5	Photograph of IITRI Short Beam Shear Test	63
7-6	Effect of Firing Temperature on Flexure Strength	65
7-7	Beam Flexure Specimen Physical Property Data (Prior to Firing)	66
7-8	Beam Flexure Specimen Physical Property Data (After Firing)	67
7-9	Individual Specimen Beam Flexure Results	68
7-10	Summary of Beam Flexure Results	69
7-11	Average Toughness Comparison of the Various Densified Materials	71
7-12	Average Flexure Strength Value Comparison of the Various Densified Materials	72
7-13	Flexural Strength Comparison of Hyperpure Slip-Cast Fused Silica with 3D Silica Woven Composite	74
7-14	Summary of Short Beam Test Results	75
7-15	Mechanical Property Summary	78
8-1	Summary ROM Cost for Full Scale Prototype 3D Woven Silica Reflective Heat Shield	80
8-2	Typical Galileo Probe Heat Shield	81

SYMBOLS

PHYSICAL PROPERTY UNITS

μm	micrometer
cm	centimeter
m	meter
cc	cubic centimeters
g or gm	grams
g/cc	grams/cubic centimeter
pcf	pounds per cubic feet

REFLECTANCE UNITS

UV	ultraviolet
IR	infrared
S/N	signal-to-noise ratio
EDGAR	Experimental Data Gathering and Reduction System
$V_S(\lambda)$	reflected intensity at wavelength
$V_L(\lambda)$	hydrogen lamp source intensity
K-M	Kubelka-Munk
S	Scattering coefficient
K	absorption coefficient (Kubelka-Munk)
δ	absorption coefficient (Beer's Law)
R_∞	reflectance of an effectively infinite thickness of a scattering material

STRENGTH UNITS

Pa	pascal--unit of stress or pressure equivalent to one newton (force) per square meter (area)
kPa	kilo-pascals (10^3 pascals)
MPa	mega-pascals (10^6 pascals)
GPa	giga-pascals (10^9 pascals)
F_{fu}	ultimate flexural strength (MPa)
F_{su}	ultimate shear strength (MPa)
F_{tu}	ultimate tension strength (MPa)
G	Modulus of rigidity (GPa)
psi	pounds force per square inch
ksi	kips (1000 pounds) per square inch
Msi	million pounds per square inch (10^6 psi)
σ_f	actual flexure stress (MPa)
E_c	compression elastic secant modulus (GPa)
E_f	flexural elastic modulus (GPa)
E_t	tension elastic modulus (GPa)

1.0 INTRODUCTION

The forebody heat shield on a Jupiter atmospheric entry probe will be required to withstand extreme heating rates upon entry into the dense atmosphere at high velocities. The heat shield must also have adequate strength and toughness to provide necessary structural integrity.

The atmosphere of Jupiter and the probe entry velocity causes the heating mode to shift from convective to predominantly radiative. Radiation heating arises from the bow shock wave generated by the probe during entry, with the radiation component making up nearly 70 percent of the total incident heat flux. A heat shield using conventional ablative materials, such as carbon-phenolic, carbon-carbon and/or 3D silica-silica, could account for as much as 40-50 percent of the total probe vehicle weight.

The concept of a reflective/ablative heat shield was demonstrated in 1971 using Teflon (Reference 1). A reflective type heat shield has the potential of more efficiently dissipating the majority of the radiative heat flux by reflecting the energy rather than absorbing it, as would carbon phenolic or carbon-carbon based materials.

Hyperpure silica has also been examined as a candidate reflecting/ablating heat shield material because of its low optical absorption of incident radiation from 0.2 to 2.3 μm , its excellent ablation characteristics, its high resistance to thermal stress, and its ready availability in several high purity forms. As a result, several high purity, highly reflective, slip cast, fused silica materials were developed as reported in References 2, 3, and 4. One heat shield material was reinforced with aggregate grain of hyperpure silica (to reduce shrinkage), and another was reinforced with hyperpure silica fiber (to reduce shrinkage and also improve toughness). However, analysis and test of the fiber-reinforced materials' strength and toughness (area under the stress-strain curve) indicated a low margin of safety.

The current program was initiated to evaluate three-dimensional (3D) reinforced continuous filament woven silica-silica composites with increased strength and toughness that would have a higher margin of safety. A layer-to-layer interlock weave pattern was selected to eliminate continuous fibers through the heat shield's thickness, thereby reducing the amount of transmittance (due to light piping) through the fibers. Silica yarns with purity levels of 500 ppm (Astroquartz) and 10 ppm (Hyperpure) were evaluated. Center-to-center Y-yarn spacings of 0.15 cm, 0.23 cm, and 0.32 cm (0.060 in., 0.090 in., and 0.125 in.) were evaluated for efficiency of densification by vacuum impregnation with hyperpure silica fines (0.4 to 0.7 μm in diameter). Optical, mechanical, and thermal properties were evaluated and a preliminary cost analysis made of fabricating a full-size heat shield from the high value candidate materials selected.

The original program plan was to evaluate 3D silica materials made of Astroquartz yarn (500 ppm impurities) and hyperpure yarn (10 ppm impurities). From this cursory analysis, selection of one material was to be made for detail material characterization. Due to late delivery of hyperpure yarn,

material selection was not possible during the scheduled Task I activity. Therefore, hyperpure silica yarn was woven into a large preform characteristic of the size required for Task II with an 0.23 cm (0.090 in.) Y-yarn spacing. The 0.23 cm (0.090 in.) yarn spacing was based upon analysis of densified Astroquartz preforms with yarn spacings of 0.15 cm (0.060 in.), 0.23 cm (0.090 in.) and 0.32 cm (0.125 in.), respectively.

2.0 PROGRAM SUMMARY

Four 3D woven silica preforms were fabricated by Fiber Materials, Inc. (FMI). A special weave design was used to minimize transmission of radiant energy through the fibers by light piping directly to the bondline or the inner surface of a typical heat shield. The Z directional yarns that travel from the surface of the specimen toward the bondline or inner surface were designed to penetrate only three fiber thicknesses in the normal X-Y plane, thereby minimizing light piping.

Three preforms were woven with Astroquartz yarn having less than 500 ppm total metallic impurities. Each preform had a different layer-to-layer fiber spacing of 0.15 cm (0.060 in.), 0.23 cm (0.090 in.), and 0.32 cm (0.125 in.), respectively. These specimens were used to determine the preferred Y-yarn spacing for optimum densification with a hyperpure silica binder developed at McDonnell Douglas Astronautics Company-St. Louis Division (MDAC-St. Louis). The fourth preform, woven with hyperpure silica yarn having 10 ppm total metallic impurities and with a Y-fiber spacing of 0.23 cm (0.090 in.), was then used to make a comparison with 3D woven Astroquartz and slip-cast hyperpure fused silica. Physical, mechanical, thermal and optical properties due to fiber spacing and purity were compared and evaluated.

The four preforms were cleaned in a variety of solvents and heat treatments to remove impurities deposited during handling and to remove the organic surface finish (sizing) placed on the fibers. Astroquartz fibers used A1100 (amino propyltriethoxy silane) as a surface finish, while hyperpure fibers were coated with polyvinyl alcohol (PVA).

The 3D silica preforms were densified with 0.7 μm hyperpure silica particles, using vacuum impregnation techniques developed by MDAC-St. Louis. The purpose of densification was to improve the mechanical properties and increase the materials' diffuse reflecting properties. Each block was impregnated to a near-maximum weight gain. Final densities of each preform were 1.31 gm/cc (82 pcf), 1.45 gm/cc (90 pcf), 1.38 gm/cc (86 pcf), and 1.30 gm/cc (81 pcf) for 0.15 cm (0.060 in.), 0.23 cm (0.090 in.), 0.32 cm (0.125 in.) Y-yarn spacing Astroquartz and 0.23 cm (0.090 in.) Y-yarn spacing hyperpure, respectively. Density gradients observed in the 0.15 cm (0.060 in.) and 0.32 cm (0.125 in.) Astroquartz preforms and in the hyperpure preform indicate that filtration resistance to impregnation had occurred.

Mechanical, optical, and thermal test specimens were machined from the preforms with diamond tooling. Some surface contamination resulted from the initial machining operation, but tools with larger diamond particles reduced the amount of surface contamination. Final clean up of test specimens was accomplished by heating at 540°C (1004°F) for 3 hours, followed by diamond-studded end mill machining.

Thermal conductivity of the 3D hyperpure silica-silica specimen was measured by a thermal comparator method between room temperature and 908°C (1667°F). The conductivity of the material ranged from 0.7 to 1.3 Cal/°C cm sec $\times 10^{-3}$ (2.1 to 3.7 Btu-in/hr ft²°f).

Optical measurements made after densification showed dramatic improvements in reflectance over measurements made before densification. Major factors influencing reflectance were density and purity. Hyperpure silica-silica specimens demonstrated the highest reflectance (99 percent at 0.8 microns). The highest density Astroquartz [0.23 cm (0.090 in.) spacing] had a reflectance of 96 percent at 0.8 microns, which was the highest value for the three Astroquartz materials evaluated.

Mechanical properties were measured at room temperature and at 1066°C (1950°F). MDAC-St. Louis fabricated all test specimens. Specimen testing was performed mainly by Illinois Institute of Technology Research Institute (IITRI) under subcontract to MDAC-St. Louis. Some limited testing was performed by MDAC-St. Louis.

Early testing performed at IITRI indicated that specimens exhibited lower than expected strengths. A study of firing temperature effects on strength and modulus was undertaken at MDAC-St. Louis with existing hyperpure specimens in an attempt to improve the strength and modulus. Firing specimens at 1037°C (1900°F) for five hours caused some strength and modulus improvements.

All four types of materials exhibited an increase in strength and toughness with increasing test temperature. For the same yarn spacing, the hyperpure had less strength at room temperature than the Astroquartz but more at the elevated temperature. Density appeared to be the major influence on room temperature strength, with the higher density specimens having higher strength. Purity was the major influence at elevated temperature.

Because of the limited number of specimens tested at any given test condition (1 to 3 specimens), the results are useful only to predict trends. Recommendations are made for future work toward increasing material strength and development of a silica heat shield material for use on outer planetary entry probes.

3.0 FABRICATION, DENSIFICATION AND MACHINING OF 3D WOVEN SILICA PREFORMS

This section describes the work performed to weave and densify 3D woven silica preforms from which test specimens were machined for subsequent testing. The original test plan was to fabricate, densify, and machine specimens from five three-dimensionally woven blocks made with either Astroquartz or hyperpure silica yarns. In Phase I, three Astroquartz preforms and one hyperpure preform were to be densified and tested. Based on limited testing in Phase I, a fifth block with optimum hyperpure silica yarn spacing was to be fabricated and more extensive tests run in Phase II. But, due to the late delivery of the hyperpure silica yarn (special material request by MDAC-St. Louis to J. P. Stevens for material with less than 10 ppm total metallic ion impurities), the hyperpure preform of Phase I was woven into a larger size to accommodate all the required test specimens intended for Phase II evaluation.

3.1 WEAVE PATTERN DESIGN

For a Jovian type entry, a large percentage of the heat flow to the heat shield will be radiant energy. This creates problems for typical 3D orthogonal-weave designs or any other weave pattern where fibers are continuous through the thickness. Energy incident on the exterior fiber ends can be directly transmitted to the back side of the material by means of light piping. Recent studies verified this phenomena (Reference 5) with 3D orthogonally-woven Astroquartz. Two different diameter Astroquartz yarns were used to obtain different fiber concentrations for two surfaces of a test specimen. When the sample was observed in front of a light source, light in the visible wavelength band could easily be seen being piped down the fibers. Reflectance measurements made on the two surfaces indicated that the higher the fiber concentration on a surface, the lower the reflectance, as shown in Figure 3-1. The light piping phenomenon can be corrected by weave patterns that do not expose the bondline to direct radiation.

To maintain a high level of reflectance, the 3D woven material must be designed to minimize light piping. In cooperation with our weaving subcontractor, Fiber Materials, Inc. (FMI), we studied several weave pattern designs that addressed the light piping problem and that also had the potential for scale up so that a full scale heat shield could be made.

The weave pattern selected for this program is a layer-to-layer interlock design shown in Figure 3-2. The advantages of this design over others considered are: a) each set of Z direction yarns penetrates only three X-Y fiber thicknesses, thereby minimizing light piping, b) each layer of Y yarns is woven to conform to the shape of the heat shield, giving a stress free condition, and c) an entire heat shield can be made without joints, thus providing a more reliable design with uniform fiber orientation at all locations on the heat shield. Figure 3-3 depicts the weave pattern orientation as it would be for a 3D heat shield configuration typical of a Jupiter entry probe.

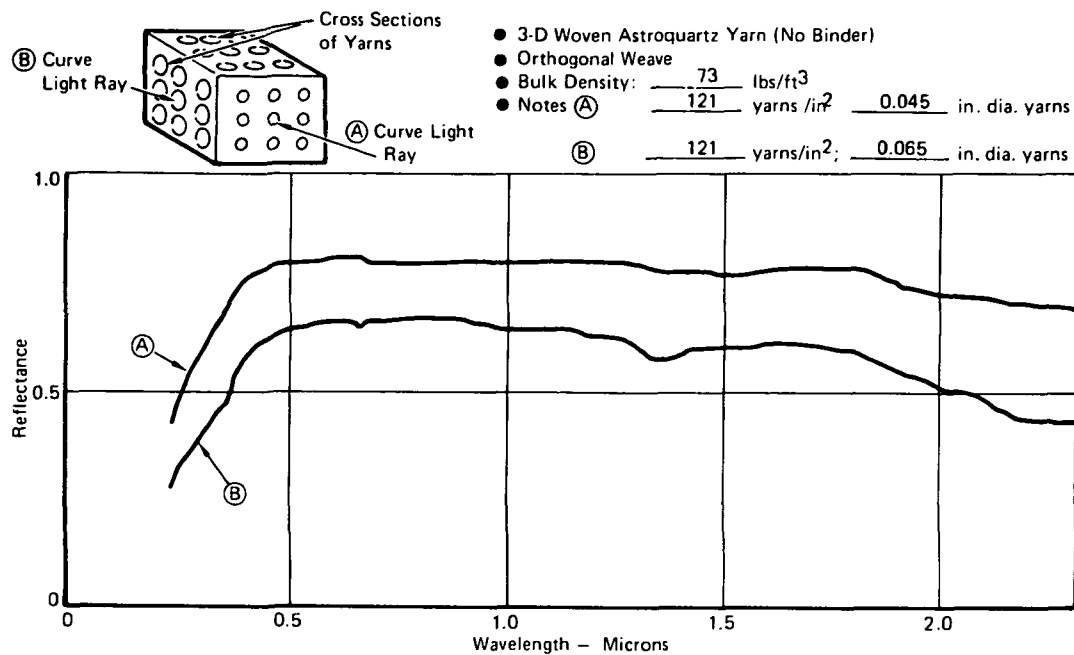


FIGURE 3-1 LIGHT PIPING PROPORTIONAL TO CONCENTRATION OF FIBERS PARALLEL TO LIGHT RAYS

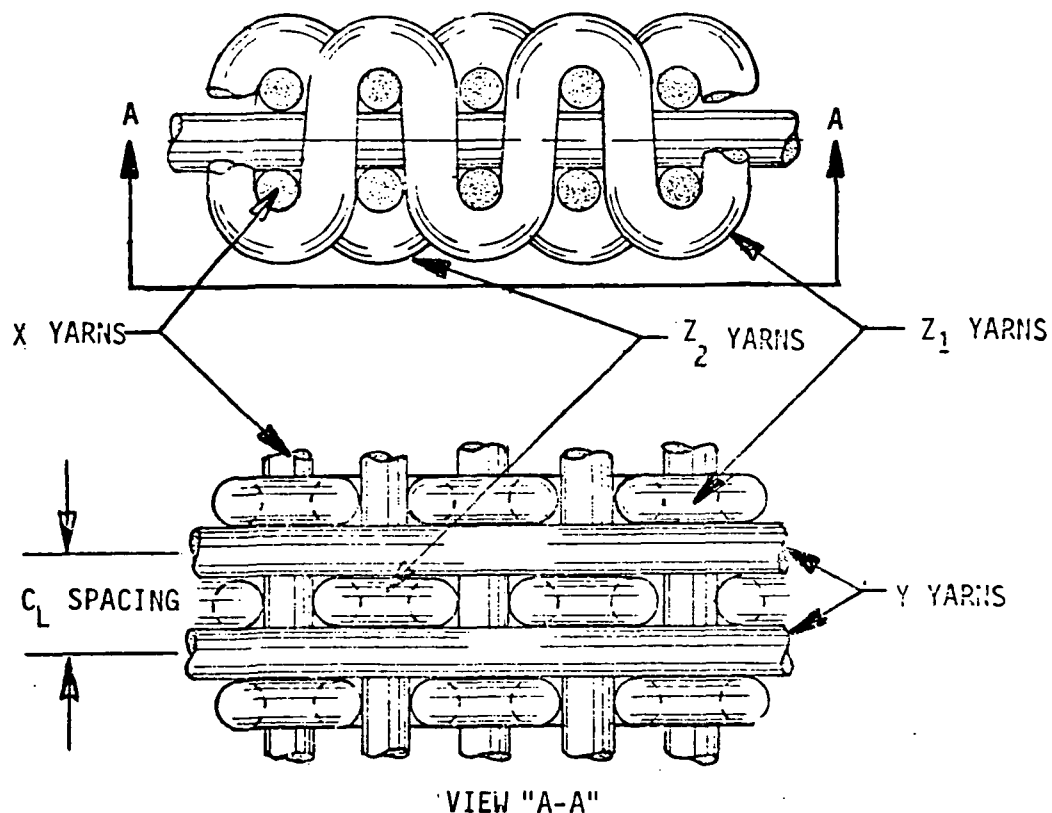


FIGURE 3-2 SELECTED LAYER TO LAYER INTERLOCK DESIGN

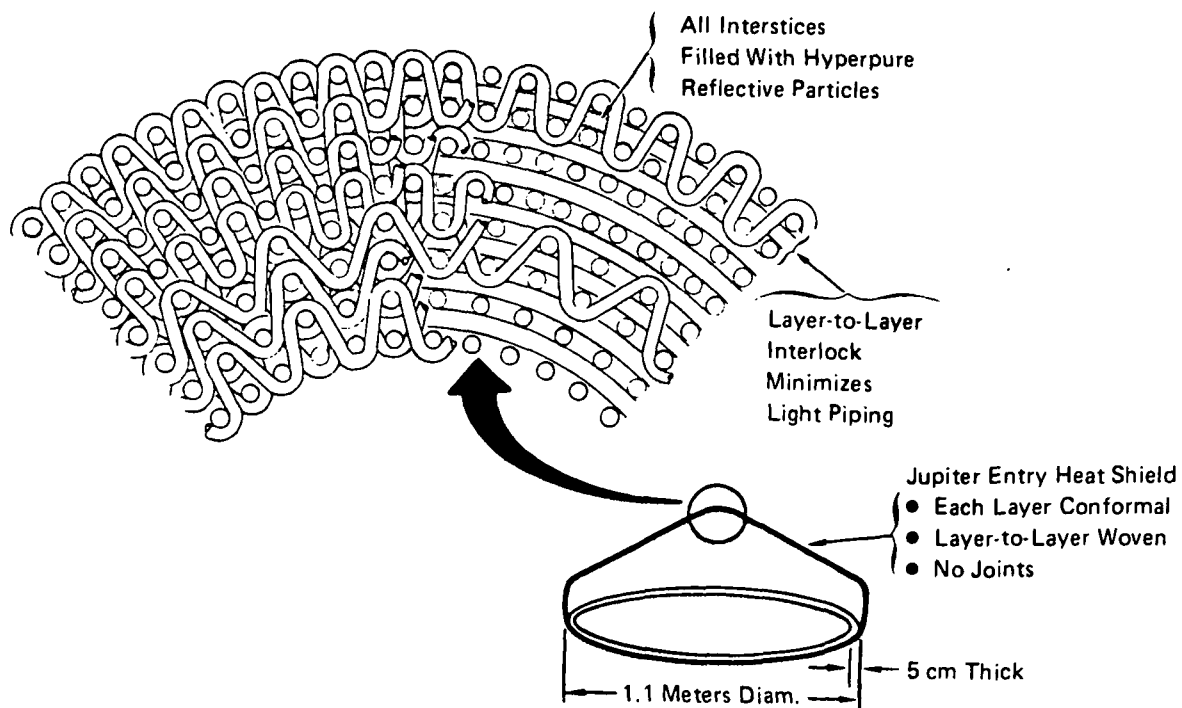


FIGURE 3-3 3D JUPITER HEAT SHIELD WEAVE PATTERN

3.2

FIBER SPACING

Three yarn spacings were chosen to evaluate their effect upon densification efficiency, resulting strength, and reflectance. As measured from Y fiber centers, the spacings selected were 0.15 cm (0.060 in.), 0.23 cm (0.090 in.), and 0.32 cm (0.125 in.). As-woven density of a preform fabricated with the layer-to-layer design and these spacings was typically $\approx 35\%$ of theoretical density. The smaller the yarn spacing, the more resistance there is to impregnation with the densifying material. A spacing that shows the greatest impregnation efficiency, adequate strength, toughness, and high reflectance is the most desirable. Generally speaking, the higher the density increase achieved through impregnation, the higher the material's strength will be.

3.3

SILICA FIBERS

Two purity grades of silica yarn were chosen for this study, Astroquartz and hyperpure. Both types were purchased through J. P. Stevens from their French fiber supplier, Quartz et Silice. Continuous fibers, about 9 microns in diameter, used to make Astroquartz yarn are made from Brazilian quartz crystals and typically contain ≈ 500 ppm total metallic ion impurities. Quartz et Silice agreed to produce the same size (9 microns diameter) continuous fibers made from their high purity (1 ppm impurities) synthetic silica (Tetrasil S.E.) rods. The impurity level of the manufactured

hyperpure fibers would be 10 ppm total metallic impurities. Comparison of optical properties of preforms made with the two types of material would show the effect of impurities on reflectance, especially in the ultra violet range 0.2 - 0.4 μm .

Three preforms were woven by FMI with Astroquartz yarn with Y-fiber spacings of 0.15 cm (0.060 in.), 0.23 cm (0.090 in.), and 0.32 cm (0.125 in.). Because the hyperpure fibers required were made in a special run for this program, the cost was much higher than originally expected, but more importantly, the time required for delivery was much longer than originally planned (7 months). To minimize program delay, the fiber spacing for the hyperpure silica preform was based on densification results of the three Astroquartz preforms. A larger size preform was made from hyperpure fibers to accommodate both Phase I and Phase II specimens. The physical characteristics of the 3D preforms obtained are presented in Figure 3-4.

SILICA YARN	WEAVE PATTERN	Y YARN SPACING	PREFORM SIZE
Astroquartz	Layer to Layer Interlock	0.15 cm (0.060 in.)	10.2 cm x 7.6 cm x 5.1 cm (4 in. x 3 in. x 2 in. thick)
Astroquartz	Layer to Layer Interlock	0.23 cm (0.090 in.)	10.2 cm x 7.6 cm x 5.1 cm (4 in. x 3 in. x 2 in. thick)
Astroquartz	Layer to Layer Interlock	0.32 cm (0.125 in.)	10.2 cm x 7.6 cm x 5.1 cm (4 in. x 3 in. x 2 in. thick)
Hyperpure	Layer to Layer Interlock	0.23 cm (0.090 in.)	10.2 cm x 20.3 cm x 5.1 cm (4 in. x 8 in. x 2 in. thick)

FIGURE 3-4 WOVEN PREFORM CHARACTERISTICS

The purchase order for the Phase I preforms required the 5.1 cm (2.0 in.) dimension as the Z direction. Due to an understandable misinterpretation, the 7.6 cm (3.0 in.) dimension was inadvertently made the Z direction on the Astroquartz preforms. When the error was discovered new layouts were made for the test specimens, and the program continued without serious loss of needed data. The hyperpure preform was fabricated with the 5.1 cm (2.0 in.) dimension being the Z direction as ordered. Photographs of the "as received" preforms from FMI are shown in Figures 3-5 through 3-8.

Radiographic examination of the "as received" preforms was made upon receipt at MDAC-St. Louis and revealed a uniformly woven structure.

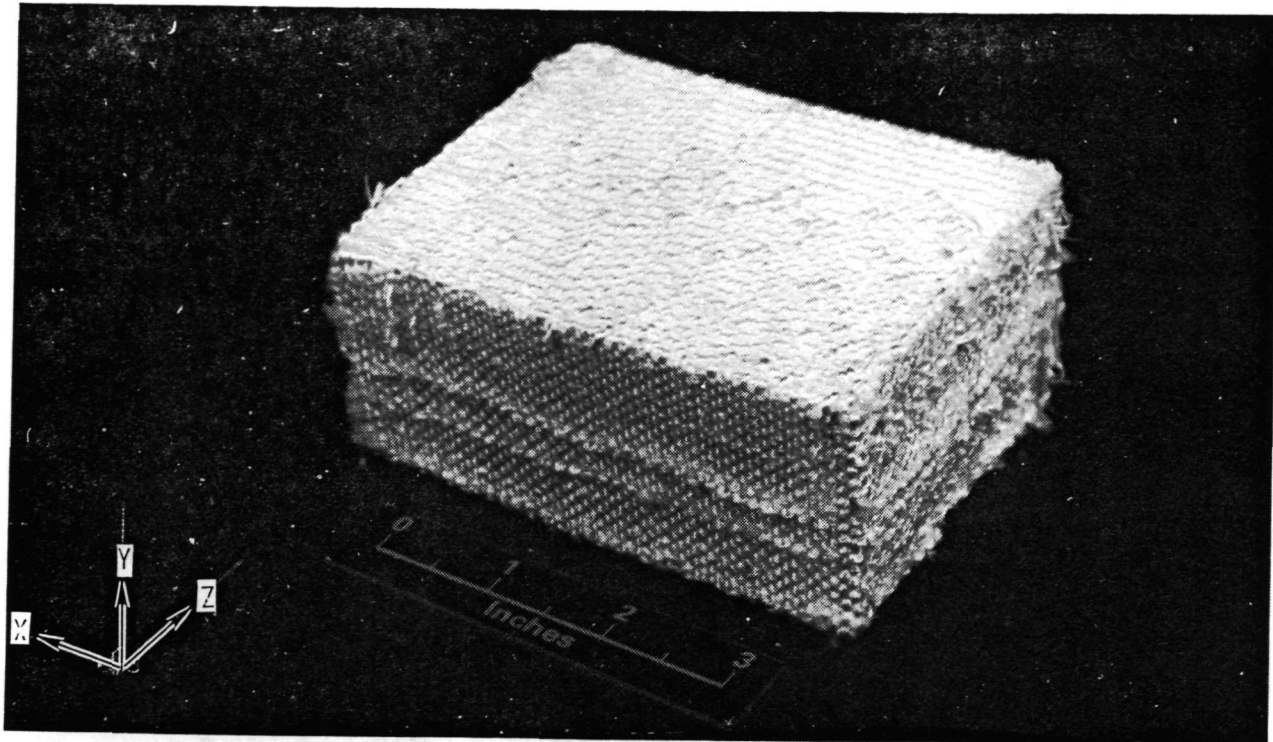


FIGURE 3-5 ASTROQUARTZ PREFORM-"AS RECEIVED" - 0.15 CM SPACING

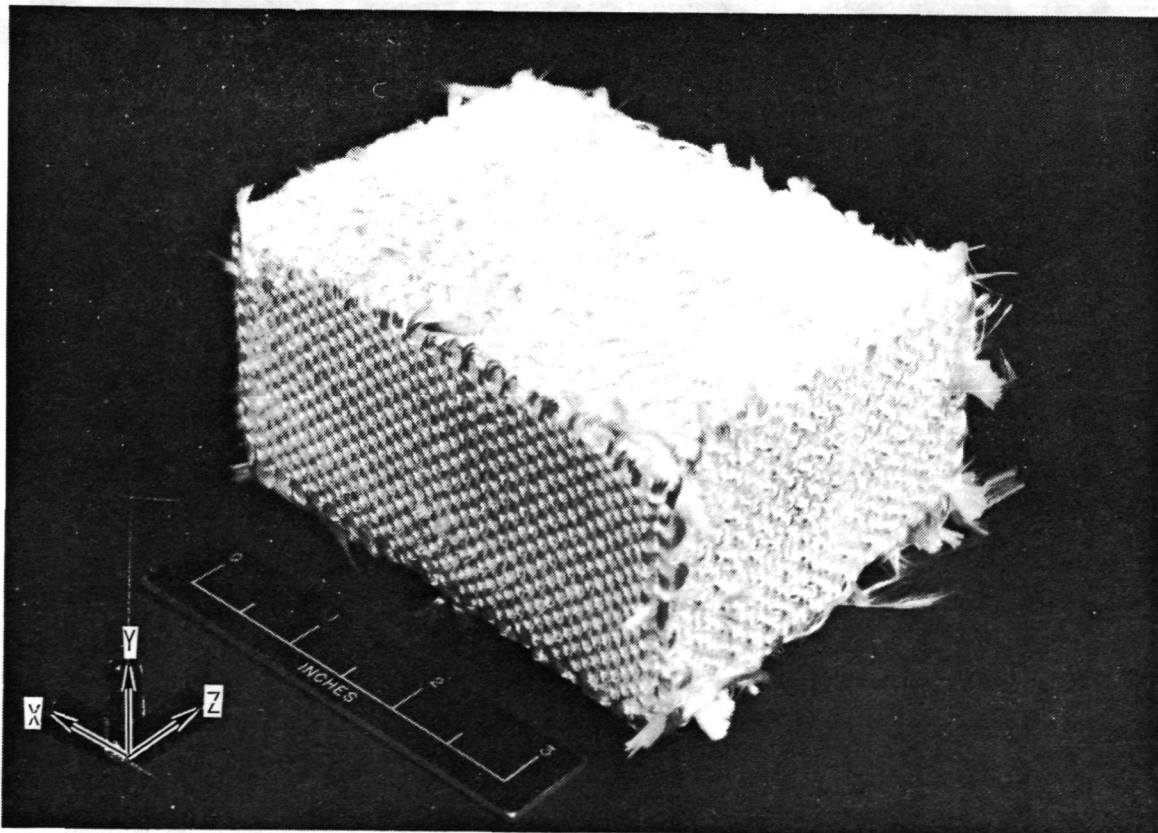


FIGURE 3-6 ASTROQUARTZ PREFORM-"AS RECEIVED" - 0.23 CM SPACING

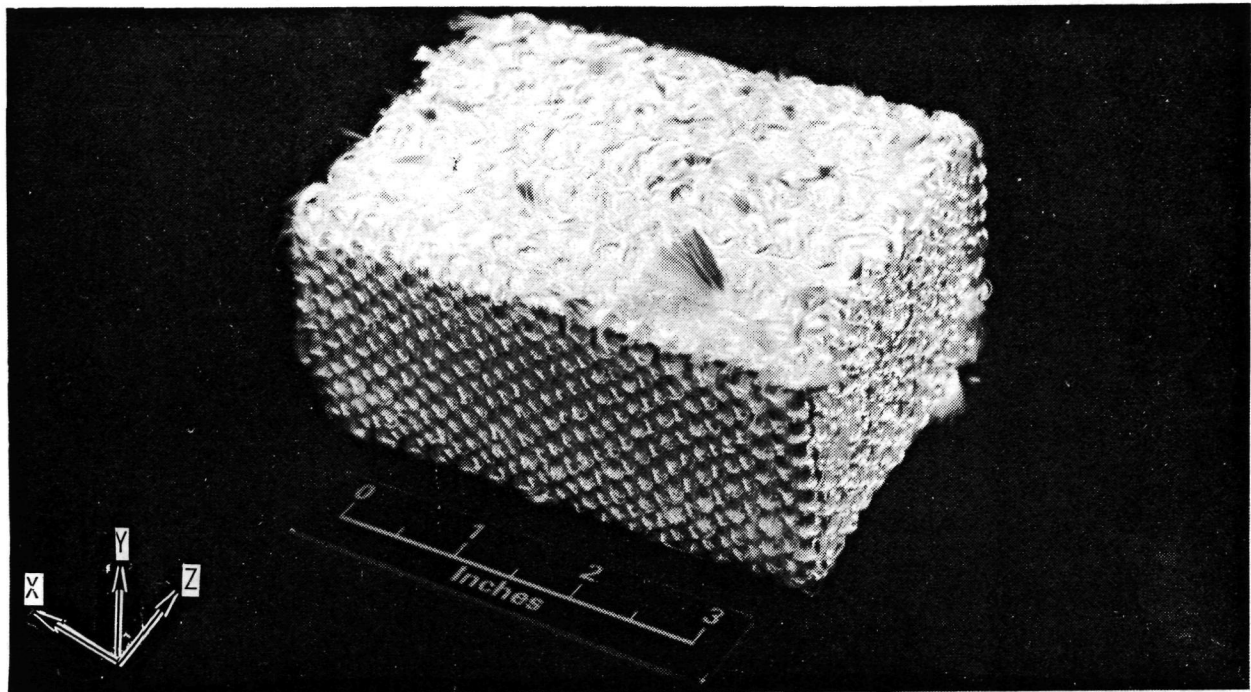


FIGURE 3-7 ASTROQUARTZ PREFORM-"AS RECEIVED" - 0.32 CM SPACING

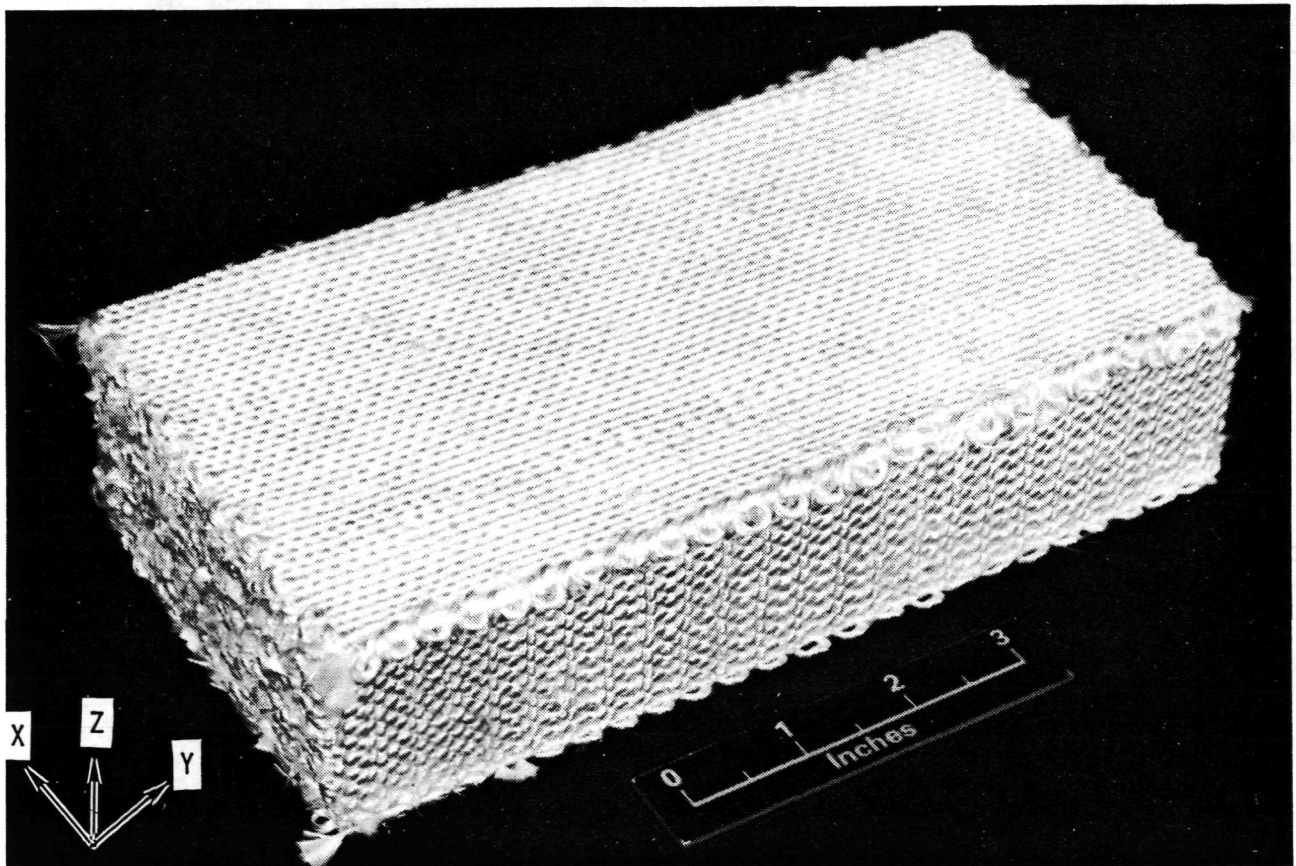


FIGURE 3-8 HYPERPURE PREFORM-"AS RECEIVED" - 0.23 CM SPACING

A series of cleaning steps was undertaken to remove any contaminants deposited on the preforms by handling of the yarn before, during, or after the weaving operation. The cleaning operation also served to remove the organic sizing placed on the yarns by J. P. Stevens. Yarn "sizing" or "surface finish" aids in the weaving operation by protecting the fibers against abrasion. The coating is placed on the fibers as they are formed. The cleaning steps taken to remove the organic sizing are listed in Figure 3-9. Preliminary studies showed that using ultrasonics and vacuum impregnation techniques to facilitate solvent penetration, do not appreciably assist in sizing removal. During and after the various cleaning steps, the preforms were handled in such a manner as to preclude further metallic contamination introduction. Preforms came in contact only with high purity silica, plastic gloves and bags, and containers that were glass or Teflon lined.

Preforms made from Astroquartz fibers exhibited some yellowing (discoloring) during various rinse cycles. Yellowing was observed throughout the organic solvent and acid cleaning steps. After each subsequent cleaning operation, the solutions had a yellow discoloration. Communications (Reference 6) with J. P. Stevens confirmed that the organic sizing used on the fibers does discolor and suggested that heat treatment should be sufficient to remove the sizing. The material used by J. P. Stevens for the sizing was Union Carbide's A1100, an amino propyltriethoxy silane.

Heat cleaning of the preforms removed most of the discoloration with the exception of the 0.15 cm (0.060 in.) Y-yarn spacing preform, which still showed some discoloration in localized areas.

The hyperpure fibers were coated with a Polyvinyl Alcohol (PVA) type sizing. The PVA sizing is soluble in water and decomposes at a lower temperature than A1100. Therefore the hyperpure preform was subjected to several hot water rinses to remove PVA sizing. Water temperatures were maintained at 77-88°C (171-190°F). The first hot water bath cleaning step showed evidence of PVA removal when the bath surface became covered with a sudsy film. This procedure was repeated approximately eight times. The final water rinse showed little evidence of additional PVA removal. After the above hot water rinses, the rest of the cleaning steps listed in Figure 3-9 were completed without visible evidence of PVA removal. During these cleaning operations, no yellowing was observed as previously noted with A1100 treated Astroquartz yarn.

Decomposition of PVA occurs at $\approx 200^{\circ}\text{C}$ (392°F) (Reference 7). Heat treatment (Step 10, Figure 3-9) of the hyperpure preform was made at 200°C (392°F) for 3 hours to remove any remaining PVA. Heat treatment at 200°C (392°F) was used instead of 540°C (1004°F) given in Figure 3-9 because of the detrimental effect the heat treatment step would have on silica fiber strength, as further discussed in subsection 3.5. Results of reflectance measurements made after the 200°C (392°F) heat treatment showed no improvement over comparable measurements made on Astroquartz, except below $0.6\text{ }\mu\text{m}$, as shown in Figure 3-10. It was rationalized that heat treatment at this temperature probably did not remove all the residual PVA on the fibers. The

hyperpure preform was then heat treated a second time at the higher temperature of 540°C (1004°F) for 3 hours and an overall higher reflectance was measured on the preform as shown in Figure 3-10.

STEP	SOLVENT	TIME	TEMPERATURE
1	DEIONIZED WATER	30 MINUTES	RT
2	DEIONIZED WATER	30 MINUTES	71°C (160°F)
3	MEK/TRICHLOROETHYLENE	30 MINUTES	RT
4	MEK/TRICHLOROETHYLENE	30 MINUTES	71°C (160°F)
5	DEIONIZED WATER	30 MINUTES	RT
6	DEIONIZED WATER	30 MINUTES	71°C (160°F)
7	5% HCl	4 HOURS	RT
8	5% HCl	4 HOURS	88°C (190°F)
9	DEIONIZED WATER TO NEUTRAL Ph	4 HOURS	RT
10	HEAT CLEANED	3 HOURS	540°C (1004°F)

FIGURE 3-9 PREFORM CLEANING SEQUENCE

3.5 EFFECTS OF CLEANING PROCESSES ON FIBER STRENGTH

Astroquartz fibers with A1100 surface finish were tested in tension after being treated with various combinations of the cleaning steps used in this study and listed in Figure 3-9. The purpose was to determine what effect the various cleaning steps had on fiber strength. Six cleaning treatments were evaluated as shown in Figure 3-11, with "as received fibers" used as a control.

Individual yarns were tested in tension in accordance with ASTM 2256, Option 1A and 1B (Reference 8). Only three yarns were tested for each condition. Therefore, the results are only an indication of the effects on yarn tensile strength because there are not enough specimens for statistical calculations. For each treatment, three yarns were tested in straight condition and three were knotted. Strength results given in Figure 3-11 indicate that heat treatment of fibers is the greatest cause for strength reduction. Solvent and acid cleaning did not appear to appreciably reduce the fiber strength.

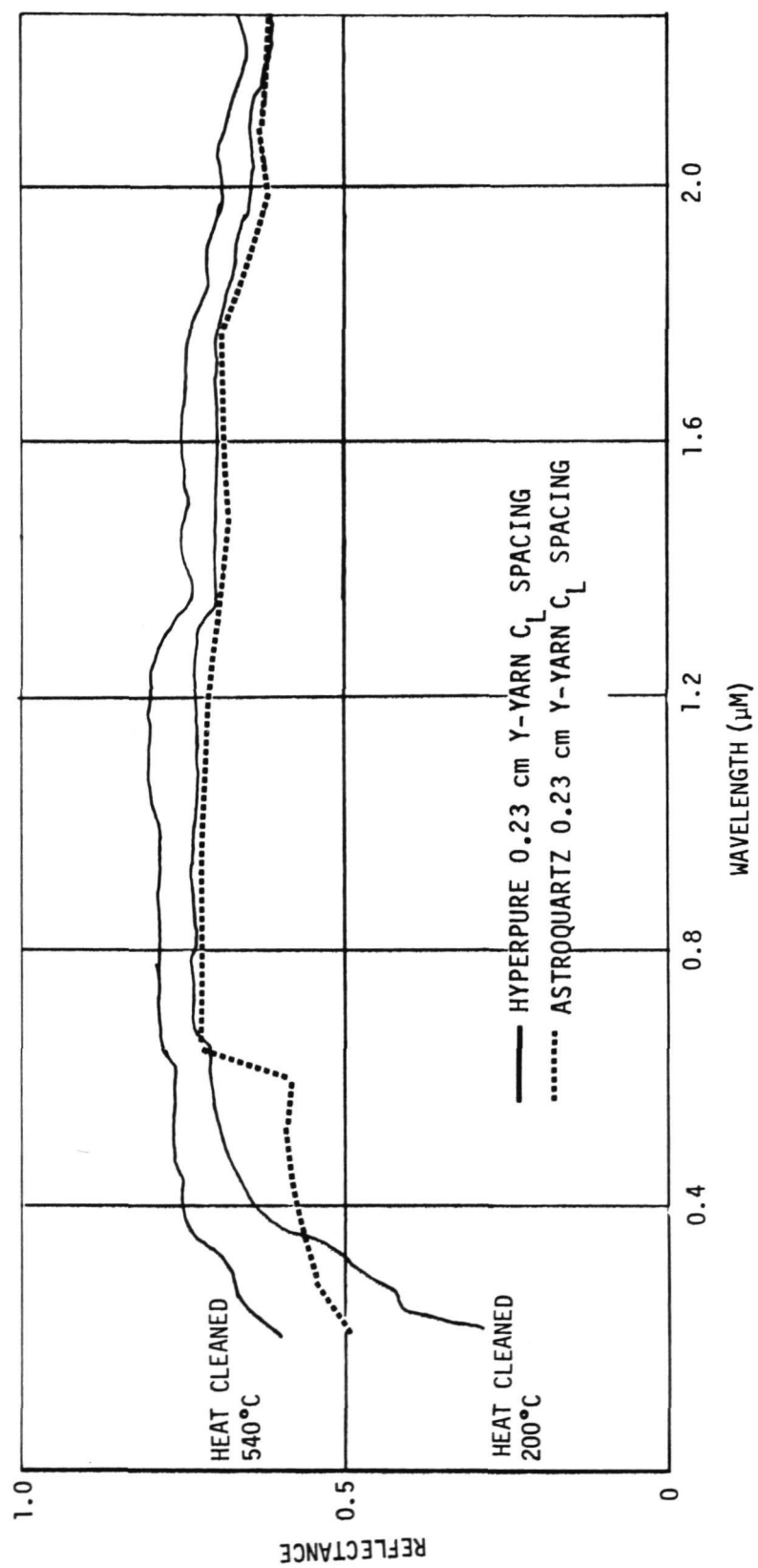


FIGURE 3-10. REFLECTANCE OF HYPERPURE PREFORM HEAT CLEANED AT 200°C AND 540°C COMPARED TO ASTROQUARTZ HEAT CLEANED AT 540°C

TREATMENT	NUMBER OF SPECIMENS		BREAKING LOAD (AVE)	
	<u>CONFIGURATION</u>			
	STRAIGHT	KNOTTED	NEWTONS	(LBS)
"AS RECEIVED"	3		116.41	(26.17)
		3	58.18	(13.09)
SOLVENT ONLY	3		103.07	(23.17)
		3	60.44	(13.60)
SOLVENT, ACID	3		107.51	(24.17)
		3	54.58	(12.27)
HEAT ONLY ¹	3 ²		29.80	(6.70)
		3	9.67	(2.17)
SOLVENT, HEAT ¹	3 ²		29.58	(6.65)
		3	7.45	(1.67)
SOLVENT, ACID, HEAT ¹	3 ²		25.88	(5.82)
		3	5.92	(1.33)
SOLVENT, HEAT ¹ , ACID	3 ²		19.88	(4.47)
		3	4.31	(0.97)

- NOTES: ¹ HEAT TREATMENT AT 540°C FOR 3 HOURS
² SPECIMENS BROKE IN GRIP
3. AVERAGE TIME TO BREAK 12.0 SEC
4. RATE OF HEAT TRAVEL WAS 0.51 CM/MIN
5. TESTED ON INSTRON UNIT
6. FIBER SIZE 4/4 ~ 1920 FILAMENTS

FIGURE 3-11 EFFECT OF PREFORM CLEANING PROCESSES ON FIBER STRENGTH

After heat treatment the fibers became brittle and difficult to handle and test effectively. All heat-treated yarns tested in the straight condition broke within the grip area of the test specimen. Aluminum foil was wrapped around the fiber ends to give them some protection, but to no avail. Knotted yarns that were heat treated tended to break at the knot. In spite of these problems, however, the main objectives of the tests were achieved. It was learned that the A100 sizing on the Astroquartz is difficult to remove without heat cleaning, but that heat treatment affects fiber strength. The strength reduction noted after heat treatment results from abrasion of the fibers due to handling both during and after removal of the sizing. The thermal cycle employed should not in itself lower the intrinsic strength of the Astroquartz to the extent indicated in Figure 3-11. It should be remembered that the organic sizing's primary function is to protect the fibers from abrasion resulting from handling and weaving of the yarn.

3.6

DENSIFICATION

The 3D silica preforms were densified with hyperpure silica grains to increase the strength of the resultant material while maintaining a high purity level and the associated high reflectance. A concerted effort was made to make the silica particles as small as possible and to maintain their high purity. Impregnation of the preforms is most efficient with a very small particle size. Achieving a colloidal size silica particle from hyperpure silica grain was not within the scope of this program. An average particle size of 0.4 to 0.7 μm was obtained during this program.

3.6.1

Binder Preparation

Small silica particles were obtained by crushing high purity Dynasil fused silica (not more than 1 ppm metallic ion impurities) in a nylon lined press. The cullet was then heat treated to remove any nylon picked up from the crushing operation. Fine particles were screened out and ground in polypropylene ball mills using high purity Dynasil grinding media and deionized water. Ceramic ball mill jars were not used because of possible contamination. Milling time was 180 hours at ≈ 40 percent solids content. After milling, the solids content of the slip was adjusted to ≈ 25 percent. Average particle size after ball milling was measured at roughly 1.3 μm . To reduce the average particle size of the slip further, the coarse material was allowed to settle out for 24 hours, resulting in a slip with a solids content of 17-18 percent and an average particle size of 0.4 - 0.7 μm , as determined by ASTM Method 422 (Reference 9).

3.6.2

Densification Technique

Once the hyperpure silica binder was prepared, both the binder and the precleaned preform were placed under a vacuum of ≈ 20 mm of mercury in the bell jar shown in Figure 3-12. The preform was held above the slip by Astroquartz yarn. While the vacuum was maintained, the preform was slowly lowered into the hyperpure silica binder and allowed to soak for ≈ 20 minutes. The 20 minute soak time was assumed to be sufficient to allow migration of the binder particles to the center of the preform. A microwave oven was then

used to dry the preform to a constant weight. Microwave drying was selected over forced air drying to avoid particle migration to the surface. This procedure was repeated until the density change versus impregnation cycle approached a constant value. Observations of densification progress were made using plots of density increases vs number of impregnation cycles and by also examining x-ray records.

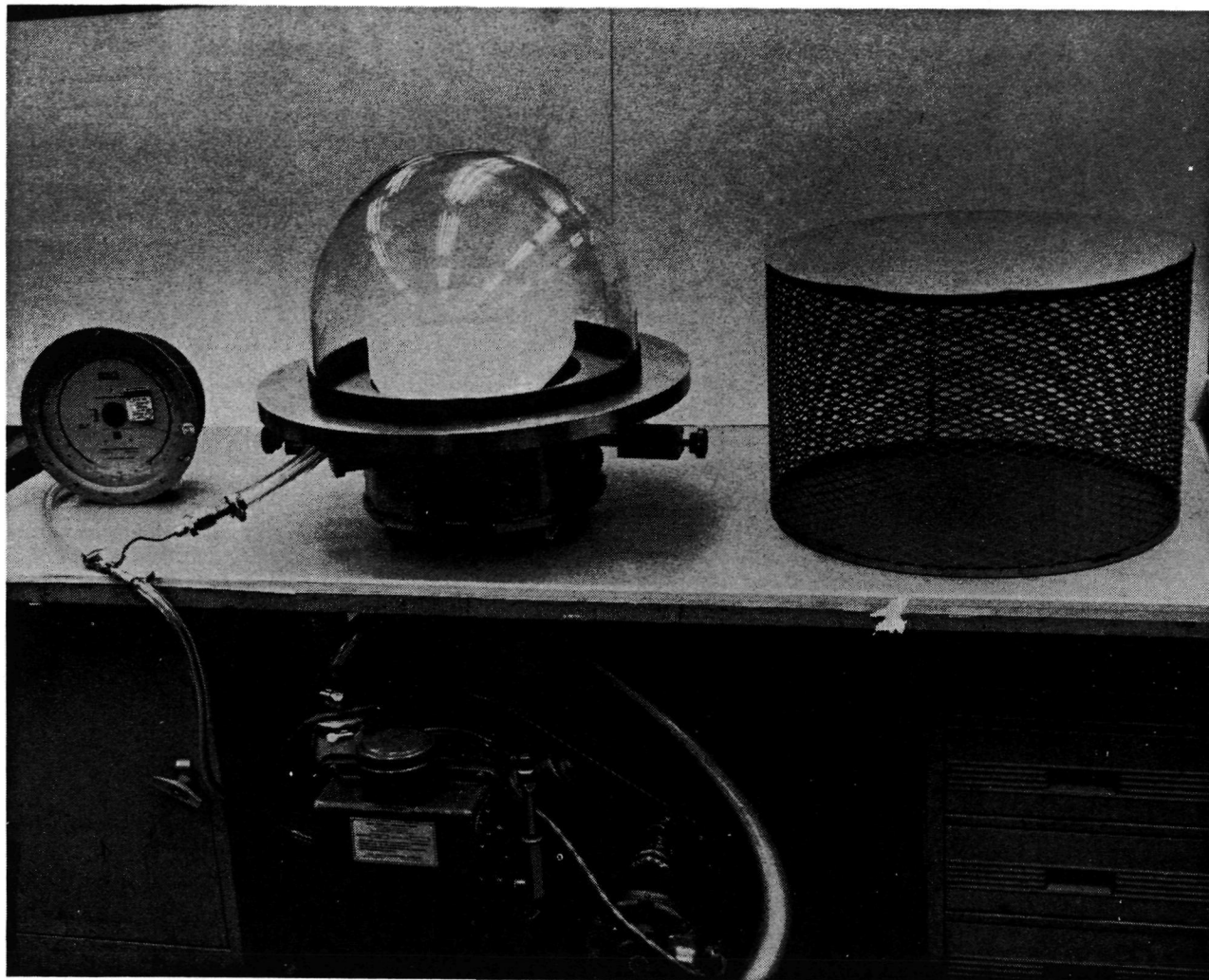


FIGURE 3-12 APPARATUS FOR VACUUM IMPREGNATION WITH HYPERPURE SILICA BINDER

3.6.3

Discussion of Densification Results

Bulk density measurements were made after each impregnation cycle. Figure 3-13 compares bulk density increase vs impregnation cycle for all three of the Astroquartz preforms. All preforms reached the maximum density levels shown in Figure 3-13 without excessive visible silica binder buildup on the surfaces, although x-rays taken between impregnation cycles indicated a small buildup. Impregnation of each preform was stopped when the curves in Figure 3-13 indicated no appreciable density increase.

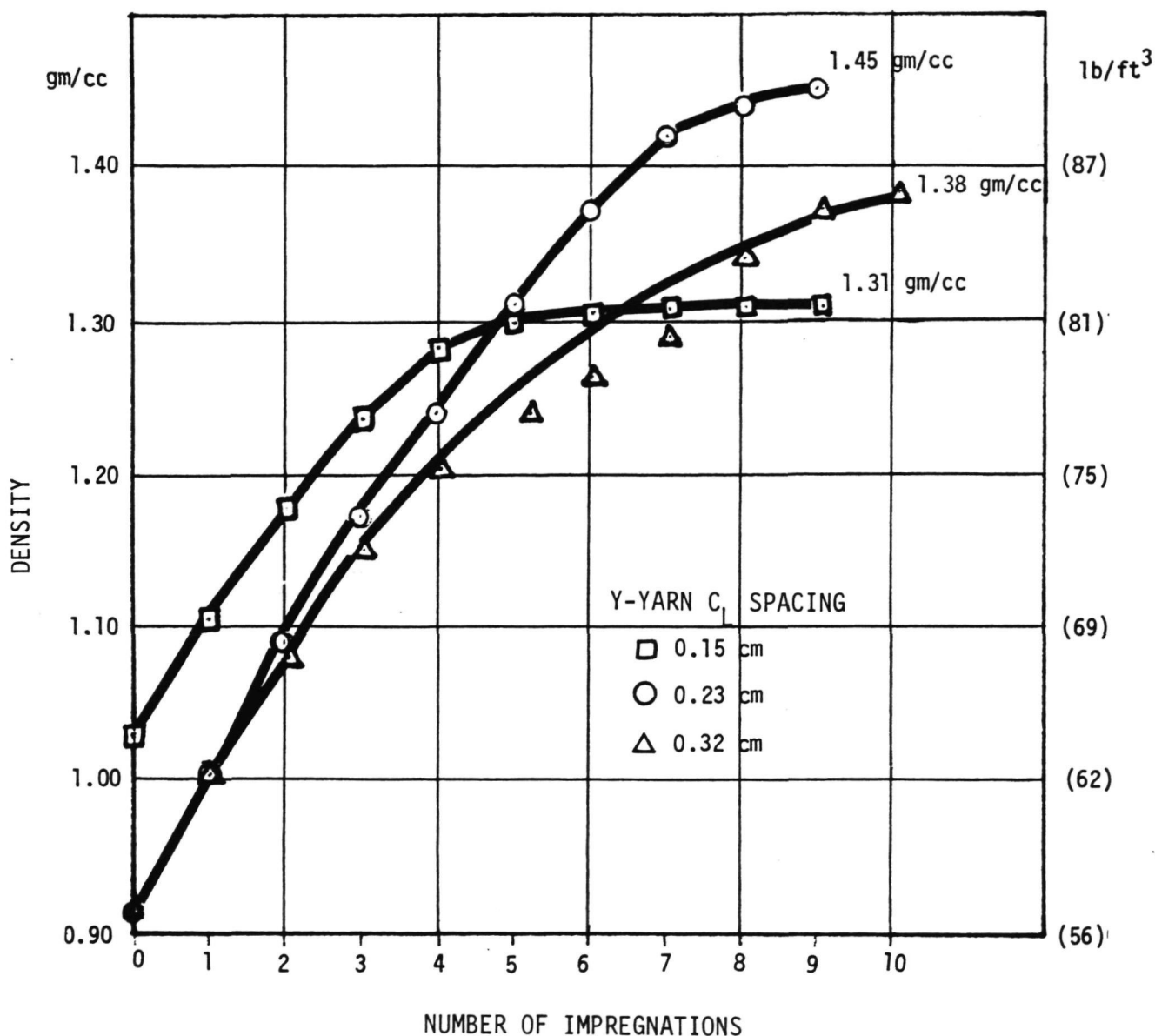


FIGURE 3-13 DENSIFICATION HISTOGRAM FOR ASTROQUARTZ PREFORMS

The 0.23 cm (0.090 in.) Y-yarn spacing preform had the highest overall density [1.45 gm/cc (90.5 pcf)] among the Astroquartz preforms after the same number of impregnation cycles. Based on this, the hyperpure preform was fabricated with a 0.23 cm (0.090 in.) Y-yarn fiber spacing. The hyperpure preform went through the same impregnation process, except that the surfaces of the preform were machined after the 5th and 7th impregnations. Machining removed a densified outer surface layer (revealed by radiographic examination) that hampered uniform densification of the 3D preform.

Figure 3-14 shows the densification progress of the hyperpure preform. For comparison, the densification progress of the 0.23 cm (0.090 in.) Y-yarn spacing Astroquartz preform is repeated. Note that large increases in density were observed for the first four impregnations on both preforms. After four impregnations, density increases for the hyperpure preform dropped slightly. The surface of the hyperpure preform appeared to be saturated with the silica binder. After the fourth impregnation, pins coated with Teflon were used to pierce the surface buildup in an attempt to increase densification efficiency. However, the density increase dropped with the fifth impregnation cycle. In order to open up the surface further, 0.25 cm (0.10 in.) was machined off both 10.2 cm (4.0 in.) x 20.3 cm (8.0 in.) surfaces, using a diamond studded end mill and high purity water coolant. After machining, the surface of the preform was rinsed with high purity water to remove loose silica. The sixth and seventh impregnations showed an increase in weight pickup, but the overall bulk density of the preform increased very little. After machining, the preform density decreased, but the loss was regained after subsequent impregnation.

A second machining step was used after the 7th impregnation. This time all surfaces were machined 0.25 cm (0.10 in.). Densification was stopped after the eighth impregnation step, because the density increase was not significant. Radiographic analysis of the preform at this time again indicated a small binder build up on the surfaces of the preform.

The final bulk density of 1.30 gm/cc (81.1 pcf) obtained for the hyperpure preform was considerably less than that of the corresponding 0.23 cm (0.090 in.) Y-yarn spacing Astroquartz preform [1.45 gm/cc (90.3 pcf)]. The overall density increase was more comparable to the 0.15 cm Astroquartz block [1.31 gm/cc (81.7 pcf)]. The low weight pickup of the hyperpure silica is believed to be due to its different weave orientation from that in the Astroquartz preforms. The Astroquartz preforms were woven with the Y direction yarns perpendicular to the largest surface (X-Z plane or surface). On the hyperpure preform the largest surface was a Z direction surface (X-Y plane or surface). The X-Y surface of the layer-to-layer interlock weave design has spaces between the Z direction yarns (refer to view A-A of Figure 3-2) which tend to become blocked with the larger hyperpure silica grains, preventing further smaller particle entrance during subsequent impregnations. The X-Z surfaces are much rougher than X-Y surfaces as can readily be seen in the photographs of the preforms in Figures 3-6 and 3-8. It is postulated that the greater roughness means more surface area for the silica impregnant to penetrate. Thus, a preform with a larger amount of rough surface would densify more efficiently.

Further, since the "straight through" or Y yarns are in the shortest dimension for the Astroquartz preforms and the longest dimension for the hyperpure preform, there also exists the possibility that impregnation through the Y direction is different from impregnation through the Z yarn directions, especially when one considers that the Z yarns which make up the largest dimension on the hyperpure block are the ones which only penetrate three other yarns (2 X and 1 Y) and then make a 180° turn.

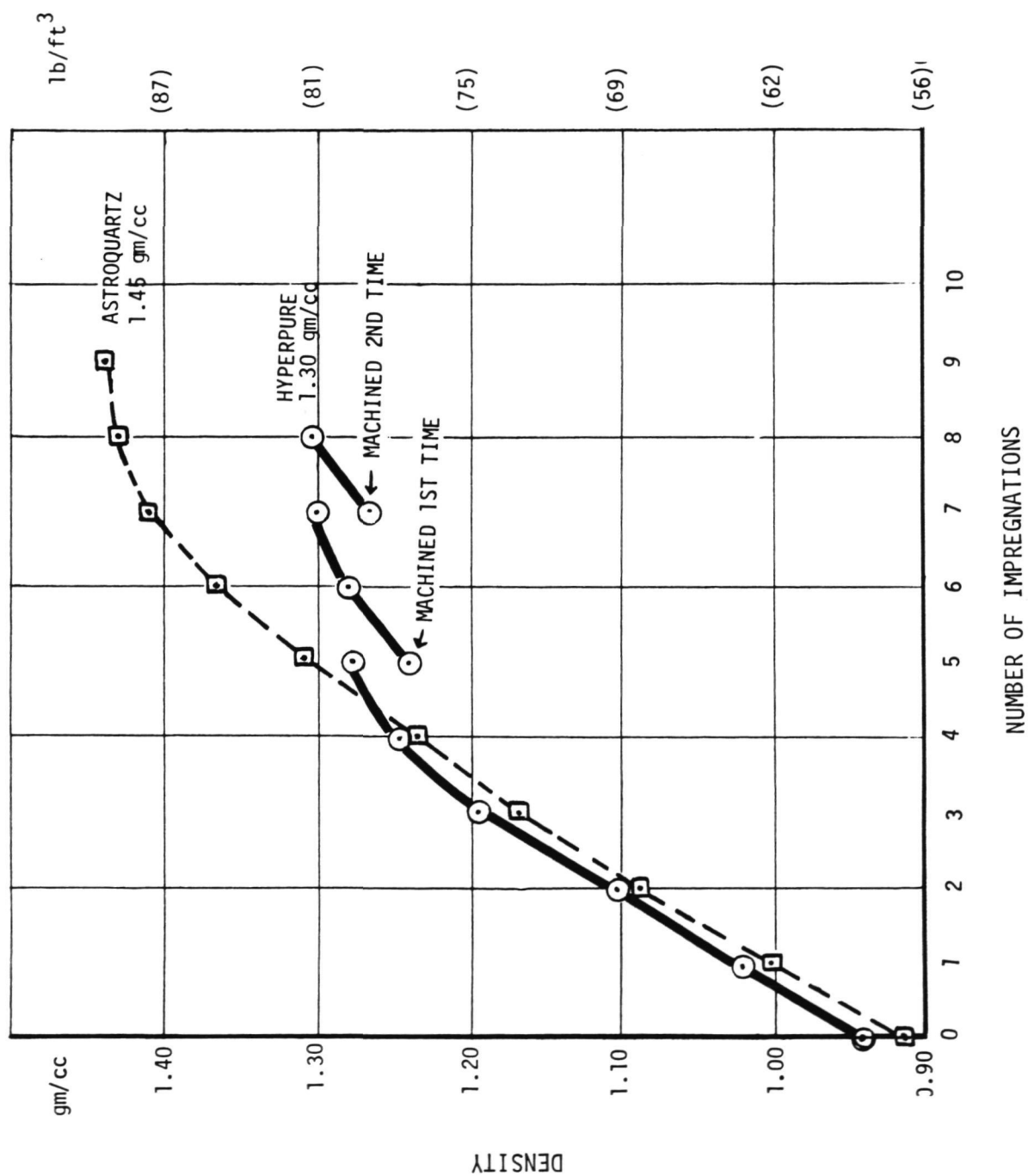


FIGURE 3-14 DENSIFICATION HISTOGRAM FOR HYPERPURE PREFORM

3.7

SPECIMEN MACHINING

Maintaining specimen purity throughout the machining operation was of primary concern. Tools used to machine specimens were all diamond impregnated. Water, used for cooling during some machining operations was high purity.

3.7.1

Specimen Layout

Layouts of test specimens machined from the Astroquartz and hyperpure silica preforms are shown in Figures 3-15 and 3-16, respectively. These layouts take into account the weave orientation change discussed in subsection 3.3. Flexure specimens were especially scrutinized and identified to ensure that they would be tested only in the Z direction. Figure 3-17 is a summary list of all specimens.

3.7.2

Machining

First all surfaces of the "as densified" Astroquartz and hyperpure preforms were machined to provide parallel surfaces to facilitate specimen layout. A diamond studded end mill was used for this purpose, with distilled deionized water as the cooling medium.

The first "blank" cut on the 0.15 cm (0.060 in.) spacing preform, made with a diamond-studded cut off wheel and employing water cooling, produced a black powder contaminant (assumed to be the cut off wheel matrix material, used to hold the diamond particles in place). The water spread the contaminant beyond the immediate area of the saw cut. It was suspected that the dark powder suspended in the cooling water was being drawn into the preform by capillary action through the fiber ends. Also, some of the silica impregnant was removed by the water coolant.

To avoid spreading the contaminant and to prevent capillary action, remaining cuts were made without water coolant. The amount of contaminant generated was approximately the same, but it remained only on the cut surface.

Surface grinding of specimens with a diamond-studded end mill was performed without contamination. The surfaces of flexure specimens were cleaned effectively using the end mill without water cooling. The surface contamination was almost completely removed, with only a few of the 0.15 cm spacing Astroquartz specimens showing some discoloration. These were specimens taken from the first slab cut with water cooling. Diamonds on the end mill used for surface grinding were of a larger grit than those on the cut off wheel, and this was believed to be the main reason the end mill did not generate contamination.

A saw blade with the same size diamond grit and matrix type used for surface grinding was purchased for the "blank" machining of the hyperpure preform. It was hoped that the procedures developed on the Astroquartz material would also hold true for the hyperpure. In general this was true, but some small amount of contamination was periodically generated even when no water coolant was employed. Removal of this contaminant was also completed with the diamond studded end mill without water cooling.

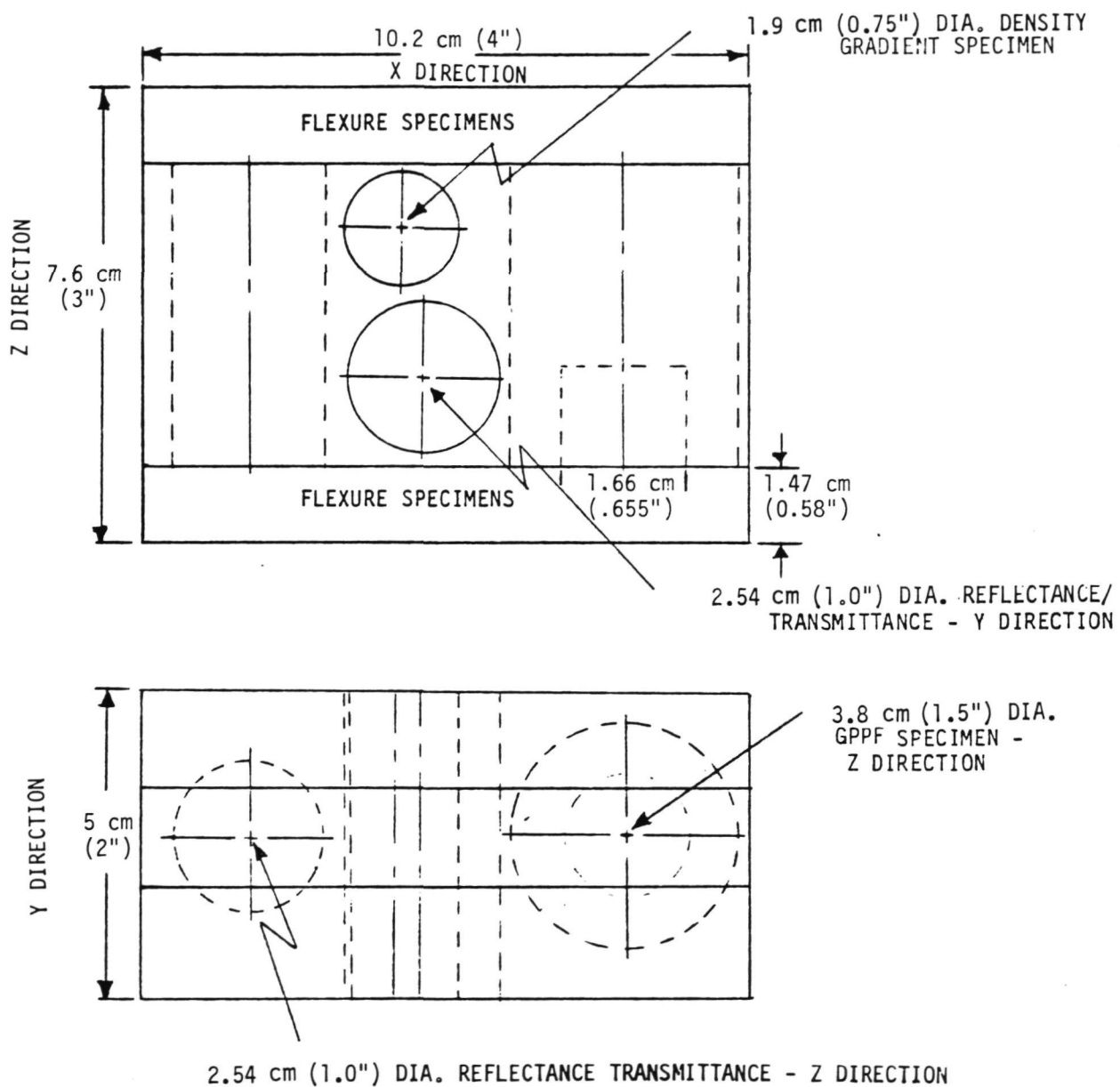


FIGURE 3-15 TEST SPECIMEN LAY-OUT FOR ASTROQUARTZ PREFORMS
(CORRECTED 3D WEAVE PATTERN ORIENTATION)

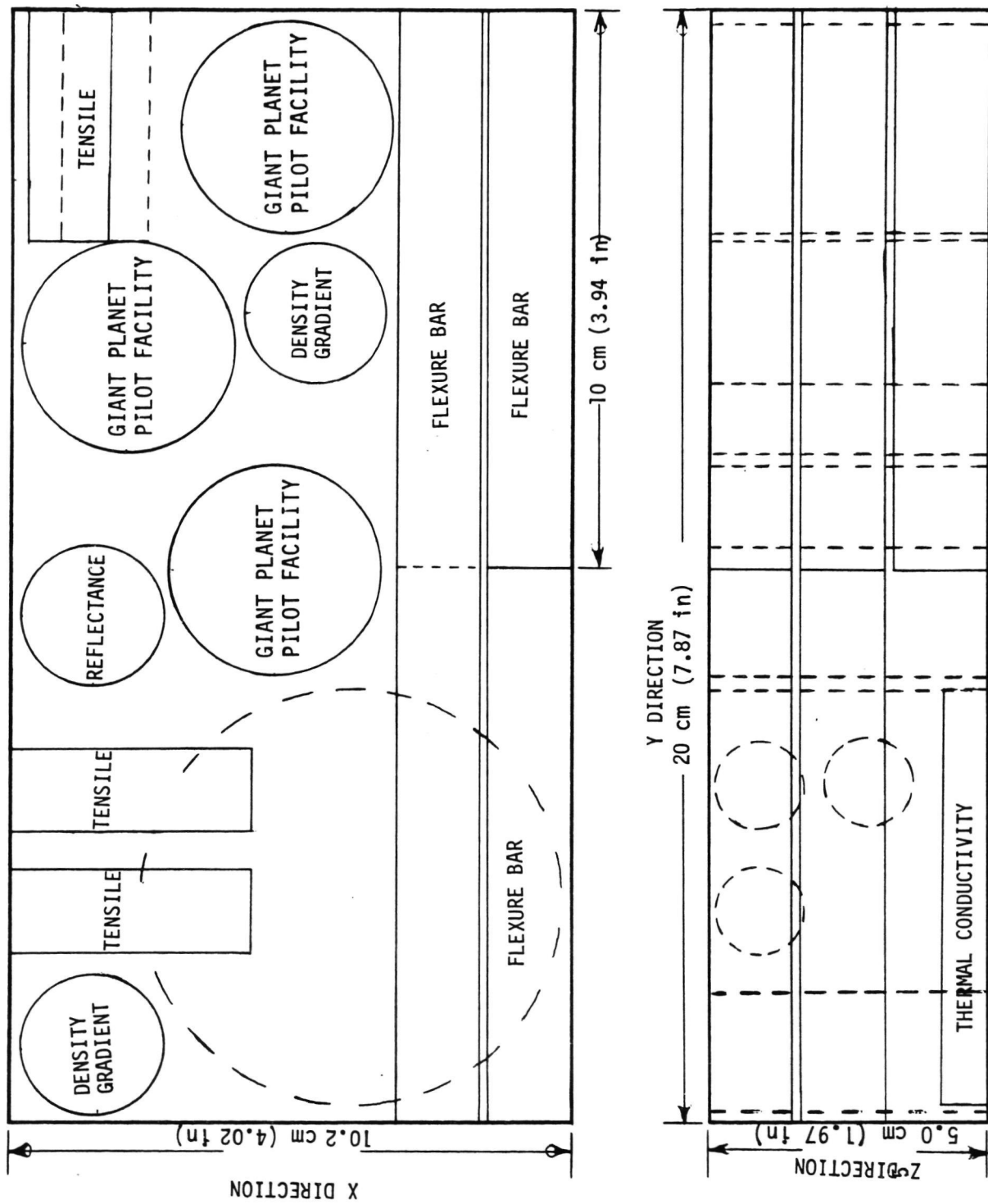


FIGURE 3-16 TEST SPECIMEN LAYOUT FOR HYPERPURE SILICA PREFORM

TEST	Y YARN SPACING/ MATERIAL	SPECIMEN DIMENSIONS	NO. OF SPECIMENS
FLEXURE	0.15 cm ASTROQUARTZ	1.3 cm x 1.3 cm x 10.2 cm	6
	0.23 cm ASTROQUARTZ	1.3 cm x 1.3 cm x 10.2 cm	6
	0.32 cm ASTROQUARTZ	1.3 cm x 1.3 cm x 10.2 cm	6
	0.23 cm HYPERPURE	1.3 cm x 1.3 cm x 10.2 cm	6
	0.23 cm HYPERPURE	1.3 cm x 1.3 cm x 20.3 cm	2
TENSILE	0.23 cm HYPERPURE	1.3 cm DIA x 3 cm	6
DENSITY GRADIENT	0.15 cm ASTROQUARTZ	1.9 cm DIA x 5.1 cm	1
	0.23 cm ASTROQUARTZ	1.9 cm DIA x 5.1 cm	1
	0.32 cm ASTROQUARTZ	1.9 cm DIA x 5.1 cm	1
	0.23 cm HYPERPURE	1.9 cm DIA x 5.1 cm	2
REFLECTANCE AND TRANSMISSION	0.15 cm ASTROQUARTZ	2.5 cm DIA x 9.1 cm	2
	0.23 cm ASTROQUARTZ	2.5 cm DIA x 9.1 cm	2
	0.32 cm ASTROQUARTZ	2.5 cm DIA x 9.1 cm	2
	0.32 cm HYPERPURE	2.5 cm DIA x 9.1 cm	1
GIANT PLANET PILOT FACILITY (GPPF)	0.15 cm ASTROQUARTZ	3.8 cm DIA x 5.1 cm	1
	0.23 cm ASTROQUARTZ	3.8 cm DIA x 5.1 cm	1
	0.32 cm ASTROQUARTZ	3.8 cm DIA x 5.1 cm	1
	0.23 cm HYPERPURE	3.8 cm DIA x 5.1 cm	3
THERMAL CONDUCTIVITY	0.23 cm HYPERPURE	7.42 cm DIA x 1.11 cm	1

FIGURE 3-17 TEST SPECIMEN IDENTIFICATION

All cylindrical specimens were machined with diamond studded core drills and no water cooling. Diamonds impregnated on the core drills were of the same size as those used on the end mills. Some gray discoloration resulted, but because of the cylindrical shape, surface grinding could not be used to clean the sides of the specimens. Flat surfaces of the larger cylindrical specimens were, however, cleaned with the end mill. All cylindrical specimens were heat cleaned at 540°C (1004°F) for three hours. This removed all visible traces of the black contaminant.

The original configuration for the tensile specimens to be machined from the hyperpure preform was a cylindrical "dog bone" shape. Three specimens were to be machined 1.5 cm (0.59 in.) in diameter by 10.2 cm (4.0 in.) long with a 0.6 cm (0.24 in.) diameter gauge section. Based upon the initial machining experience, the gauge section was determined to be too thin to machine successfully. Therefore, the "dog bone" configuration was dropped in favor of an alternative specimen geometry. The alternate geometry consisted of a 1.3 cm (.5x1 in.) diameter by 4.3 cm (1.7 in.) long test specimen that could be core drilled directly from the densified preform. Because these specimens were considerably smaller than those originally conceived, additional test specimens could be obtained. Three specimens were core drilled in both the X and Y directions. They were slightly twisted because of their low strength which is directly proportional to the low density [1.3 gm/cc (81 pcf)].

An attempt was made to obtain specimens in the Z direction. One specimen was core drilled, but it was severely twisted and would be unacceptable for testing. Further efforts to obtain useful specimens were dropped.

As a result of the fiber orientation problem discussed in subsection 3.3, only one Giant Planet Pilot Facility (GPPF) specimen could be core drilled from each Astroquartz preform instead of the two test specimens previously thought possible. However, two reflectance and transmittance specimens were obtained in the Y and Z directions. Flexure specimens were marked with a felt tip pen as they were machined so that correct weave orientation could be verified.

Figures 3-18 and 3-19 are photographs of typical specimens machined from both the Astroquartz and hyperpure densified preforms ready. The specimens are ready for testing.



FIGURE 3-18 TYPICAL SPECIMENS MACHINED FROM THE 0.23 cm Y-YARN
SPACING ASTROQUARTZ PREFORM

ORIGINAL PAGE IS
OF POOR QUALITY

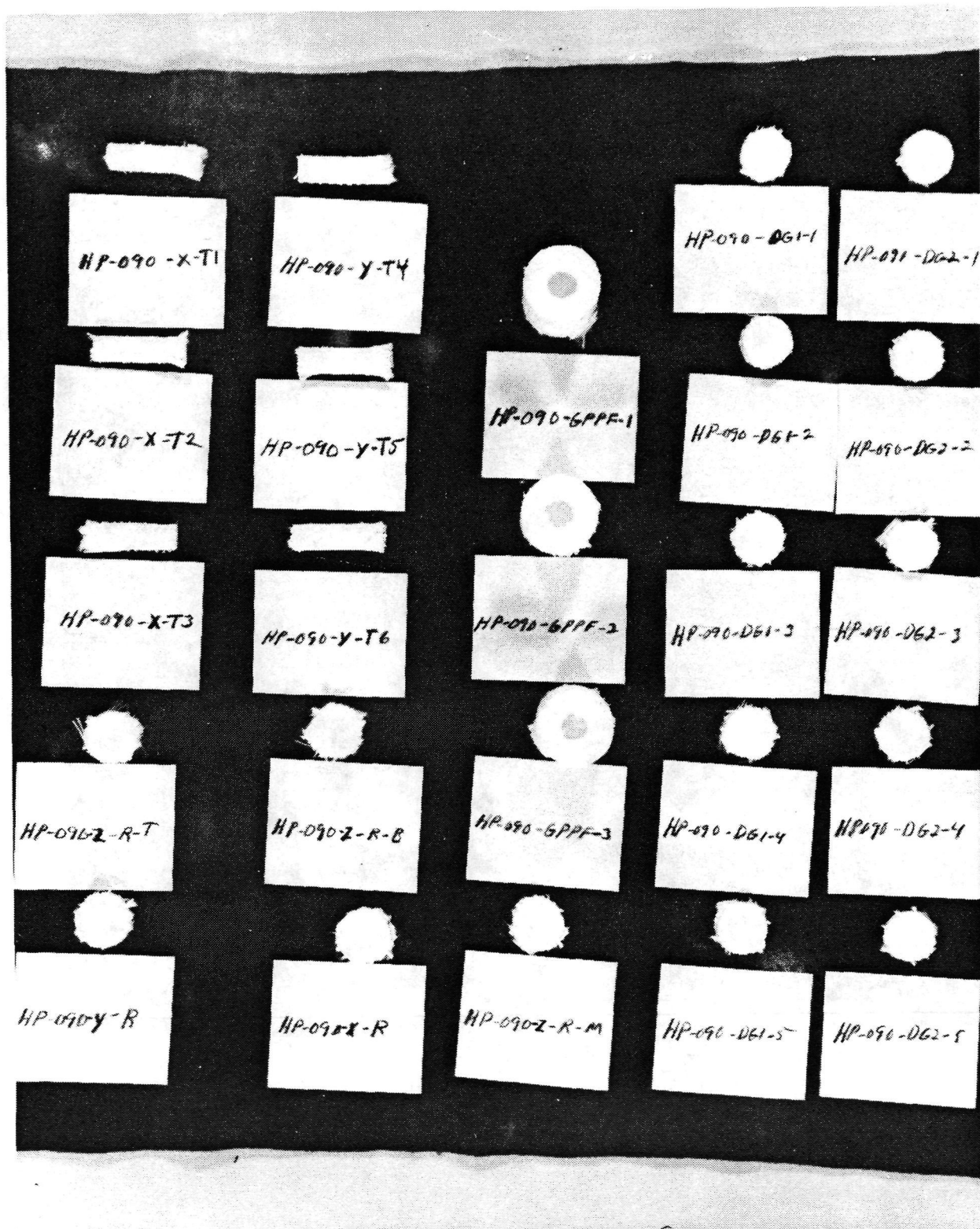


FIGURE 3-19 TYPICAL SPECIMENS MACHINED FROM THE 0.23 cm Y-YARN
SPACING HYPERPURE PREFORM

4.0 DENSITY GRADIENT MEASUREMENTS

4.1

SPECIMEN DESCRIPTION

Specimens were core drilled from the center of each Astroquartz preform in the 5.0 cm (2.0 in.) dimension, as shown in Figure 3-15. Two specimens were obtained from the hyperpure preform in the 5 cm (2.0 in.) dimension; one from the center and one at the edge, as shown in Figure 3-16. Each core was then cut into five slices approximately 1 cm (0.4 in.) thick. Density checks and visual observations were made on each slice.

The rough surfaces of the specimens made accurate dimensional measurements difficult. Presence of loose impregnant eliminated the possibility of using any immersion techniques to determine density. All density measurements were determined from volume measurements made with calipers, and the accuracy of the measurements was therefore impaired by size and roughness of the specimen. A larger specimen obviously would provide more accurate results.

4.2

MEASUREMENT RESULTS

The densified 3D Astroquartz specimen with the 0.15 cm Y-yarn spacing was not uniformly densified by the vacuum procedure outlined in subsection 3.5. Densities of approximately 1.34 gm/cc (83.6 pcf) were measured for the slices taken near one outer edge, while densities as low as 1.15 gm/cc (71.8 pcf) were measured for slices taken from the center of the specimen. Figure 4-1 depicts the observed density gradient through the thickness of the preform at one location.

Increasing the Astroquartz Y-yarn spacing from 0.15 cm (0.060 in.) to 0.23 cm (0.090 in.) in a 3D woven specimen densified by the same procedure resulted in a more uniform density. The first four slices exhibited, a fairly uniform density, as shown in Figure 4-2. The 5th slice taken from this specimen, was not considered in data analysis because of its obvious nonuniform condition. The outer surface slices had a density of approximately 1.35 gm/cc (84.2 pcf), while the slices taken near the center of the densified preform had a density of 1.32 gm/cc (82.4 pcf). The individual slices from this specimen were nearly the same in density except for the fifth slice, which did have a rough surface, which could account for its apparent lower density.

The largest spacing Astroquartz preform, with a 0.32 cm (0.125 in.) Y-yarn spacing, was not as uniformly densified as the 0.23 cm (0.090 in.) Y-yarn spacing, but was better than the 0.15 cm (0.060 in.) Y-yarn preform. Figure 4-3 shows that density values varied from 1.25 gm/cc (78 pcf) to 1.26 gm/cc (78.6 pcf) for the outer slices while the center slices varied between 1.19 gm/cc (74.3 pcf) and 1.28 gm/cc (79.9 pcf).

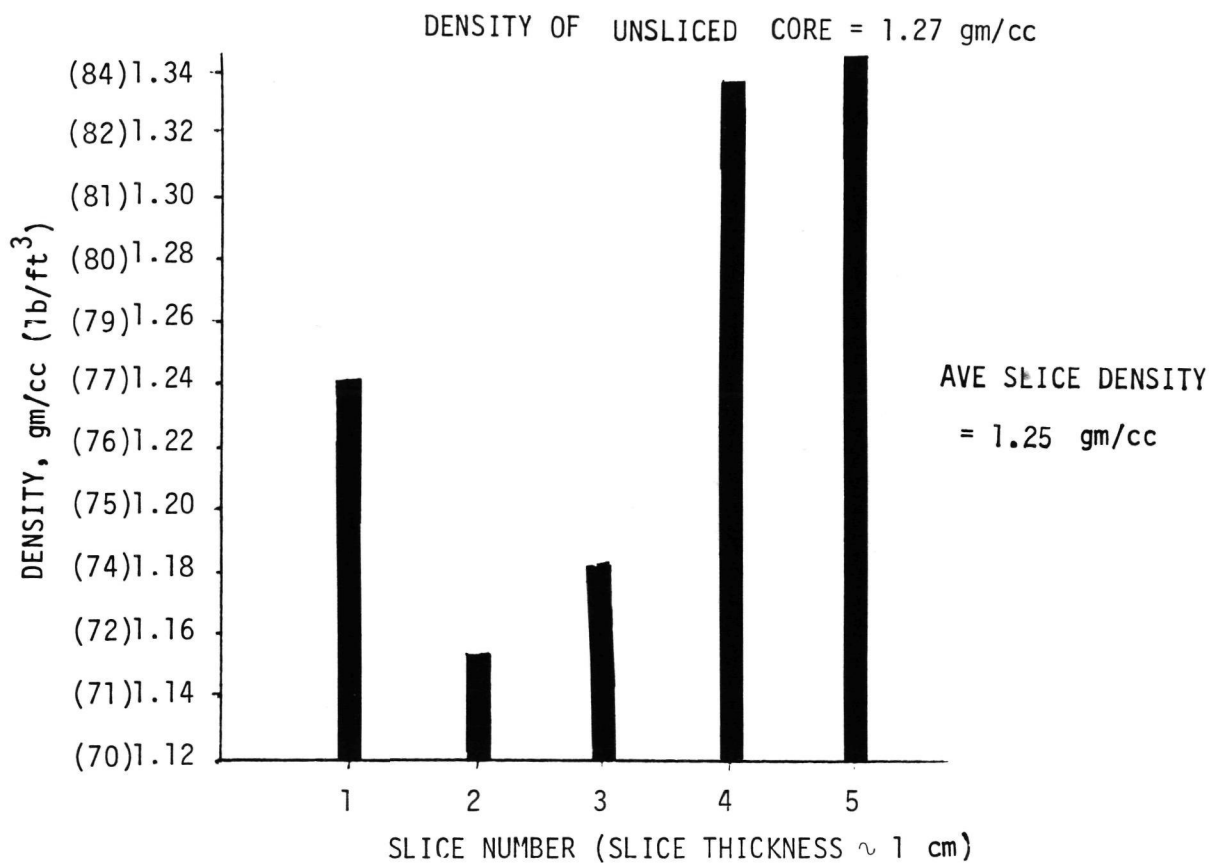


FIGURE 4-1 DENSITY GRADIENT FOR THE 0.15 cm SPACING DENSIFIED ASTROQUARTZ
(SPECIMEN CORE DRILLED FROM THE CENTER)

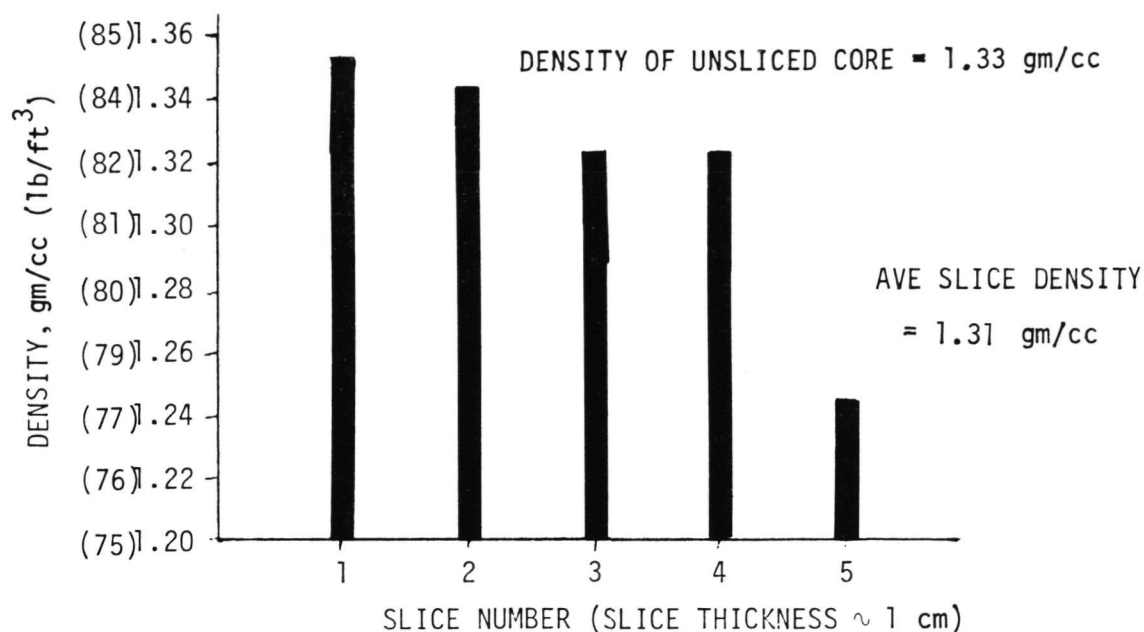


FIGURE 4-2 DENSITY GRADIENT FOR THE 0.23 cm SPACING DENSIFIED ASTROQUARTZ (SPECIMEN CORE DRILLED FROM THE CENTER)

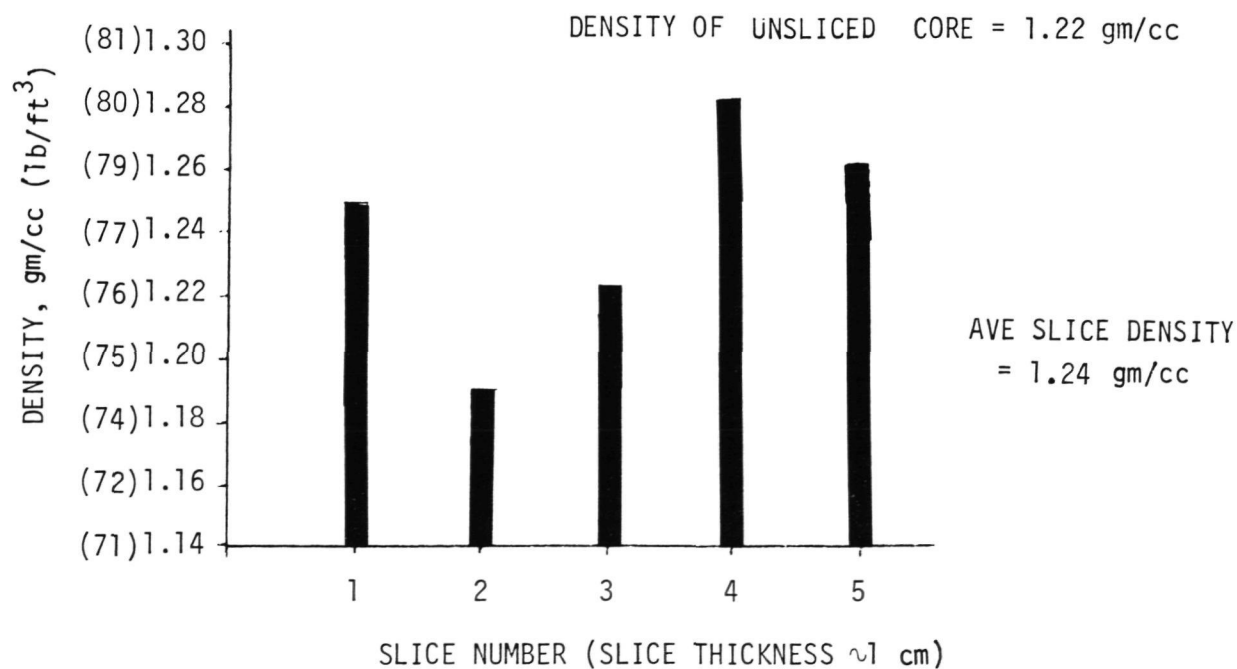


FIGURE 4-3 DENSITY GRADIENT FOR THE 0.32 cm SPACING DENSIFIED ASTROQUARTZ (SPECIMEN CORE DRILLED FROM THE CENTER)

Density gradient data from specimens machined from the 0.15 cm (0.060 in.) and 0.32 cm (0.125 in.) Y-yarn spacing specimens indicate in general a buildup of impregnate on the outer surfaces, as shown in Figures 4-1 and 4-3 respectively. The 0.23 cm (0.090 in.) Y-yarn spacing specimen did not have this same trend.

Based on the results of density measurements made on all three densified Astroquartz preforms, the 0.23 cm (0.090 in.) Y-yarn spacing, which showed the most uniform density, was chosen as the baseline for the 3D hyperpure silica preform.

Following densification of the 3D hyperpure silica preform, core-drilled density gradient specimens taken from the center and corner of the hyperpure preform indicated a density gradient. Figures 4-4 and 4-5 both show higher densities for specimens taken near the surface than for those near the center. There also appears to be a large density difference between the center specimen and the corner specimen: 1.30 gm/cc (81.1 pcf) for the corner specimen versus 1.18 gm/cc (73.6 pcf) for the center specimen. These results, although somewhat surprising because they do not exhibit the uniformity of the 0.23 cm (0.090 in.) spacing Astroquartz block, are nonetheless perhaps indicative of the unusual densification histogram generated and plotted in Figure 3-14.

4.3 DISCUSSION OF THE DENSITY GRADIENT RESULTS

As discussed in subsection 3.6, the greater bulk density achieved for the 0.23 cm (0.090 in.) spacing Astroquartz preform was attributed to several factors, including rough surface texture and weave configuration. The smoother surface resulting from the specific weave used may have caused a greater binder buildup, because of its improved filtering properties.

The average density of slices machined from removed cores from both hyperpure and Astroquartz densified preforms was lower than the density of the core before machining. Both the cores and their slices tended to have even lower densities than the densified preform they were taken from. This is because machining of cores removed some of the impregnate at the surface of the specimens and a small loss of binder would greatly affect the calculated density of a specimen.

Slices made from the density gradient specimens of Astroquartz preforms consistently deviated about 0.02 gm/cc (1.25 pcf) from the density of the core they were machined from. Hyperpure slices deviated much more. Observations of the specimens show that the densified hyperpure slices were rougher and more frayed than the Astroquartz slices. The density gradient specimens from the densified hyperpure preform were machined in the Z direction and those from Astroquartz were from the Y direction. As previously stated in paragraph 3.7.2, core drilled specimens made in the Z direction became twisted. The hyperpure density gradient specimens were also twisted. During machining of the hyperpure slices, excessive material loss resulted in lower slice densities than the original core density and the rougher surfaces reduced accuracy in dimension measurements.

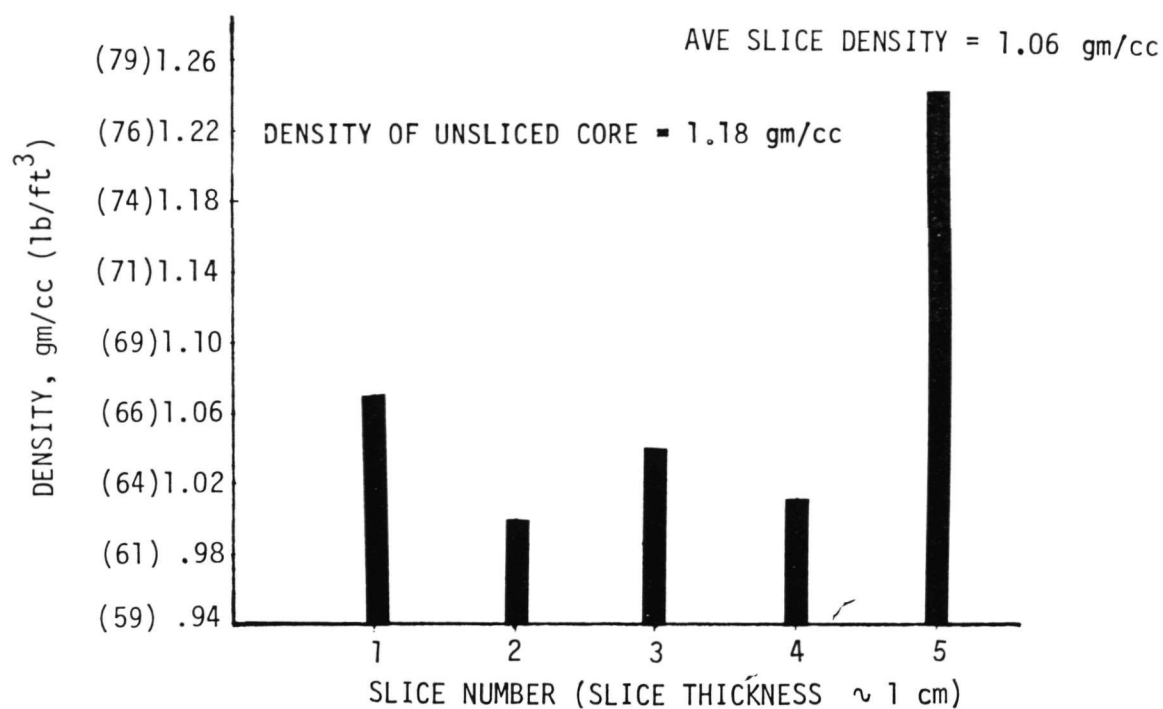


FIGURE 4-4 DENSITY GRADIENT FOR THE 0.23 cm DENSIFIED HYPERPURE PREFORM (SPECIMEN CORE DRILLED FROM THE CENTER)

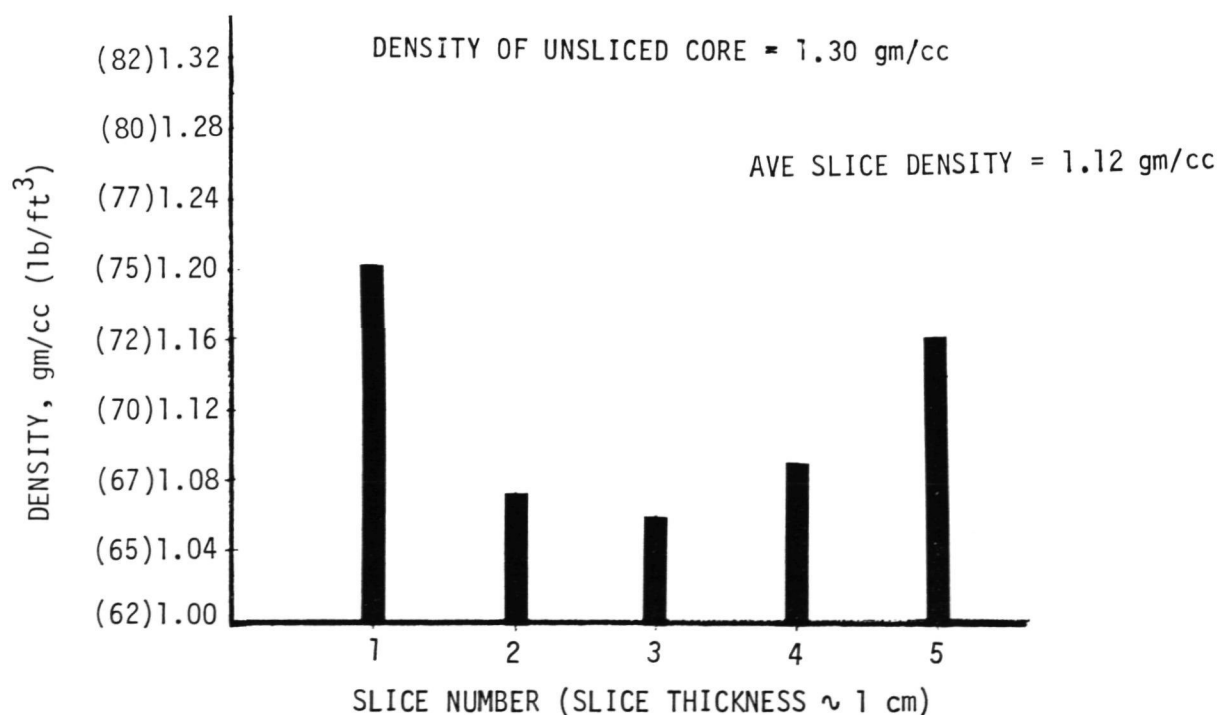


FIGURE 4-5. DENSITY GRADIENT FOR THE 0.23 cm DENSIFIED HYPERPURE PREFORM (SPECIMEN CORE DRILLED FROM THE CORNER)

5.0 THERMAL CONDUCTIVITY MEASUREMENTS

5.1

TEST DESCRIPTION

The thermal conductivity of the hyperpure 3D woven silica composite was measured between room temperature and 908°C (1667°F) in a helium atmosphere at ambient pressure, using a thermal comparator method. The thermal comparator apparatus, shown in Figure 5-1, employs a 7.6 cm (3.0 in.) diameter specimen.

Figure 5-2 shows a schematic of the thermal comparator. The test specimen was placed between two reference materials whose thermal conductivity is known. Pyrex 7740 was used as the reference material for testing below 260°C (500°F), and Pyrocera 9606 was used above 260°C (500°F). All three components are in the shape of disks and form a stack in which heat flows parallel to the centerline of the disks. A main heater placed on top of the stack supplies the heat flow through the stack. An auxiliary heater with a cooling plate was placed below the stack for controlling the heat flow through the stack. For testing above 260°C (500°F), a thin sheet of insulation was inserted between the auxiliary heater and the cooling plate. A guard heater and fibrous insulation were placed around the stack to diminish radial heat loss. The temperature within the stack was measured with thermocouples at locations 1 through 10, as shown in Figure 5-2.

All thermocouples and electrical leads were electrically insulated with ceramic beads and tubing. The first eight thermocouples were connected directly to a computer for real time data analysis. Thermocouples 9 and 10, with an adjustable DC offset, were used to control the main and auxiliary heaters.

Thermal conductivity was determined by establishing a constant heat flow through the stack with the heaters and cooling plate. The guard heater was maintained at the mean temperature of the specimen to average the radial heat loss along the stack height. Once uniform heat flow was established, a value for thermal conductivity (K_S) was computed for the specimen using the following equation:

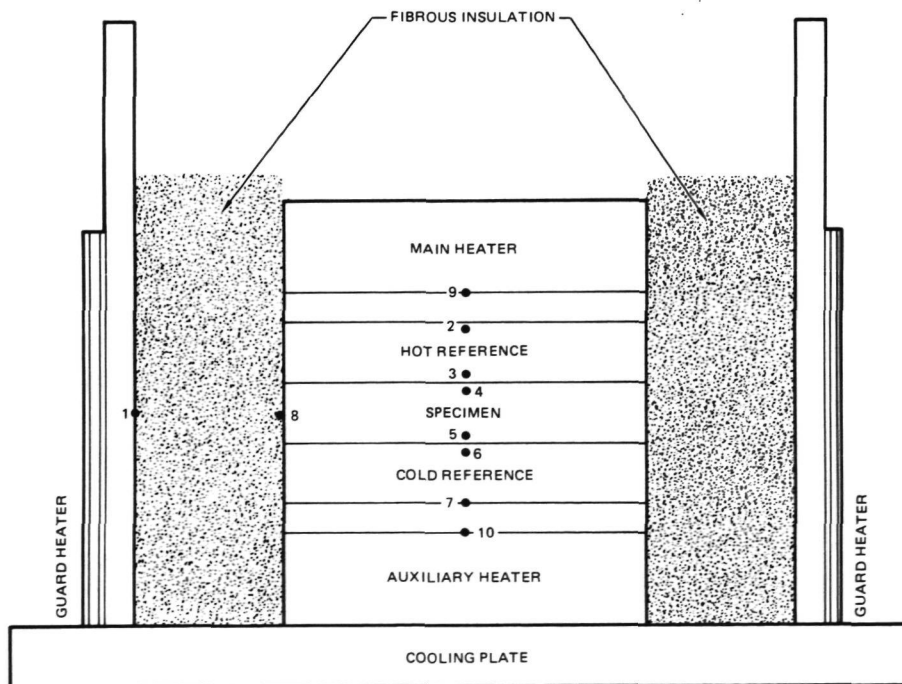
$$K_S = \frac{X_S}{T_S} \cdot \frac{1}{2} \cdot \left(\frac{K_{HR} \cdot T_{HR}}{X_{HR}} + \frac{K_{CR} \cdot T_{CR}}{X_{CR}} \right)$$

where K_S is the calculated thermal conductivity of the specimen and

X_S , X_{HR} , X_{CR}	are the thicknesses of the specimen, hot reference and cold reference, respectively;
T_S , T_{HR} , T_{CR}	are the temperature differences across the specimen, hot reference, and cold reference, respectively;
K_{HR} , K_{CR}	are the thermal conductivities of the reference materials.



FIGURE 5-1 THERMAL COMPARATOR EQUIPMENT FOR DETERMINING THERMAL CONDUCTIVITY



NOTE: NUMBERS REFER TO THERMOCOUPLE LOCATIONS
FIGURE 5-2 THERMAL COMPARATOR APPARATUS SCHEMATIC

Temperatures reached during the test did not affect the physical characteristics of the specimen. There was no measurable shrinkage or observable surface effects. Calculated thermal conductivity data for the specimen is presented in Figure 5-3.

In comparison to the high density [1.7 to 1.9 gm/cc (106 to 118.6 pcf)] of slip-cast fused silica, originally evaluated as a candidate reflective heat shield material (References 2, 3 and 4) the densified hyperpure silica composite [1.3 gm/cc (81.1 pcf)] had a considerably lower measured thermal conductivity. Typical conductivity values for fused silica shown in Figure 5-3 were taken from Reference 10. The lower values measured for the hyperpure silica composite are believed due to its low density. The lower density material contains many pores that are small and numerous enough to have a significant effect in lowering the overall conductivity by reducing solid conduction. The small binder particles contained in the matrix of the 3D hyperpure composite also serve as radiant inhibitors that further help to reduce heat transfer through the material.

Error analysis indicates that the thermal comparator method of determining thermal conductivity is accurate within 10 percent, with the greatest error occurring at higher temperatures. The main source of error is due to thermocouple reading.

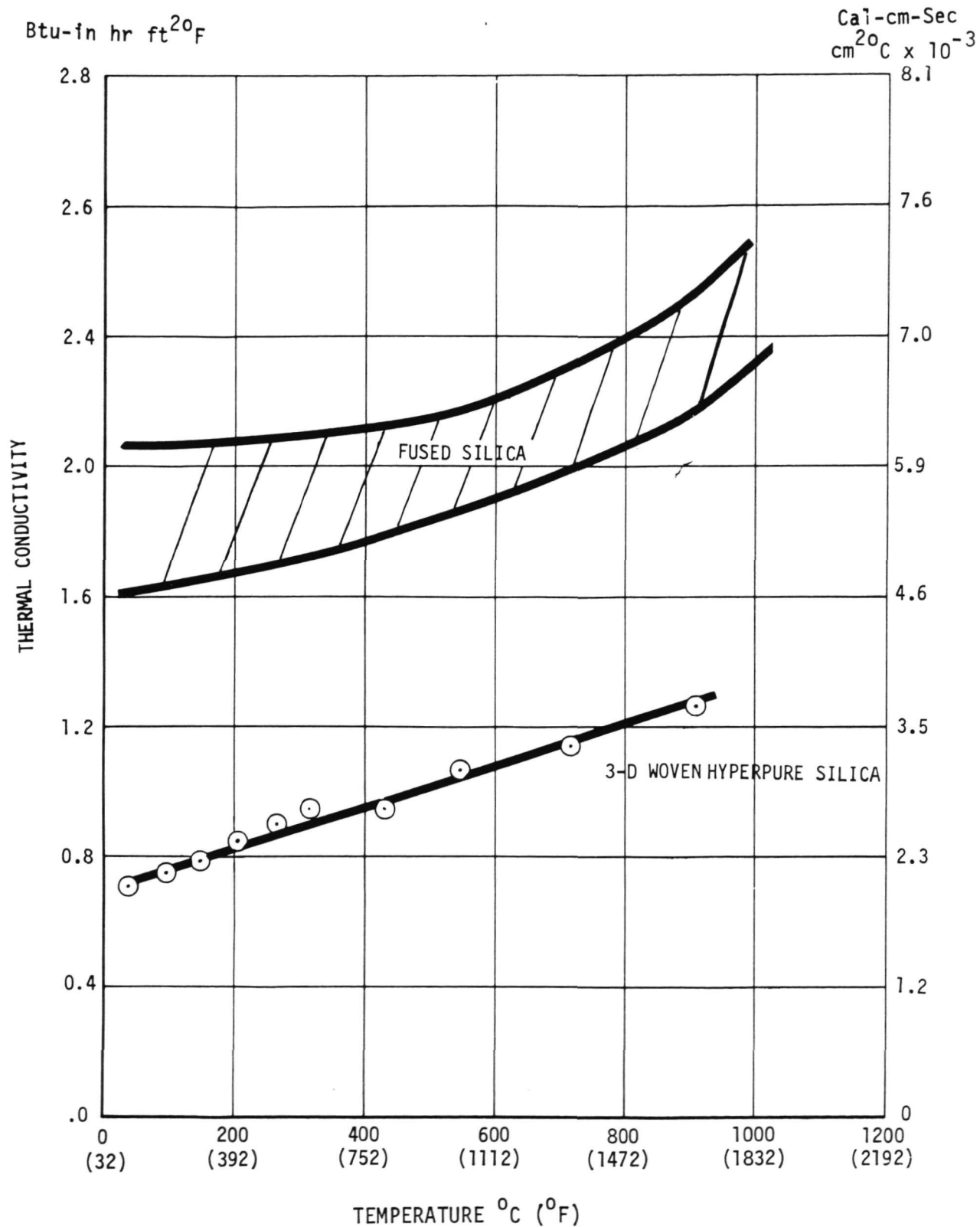


FIGURE 5-3. THERMAL CONDUCTIVITY OF 3D WOVEN HYPERPURE SILICA

6.0 OPTICAL PROPERTY MEASUREMENTS

6.1

TEST DESCRIPTION AND RATIONALE

The purpose of optical measurements was to determine the infinite thickness reflectance, as well as to calculate scattering and absorption coefficients from transmission measurements, to get a better understanding of the materials' total reflective characteristics. Room-temperature measurements were made using a Beckman DK-2A integrating sphere spectrophotometer at wavelengths ranging from 0.25 to 2.4 μm . The method used for measurements is identical to that detailed in Reference 4. Figure 6-1 contains the test matrix for the optical properties determined. As the figure indicates, not all the data is reported, even though it was developed since it did not alter conclusions drawn from the data presented and its publication would serve no useful purpose.

Effects due to fiber purity, light piping, fiber spacing and densification were of primary interest, in addition to detecting differences between the different silica forms (3D woven hyperpure silica, 3D woven Astroquartz, and fiber-reinforced hyperpure slip-cast silica). Measurements accounted for the effects both of light piping and diffuse scattering from the surfaces of both the fibers and silica grain. The two effects were not separated, since the effects of light piping were included automatically in the absorption and scattering calculations performed using transmittance data.

Figure 6-2 is a sketch of both an Astroquartz (typical) and a hyperpure densified preform and identifies the location of the specimens removed and used to make the various optical property measurements. Use of the sketch should eliminate confusion in terminology. Any subsequent reference to test specimens will be by the alpha designation given to the specimen surface for which the optical measurement is made; i.e., a Y direction transmittance means the transmission test was performed on the specimen surface that is perpendicular to the Y direction fibers. The sketch also shows the location of a Y direction sample removed from the hyperpure preform. This sample was not originally laid out (Figure 3-16), but was cored out after the specimens identified in Figure 3-16 were obtained and when it became desirable to make a correlation with Y direction samples from the Astroquartz preforms.

It has been demonstrated in Reference 2 that higher purity silica raw materials can increase the overall reflectance of slip cast fused silica, especially in the ultra violet range. Since radiation from the gas cap during a Jupiter entry is predominantly at the shorter wavelengths, the importance of purity material on optical properties becomes obvious. For this reason woven hyperpure fibers at 10 ppm total metallic ion impurities were compared to Astroquartz (500 ppm total metallic ion impurities). This comparison can play an important part in the final selection of a highly efficient reflective heat shield material.

PREFORM MATERIAL	Y-YARN SPACING	SPECIMEN CONDITION Cm	SPECIMEN THICKNESS Cm	MEASUREMENT SURFACE	DATA LOCATION	
					REFLECTANCE (NUMBERS REFER TO FIGURES IN SECTION 6.)	SCATTERING AND ABSORPTION (NUMBERS REFER TO FIGURES IN SECTION 6.)
ASTROQUARTZ	.15	WOVEN AND CLEANED	5.0	Y	6-3	-
ASTROQUARTZ	.15	DENSIFIED	5.0	Y	6-3	-
ASTROQUARTZ	.15	MACHINED	.50	Y	NOT REPORTED	6-13
ASTROQUARTZ	.15	MACHINED	.50	Z	6-7	6-14
ASTROQUARTZ	.15	MACHINED	.25	Z	NOT REPORTED	6-14
ASTROQUARTZ	.23	WOVEN AND CLEANED	5.0	Y	6-4	-
ASTROQUARTZ	.23	DENSIFIED	5.0	Y	6-4	-
ASTROQUARTZ	.23	MACHINED	.50	Y	6-10	6-15
ASTROQUARTZ	.23	MACHINED	.50	Z	6-7, 6-10, 6-11	6-16
ASTROQUARTZ	.23	MACHINED	.25	Z	6-11	6-16
ASTROQUARTZ	.32	WOVEN AND CLEANED	5.0	Y	6-5	-
ASTROQUARTZ	.32	DENSIFIED	5.0	Y	6-5	-
ASTROQUARTZ	.32	MACHINED	.50	Y	NOT REPORTED	6-17
ASTROQUARTZ	.32	MACHINED	.50	Z	6-7	6-18
HYPERPURE	.23	WOVEN AND CLEANED	20.0	Y	6-6	-
HYPERPURE	.23	WOVEN AND CLEANED	5.0	Z	NOT REPORTED	-
HYPERPURE	.23	DENSIFIED	20.0	Y	6-6	-
HYPERPURE	.23	DENSIFIED	.50	Z	NOT REPORTED	-
HYPERPURE	.23	MACHINED	.50	Y	6-9	6-19
HYPERPURE	.23	MACHINED	.50	Z	5-7, 6-9	6-20

FIGURE 6-1 OPTICAL PROPERTY TEST MATRIX

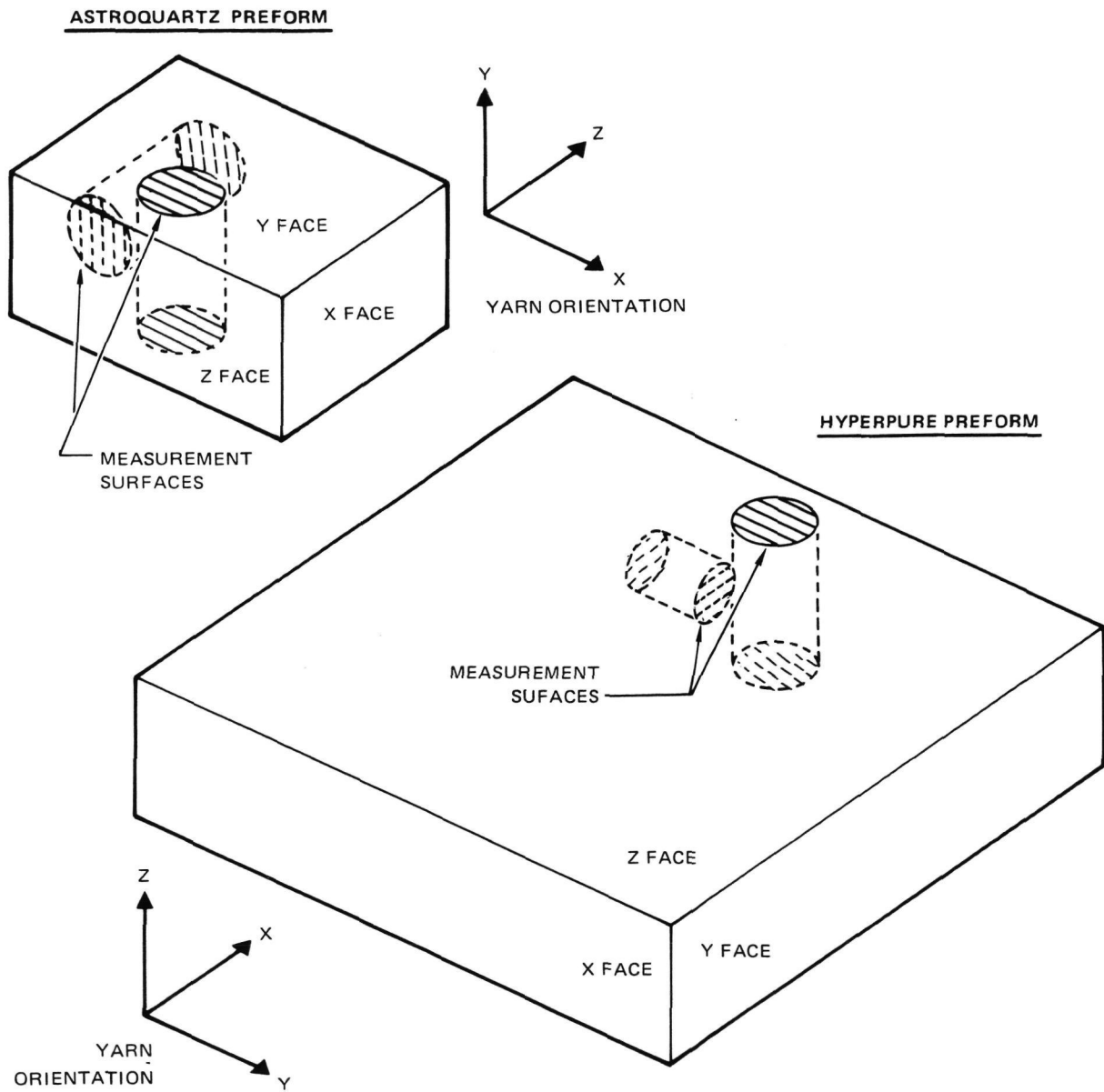


FIGURE 6-2 OPTICAL PROPERTY SPECIMEN ORIENTATION AND DESIGNATION

Spectral reflectance data was obtained on all preforms before and after densification. Individual specimens were taken from the densified preforms and used to measure transmittance in two directions (thickness direction and perpendicular to the thickness). The specimens were machined to thicknesses of 0.25 cm to 0.5 cm (0.1 in. to 0.2 in.).

6.2.1

"As Woven" Reflectance

Reflectance measurements taken of "as cleaned" surfaces of preforms indicates the influence of fiber spacings and purity. Results are shown in Figure 6-3 for measurements taken on the Y surface (maximum light piping direction). Measurements in the Z direction were not made on the "as received" Astroquartz preforms because of the mistake in the weave orientation. For the sake of comparison, the "as cleaned" hyperpure preform was analyzed in the Y direction as well.

In the longer wavelengths (0.7 to 2.4 μm), the Astroquartz preform with the smallest weave spacing has the highest reflectance. As expected, the order of reflectance goes from the 0.15 cm (0.060 in.) preform (smallest spacing), to the 0.23 cm (0.090 in.) preform, and finally to the 0.32 cm (0.125 in.) preform. The total difference between the three is not more than a few percent. At the shorter wavelengths (0.22 to 0.7 μm), the order is reversed, as shown in Figure 6-3. The larger difference in the U.V. region represents more absorption due to light piping, where the higher the fiber concentration at the surface, the greater the absorption. The 0.15 cm (0.060 in.) preform had the greatest fiber concentration in the Y direction, followed by the 0.23 cm (0.090 in.) preform and then the 0.32 cm (0.125 in.) preform.

The hyperpure silica preform had an overall higher reflectance (at all wavelengths) than any of the Astroquartz preforms, which is directly attributable to the higher purity of the hyperpure fibers (10 ppm impurities versus 500 ppm for Astroquartz), as reported in References 2 and 4.

6.2.2

"As Densified" Reflectance

Following densification, reflectance measurements were made of the unmachined preform surfaces to determine any changes made over the "as woven" condition. The densification with hyperpure grains (1 ppm impurities) improved the reflectance of all preforms considerably, as the data plotted in Figures 6-4 through 6-7 indicates. All measurements on unmachined specimens were made in the Y direction for reasons explained in paragraph 6.2.1. The largest increase in reflectance occurred in the shorter wavelengths for all preforms. The difference between the curves decreases with increasing wavelength, until the curves meet or cross at 2.2 microns.

6.2.3

"As Machined" Reflectance

Measurements were made in the Z direction on each type of material, with a specimen thickness of 0.5 cm (0.2 in.). Figure 6-8 is a plot of the measurements made.

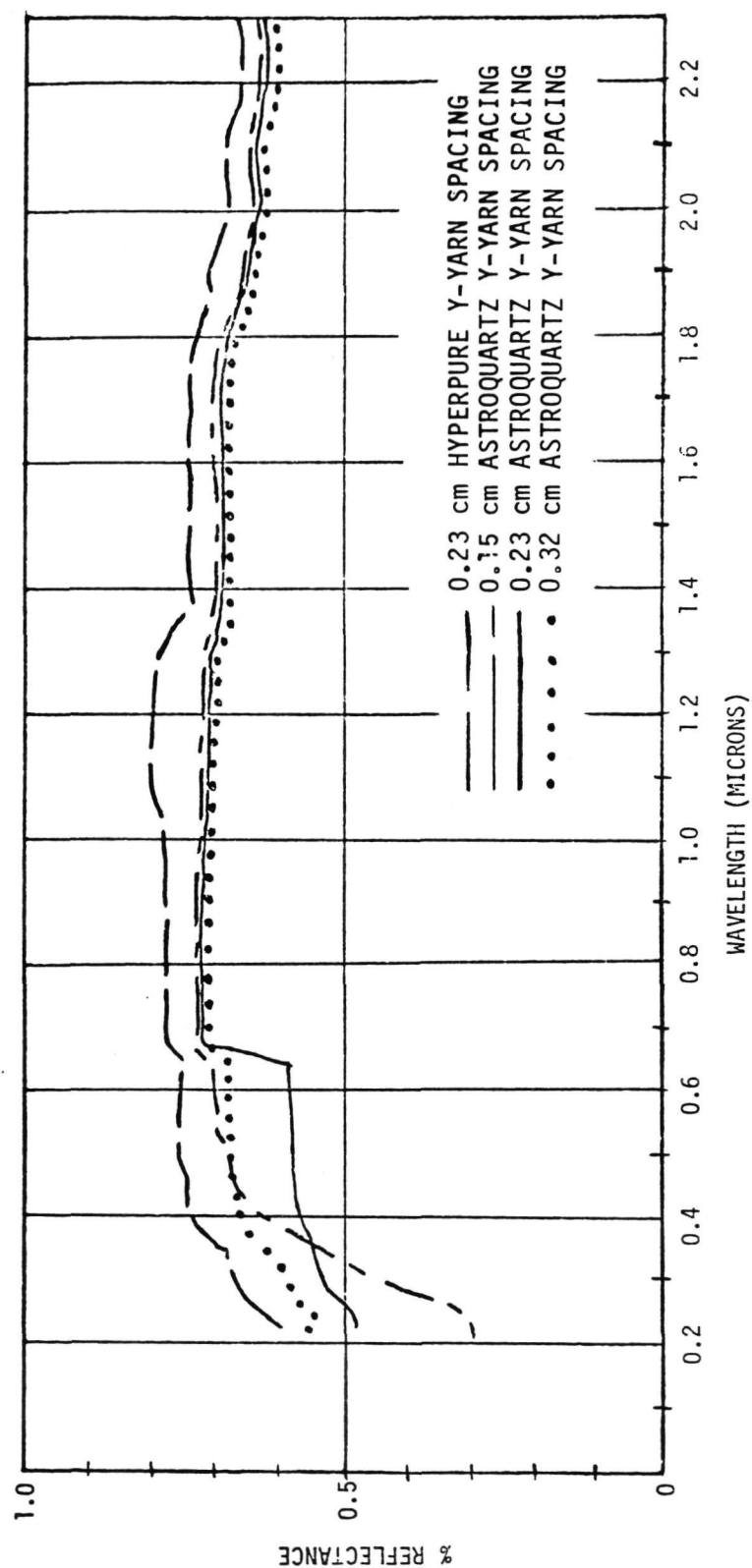


FIGURE 6-3 ROOM TEMPERATURE REFLECTANCE OF 3D WOVEN ASTROQUARTZ AND HYPERPURE PREFORMS IN THE "AS CLEANED" CONDITION AND MEASURED ON THE Y SURFACE

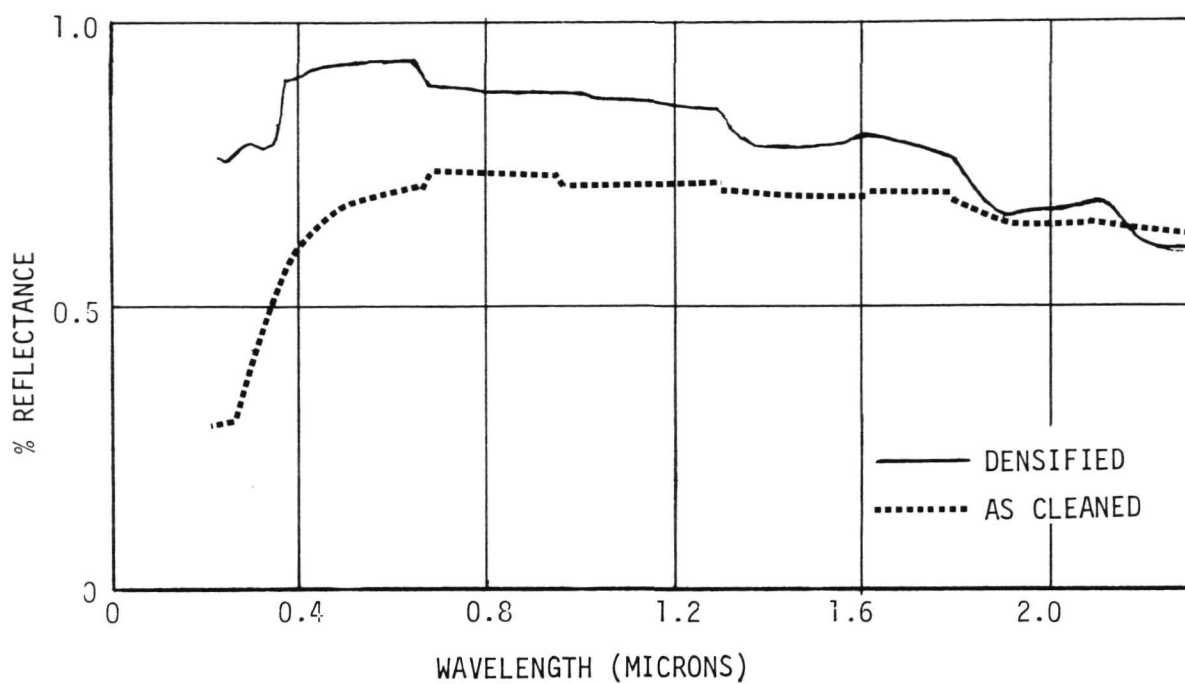


FIGURE 6-4 COMPARISON OF "AS CLEANED" AND "DENSIFIED" REFLECTANCE FOR 0.15 cm ASTROQUARTZ PREFORM MEASURED ON THE Y SURFACE

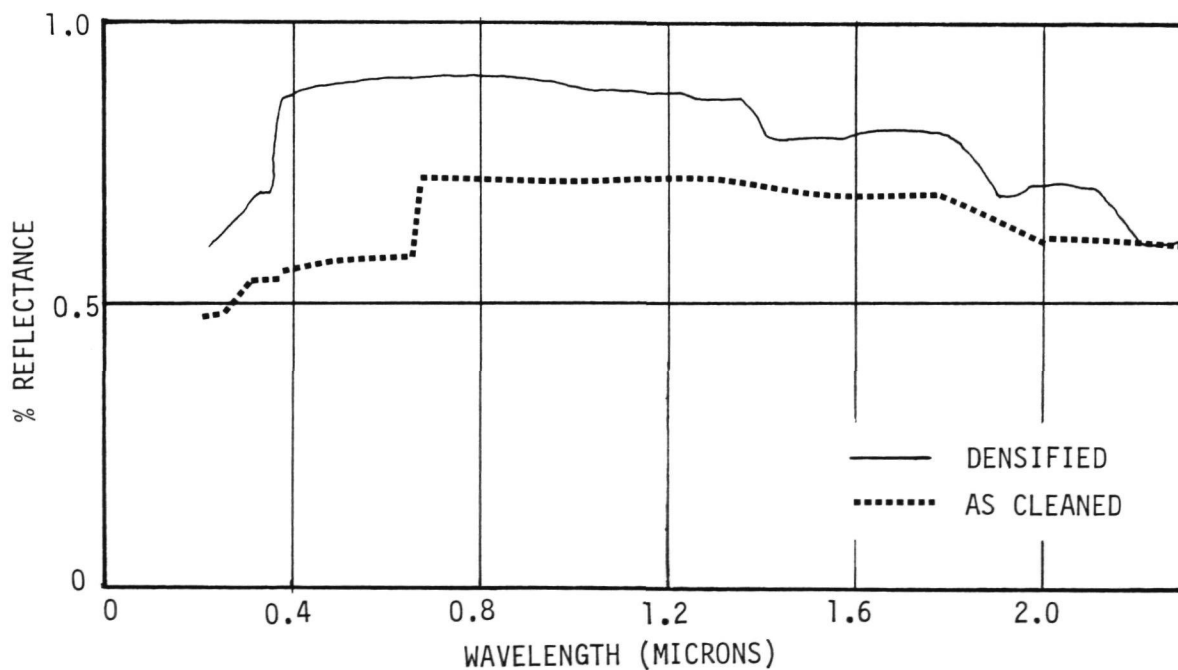


FIGURE 6-5 COMPARISON OF "AS CLEANED" AND "DENSIFIED" REFLECTANCE FOR 0.23 cm ASTROQUARTZ PREFORM MEASURED ON THE Y SURFACE

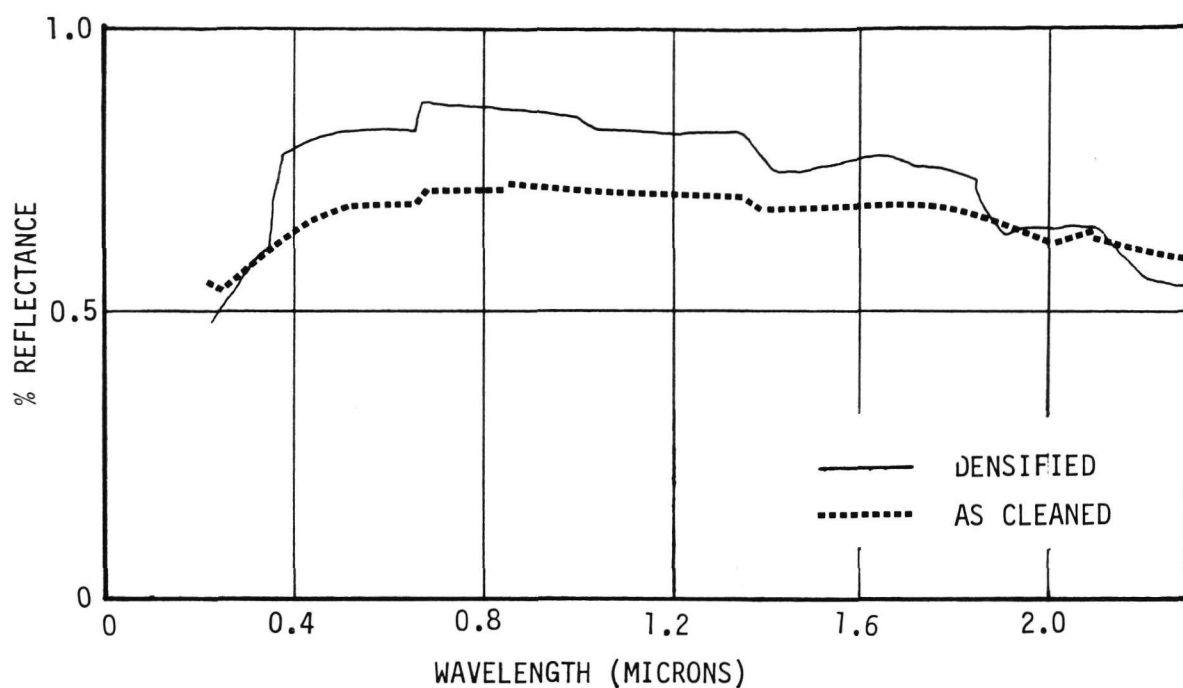


FIGURE 6-6 COMPARISON OF "AS CLEANED" AND "DENSIFIED" REFLECTANCE FOR 0.32 cm ASTROQUARTZ PREFORM MEASURED ON THE Y SURFACE

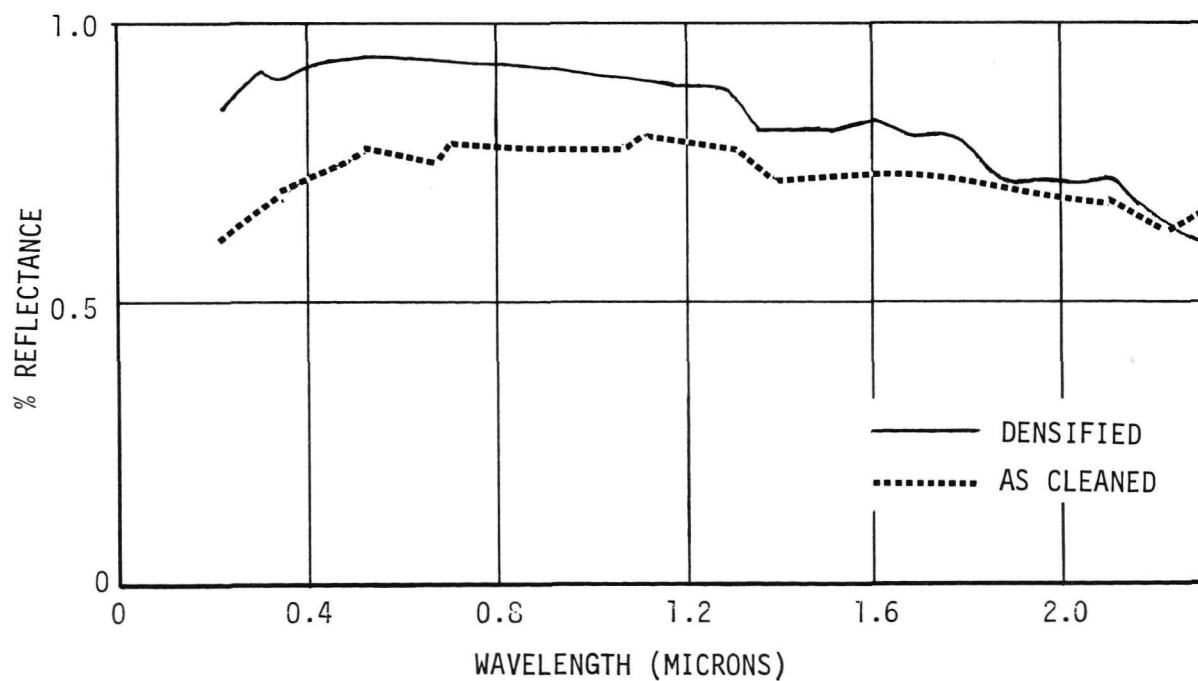


FIGURE 6-7 COMPARISON OF "AS CLEANED" AND "DENSIFIED" REFLECTANCE FOR 0.23 cm HYPERPURE PREFORM MEASURED ON THE Y SURFACE

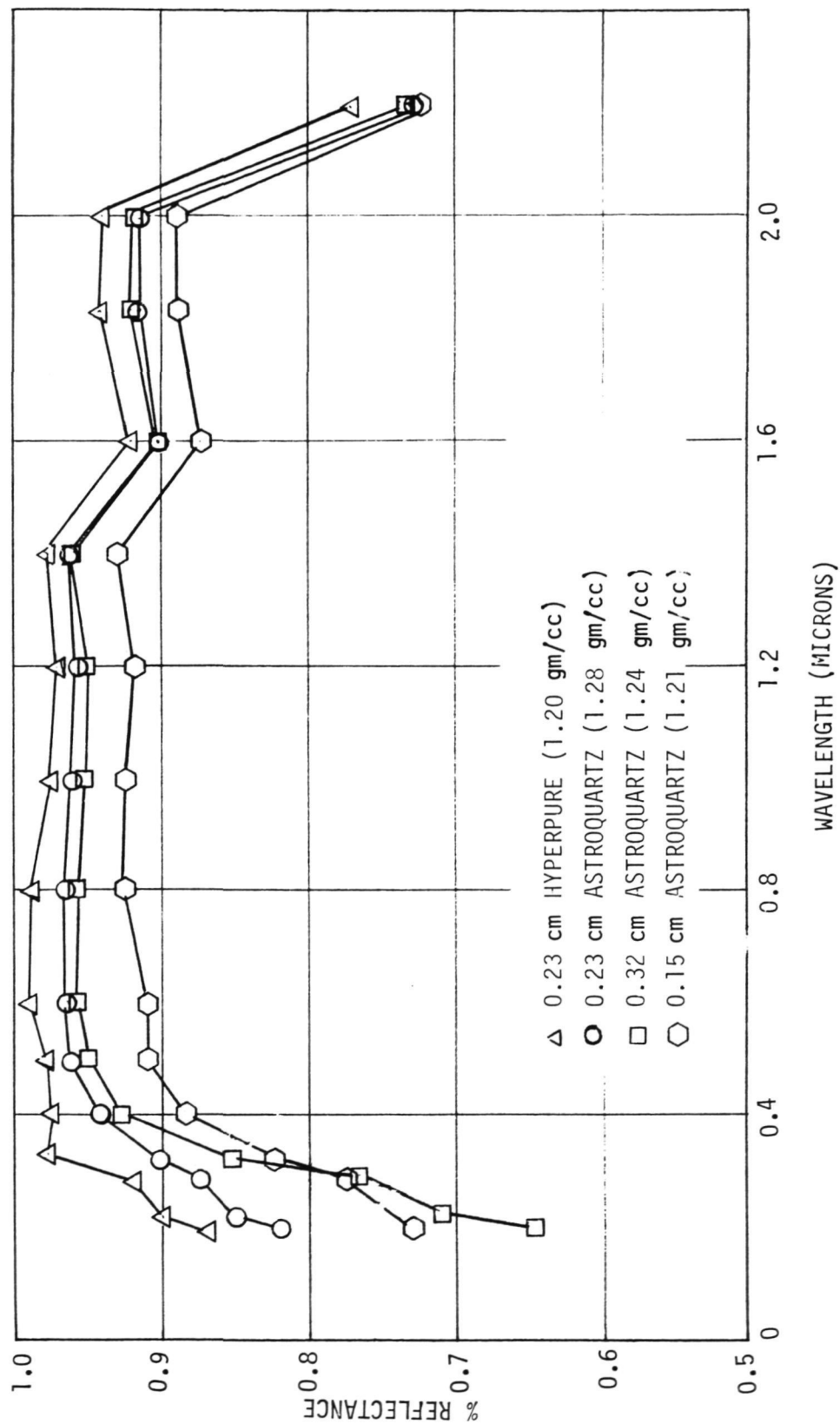


FIGURE 6-8 Z DIRECTION REFLECTANCE OF 0.5 cm THICK SILICA (3D WOVEN-DENSIFIED)

As described in subsection 3.7, 2.54 cm (1.0 in.) diameter specimens were drilled from the center of the densified Astroquartz and hyperpure silica preforms. Specimens were then machined into the appropriate thicknesses shown in Figure 6-1 for reflectance measurements. Prior to making the reflectance measurements, all specimens were heat treated at 540°C (1004°F) to remove hydroxyl ions.

Reflectance of the densified and machined Astroquartz preforms appears to be more dependent on density than fiber spacing. The high density Astroquartz 0.23 cm (0.090 in.) Y-yarn spacing specimen had the highest overall reflectance of the three Astroquartz materials. The Astroquartz 0.15 cm (0.060 in.) Y-yarn spacing specimen had the lowest reflectance and the lowest density of the Astroquartz materials. However, the hyperpure specimen, which had a density lower than any of the Astroquartz specimens, exhibited the highest overall reflectance of all materials tested. Purity level of the hyperpure preform is the major reason for its higher reflectance. It can be expected that at higher densities the hyperpure and the Astroquartz materials will have even higher reflectances. The increased number of small particles per unit of volume will increase the scattering sights, thus forming an improved diffuse reflector.

Comparing reflectance of fiber-reinforced hyperpure slip-cast fused silica, developed under previous studies (Reference 3), to the hyperpure and Astroquartz woven silica composites shows that the hyperpure slip-cast fused silica reflectance is higher at all wavelengths measured. The differences shown in Figure 6-9 between the slip cast fused silica and the hyperpure silica woven composite are mainly due to density differences (1.55 gm/cc [96.7 pcf] versus 1.3 gm/cc [81.2 pcf] for slip cast and hyperpure, respectively.) Reflectance differences between hyperpure and Astroquartz are mainly due to increased absorption in the Astroquartz, which had a higher impurity content.

Light piping effects caused by transmission through fiber ends open at the surface can be seen in Figures 6-10 and 6-11 for Astroquartz and hyperpure 3D silica woven composites, respectively. These measurements were taken from specimens machined to a 0.5 cm (0.2 in.) thickness. It is also apparent from these figures, when compared to Figures 6-6 and 6-7, that machined surfaces have a greater reflectance than unmachined surfaces. This is not unexpected, since rough surfaces tend to absorb more incident radiant energy.

Figure 6-12 shows reflectance data for Astroquartz (0.32 cm Y-yarn spacing) in the Z direction at two thicknesses, 0.5 cm (0.2 in.) and 0.25 cm (0.098 in.). The accuracy of reflectance measurements on diffuse surfaces is typically $\Delta R/R = \pm 0.02$ for the type of integrating sphere (a comparison sphere) employed, due to the inaccuracy in the reflectance of the standard material (barium sulfate). The observable difference shown is within the error of measurement and therefore indicates a single curve.

6.2.4

"As Machined" Transmittance

Transmittance measurements were made for all specimens identified in Figure 6-1 for which scattering and absorption coefficients were needed.

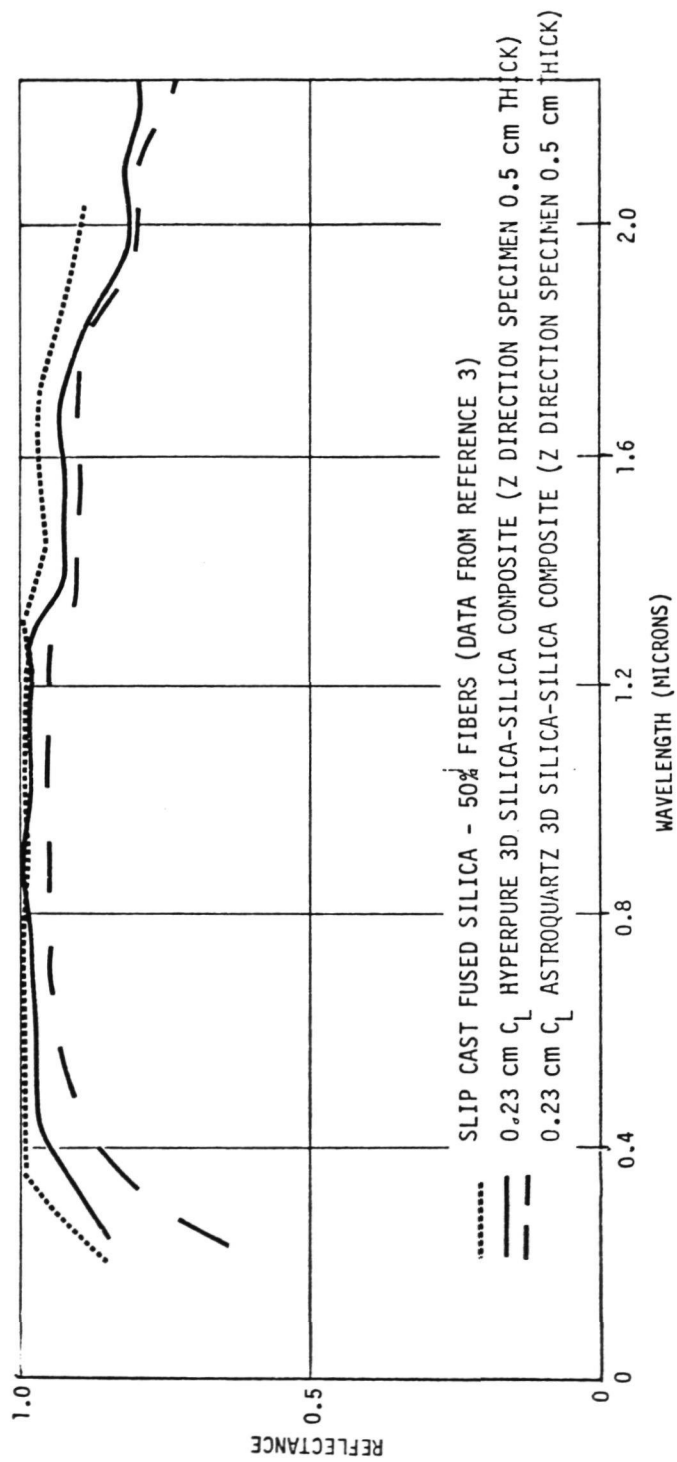


FIGURE 6-9 EFFECTS OF PURITY ON REFLECTANCE

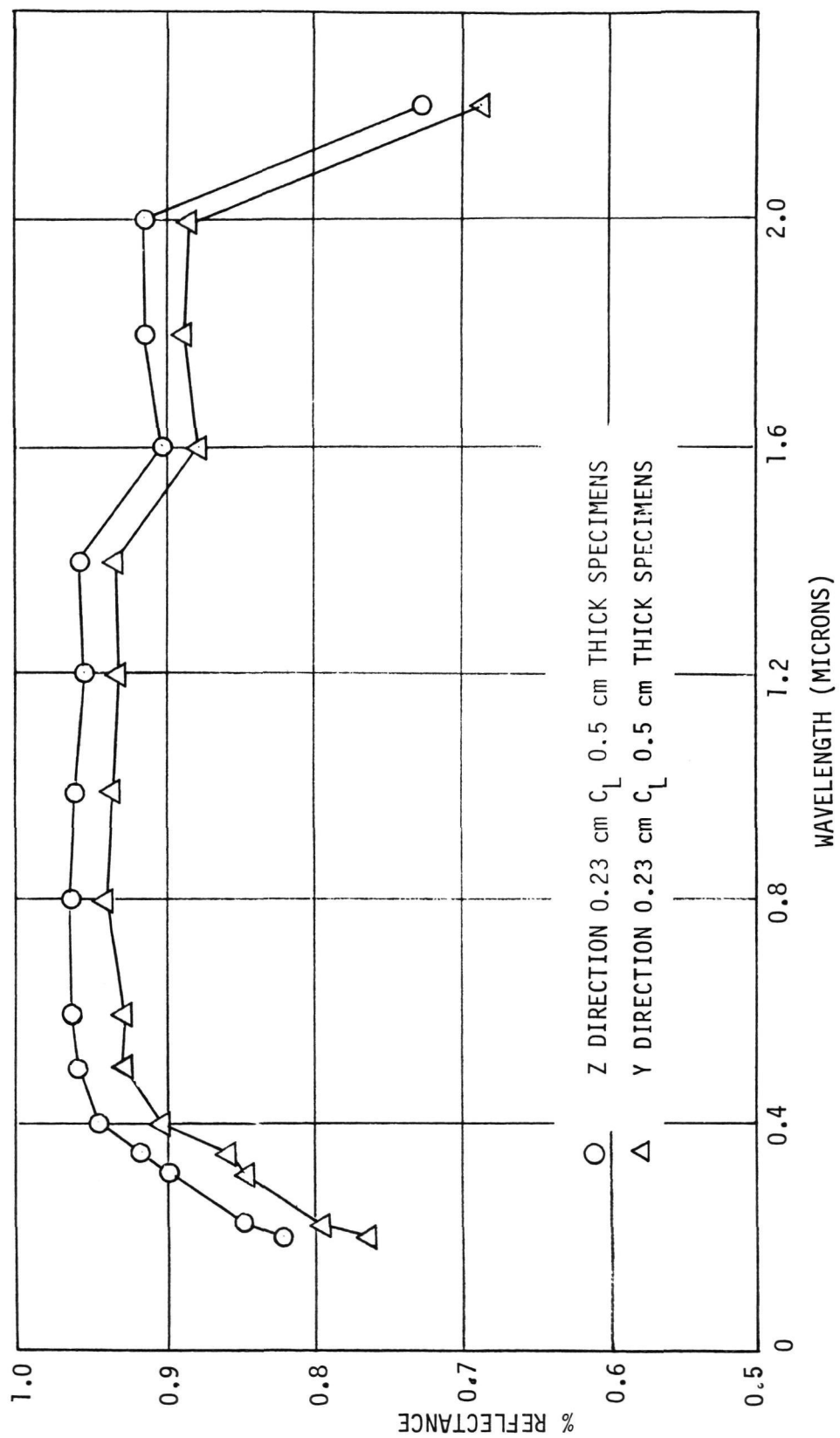


FIGURE 6-10 LIGHT PIPING IN ASTROQUARTZ 3D SILICA WOVEN COMPOSITE

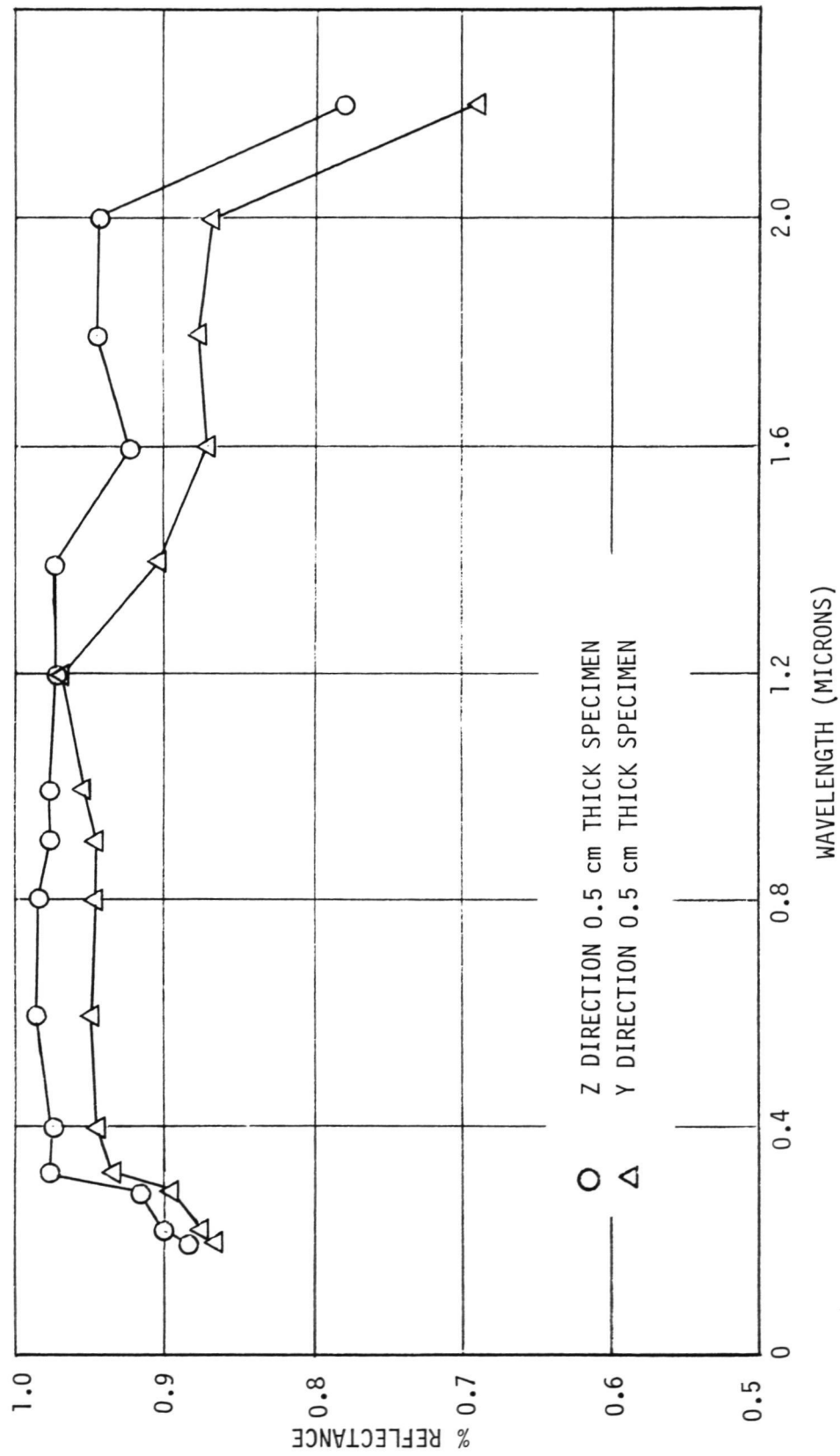


FIGURE 6-11 LIGHT PIPING IN HYPERPURE 3D SILICA WOVEN COMPOSITE

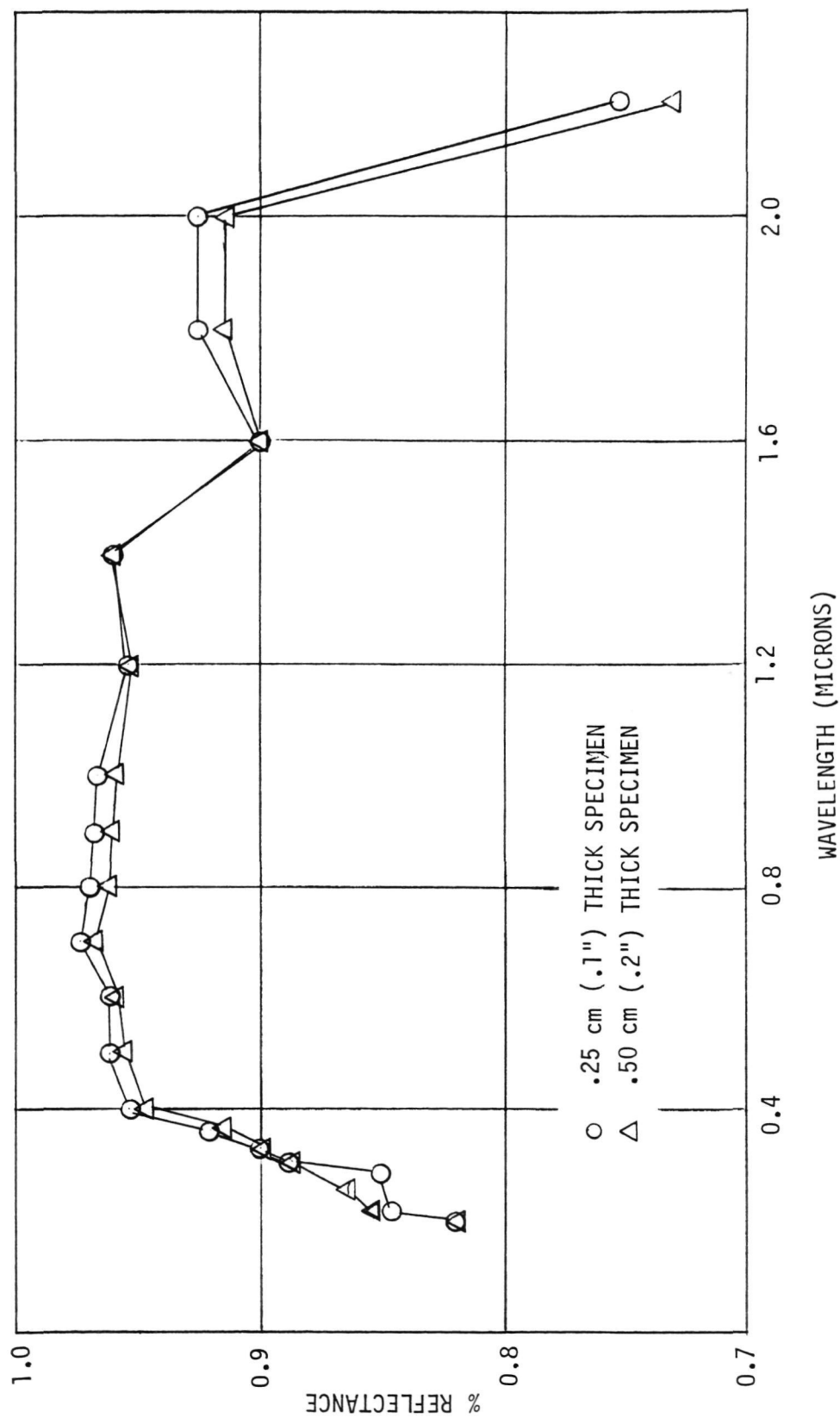


FIGURE 6-12 EFFECT OF THICKNESS ON REFLECTANCE OF 0.23 cm Y-YARN SPACING ASTROQUARTZ (Z DIRECTION)

The equipment and test procedure are detailed in Reference 4. The raw transmittance data was then used to calculate the K-S coefficients discussed in the following section.

6.2.5

Scattering and Absorption Coefficients

For most machined specimens, both reflectance and transmittance were measured for several thicknesses and in two of the three orthogonal directions. This data is basic information used in conduction-radiation heat transfer models developed for analyzing reflective silica heat shields thermal performance. To correlate experimental test data, scattering and absorption coefficients have been calculated as described below. Coefficients have been derived for the Y and Z directions for both Astroquartz and hyperpure 3D woven silica materials to check for anisotropy in the transport of radiant heat through these materials. Figures 6-13 through 6-20 contain plots of calculated values for the specimen conditions identified in Figure 6-1.

The scattering (S) and absorption (K) coefficients were calculated from measurements of reflectance (R) and transmittance (T) using the traditional Kubelka-Munk (K-M) scattering theory as modified by Reichman in Reference 11. The Reichman Theory provides relations between R and T and two parameters, γ and ω ,

$$R = \left(\frac{\omega}{2}\right) \frac{3R_{\infty} - (1-R_{\infty}^2)e^{-(1+\alpha)\tau} - 1-R_{\infty}(3-R_{\infty})e^{-2\alpha\tau}}{(4\omega-3)(1-R_{\infty}^2e^{-2\alpha\tau})} \quad \text{Equation 1}$$

$$T = \left(\frac{\omega}{2}\right) \frac{3(1-R_{\infty}^2)e^{-\alpha\tau} - (3-R_{\infty})e^{-\tau} + R_{\infty}(3R_{\infty}-1)e^{-(\tau+2\alpha\tau)}}{(4\omega-3)(1-R_{\infty}^2e^{-2\alpha\tau})} + e^{-\tau} \quad \text{Equation 2}$$

$$\alpha = 2 \sqrt{1-\omega} \quad \text{Equation 3}$$

$$R_{\infty} = \frac{2}{\omega} - 1 - \frac{2}{\omega} \sqrt{1-\omega} \quad \text{Equation 4}$$

$$\tau = (k+\sigma)\delta \quad \text{Equation 5}$$

where:

δ = sample thickness (cm)
 κ = Reichman absorption coefficient (cm^{-1})
 σ = Reichman scattering coefficient (cm^{-1})
 R_{∞} = infinite thickness reflectance

$$\omega = \sigma / (\sigma + \kappa) \quad \text{Equation 6}$$

The Reichman coefficients are related to the usual K-M coefficients K and S:

$$K = 2\kappa \quad \text{Equation 7}$$

$$S = \sigma \quad (\text{for isotropic scattering}) \quad \text{Equation 8}$$

A pair of R and T measurements on a sample yields a corresponding pair (τ, ω) from which κ and σ (given δ) can be calculated.

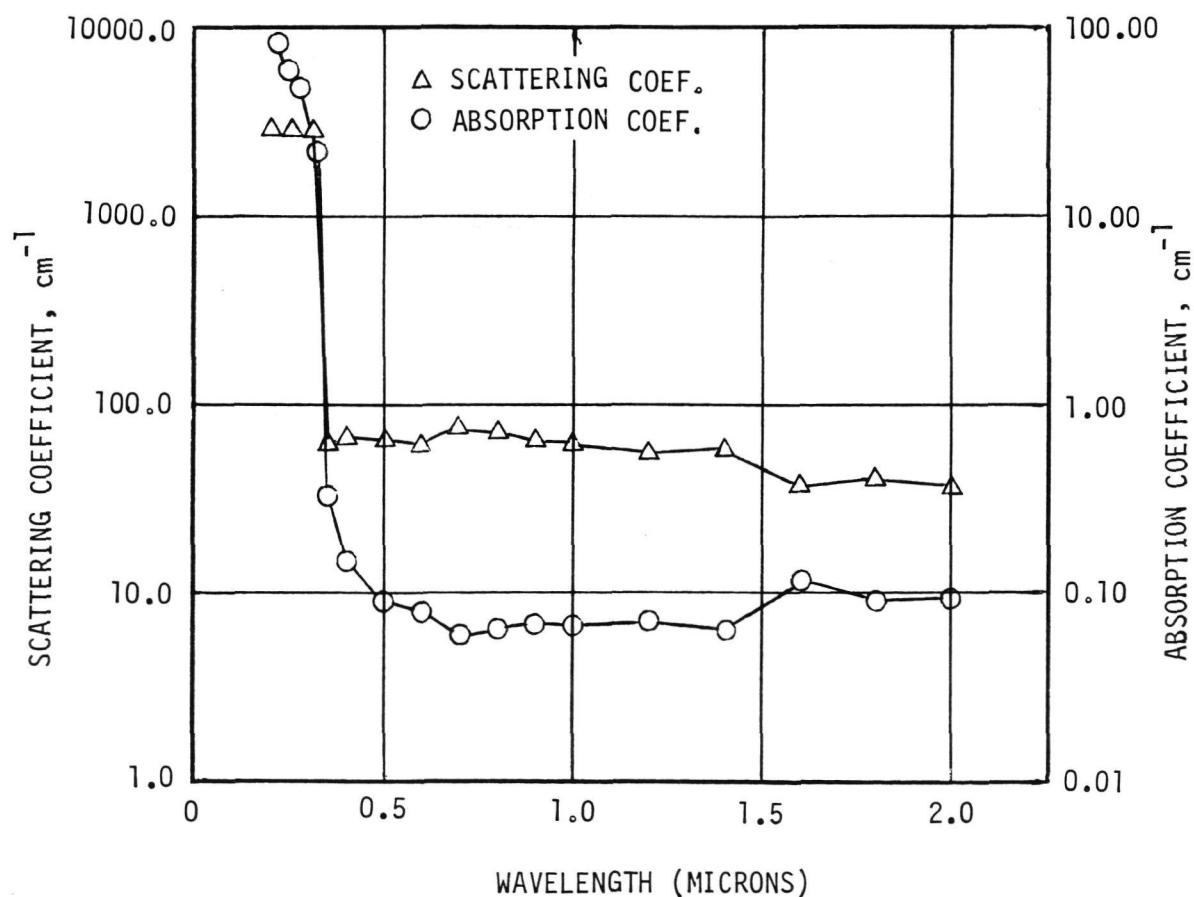
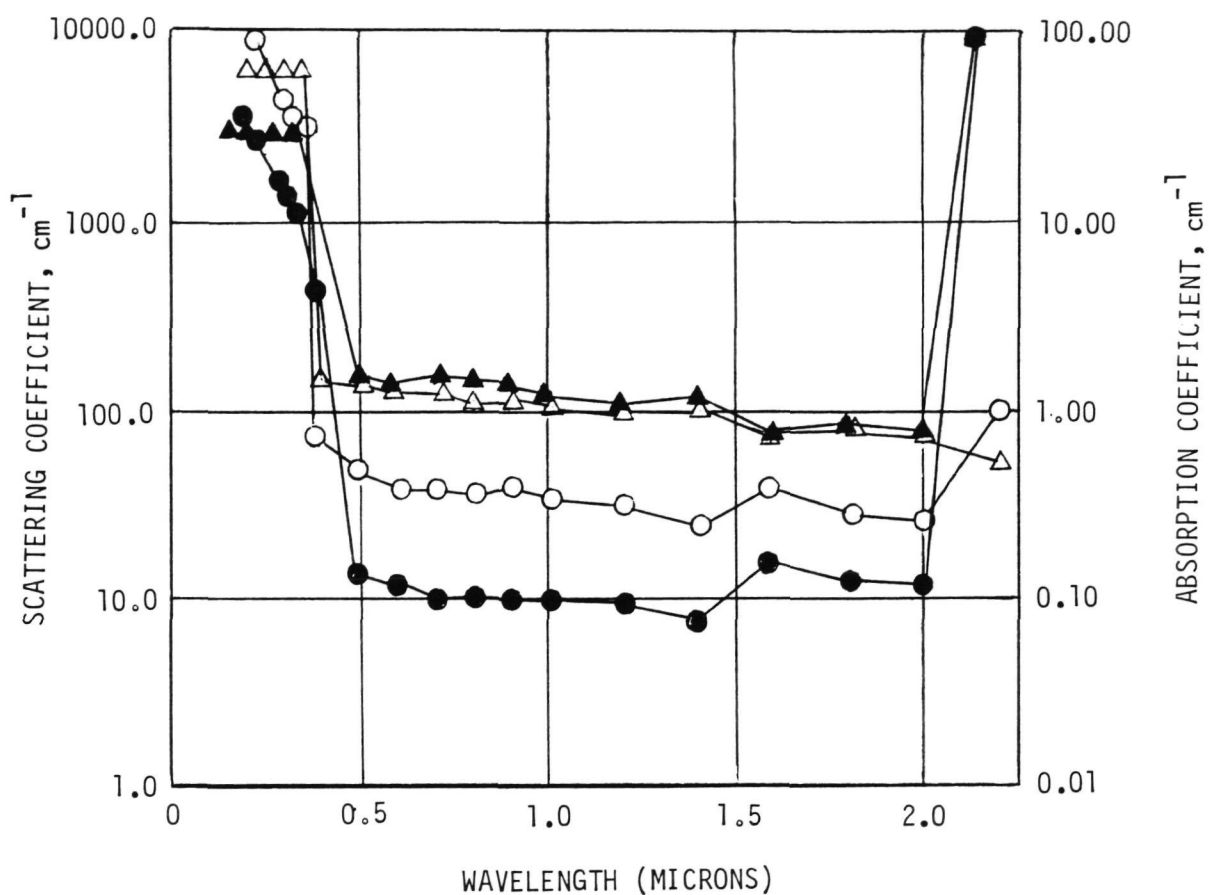


FIGURE 6-13 SCATTERING AND ABSORPTION COEFFICIENTS FOR 0.5 cm (0.20 in) THICK 0.15 cm Y YARN SPACING ASTROQUARTZ (Y DIRECTION)



- Δ SCATTERING COEF. (0.25 cm (0.10 in) THICK)
- \blacktriangle SCATTERING COEF. (0.50 cm (0.20 in) THICK)
- \circ ABSORPTION COEF. (0.25 cm (0.10 in) THICK)
- \bullet ABSORPTION COEF. (0.50 cm (0.20 in) THICK)

FIGURE 6-14 THICKNESS EFFECTS ON SCATTERING AND ABSORPTION COEFFICIENTS FOR 0.15 cm Y-YARN SPACING ASTROQUARTZ (Z DIRECTION)

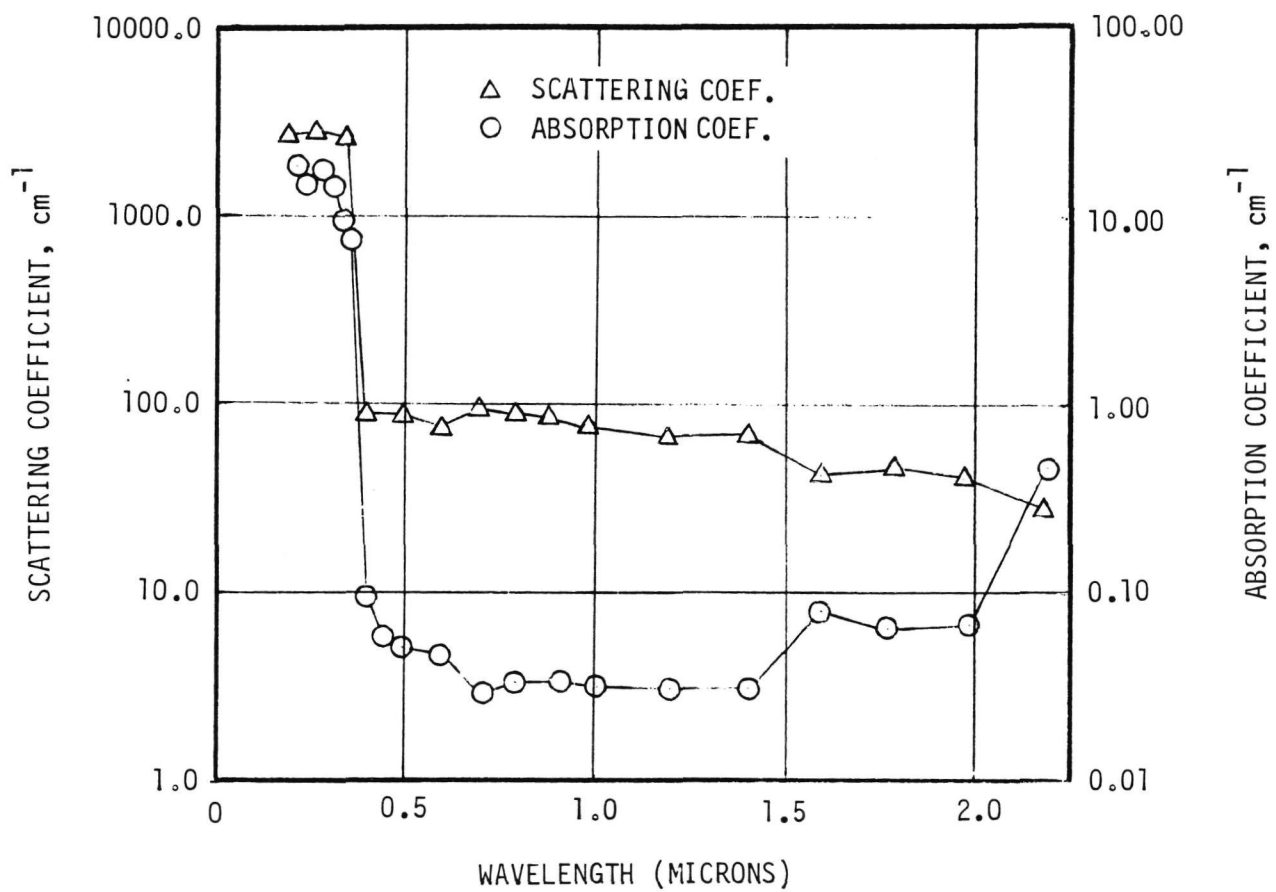
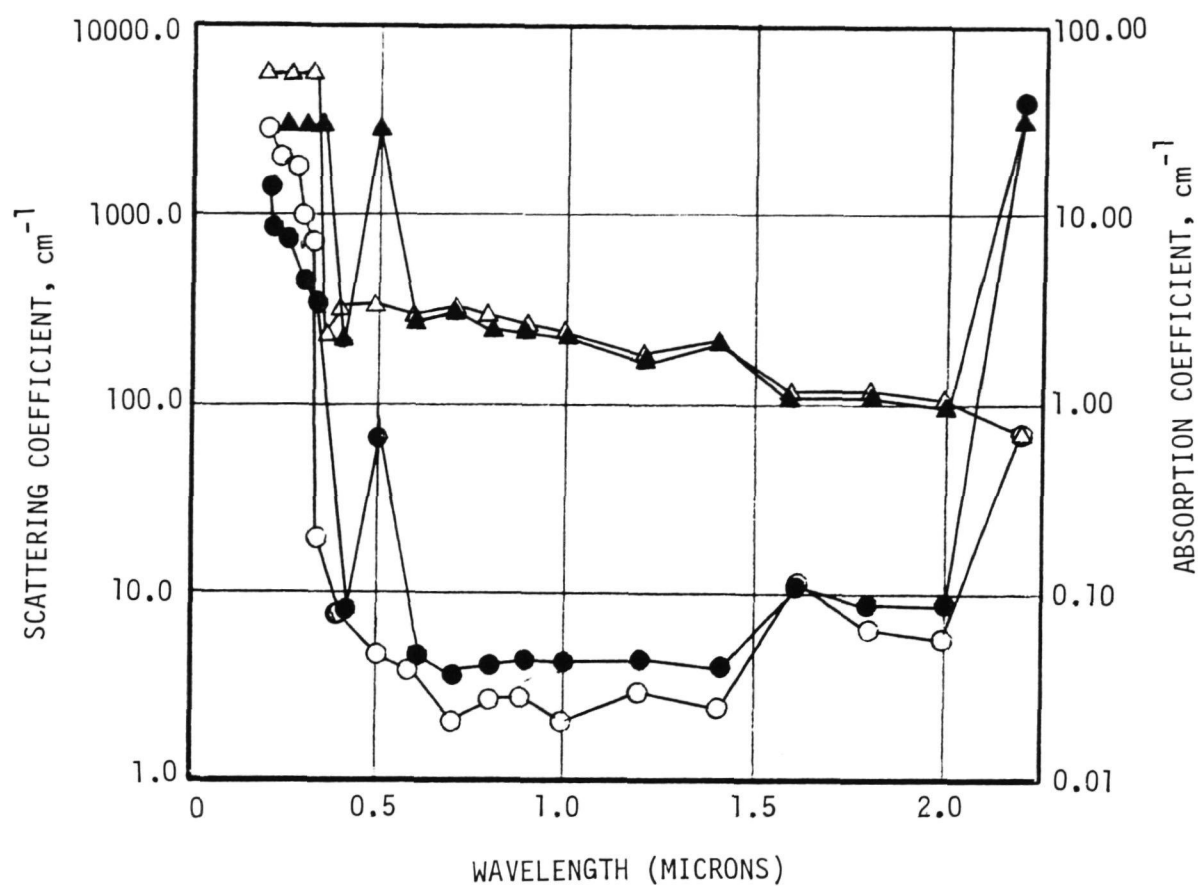


FIGURE 6-15 SCATTERING AND ABSORPTION COEFFICIENTS FOR 0.50 cm (0.20 in) THICK 0.23 cm Y-YARN SPACING ASTROQUARTZ (Y DIRECTION)



- Δ THICK SCATTERING COEF. (0.25 cm (0.10 in) THICK)
- \blacktriangle THICK SCATTERING COEF. (0.50 cm (0.20 in) THICK)
- \circ THICK ABSORPTION COEF. (0.25 cm (0.10 in) THICK)
- \bullet THICK ABSORPTION COEF. (0.50 cm (0.10 in) THICK)

FIGURE 6-16 THICKNESS EFFECTS ON SCATTERING AND ABSORPTION COEFFICIENTS FOR 0.23 cm Y-YARN SPACING ASTROQUARTZ (Z DIRECTION)

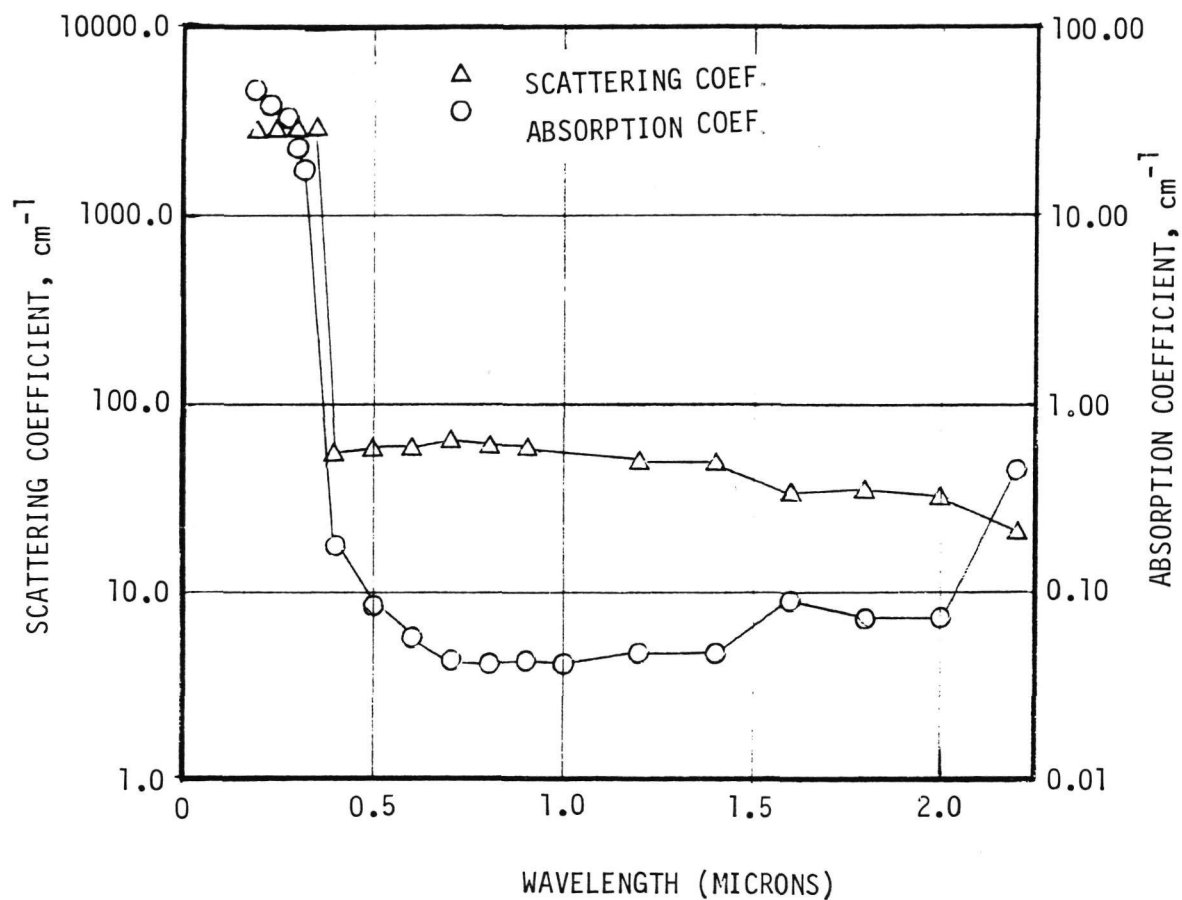


FIGURE 6-17 SCATTERING AND ABSORPTION COEFFICIENTS FOR 0.50 CM (0.20 in) THICK 0.32 cm Y-YARN SPACING ASTROQUARTZ (Y DIRECTION)

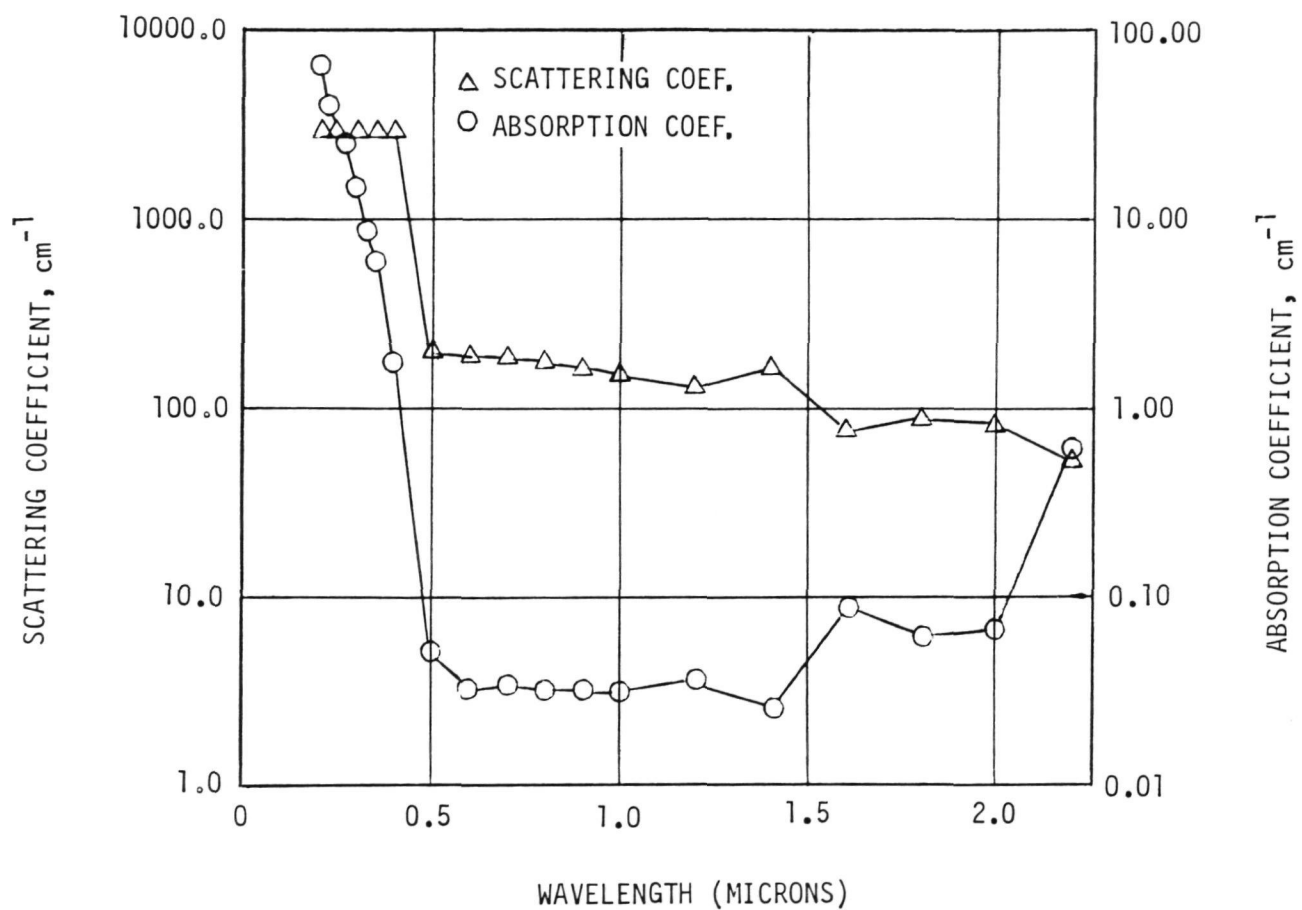


FIGURE 6-18 SCATTERING AND ABSORPTION COEFFICIENTS FOR 0.50 cm (0.20 in) THICK 0.32 cm Y-YARN SPACING ASTROQUARTZ (Z DIRECTION)

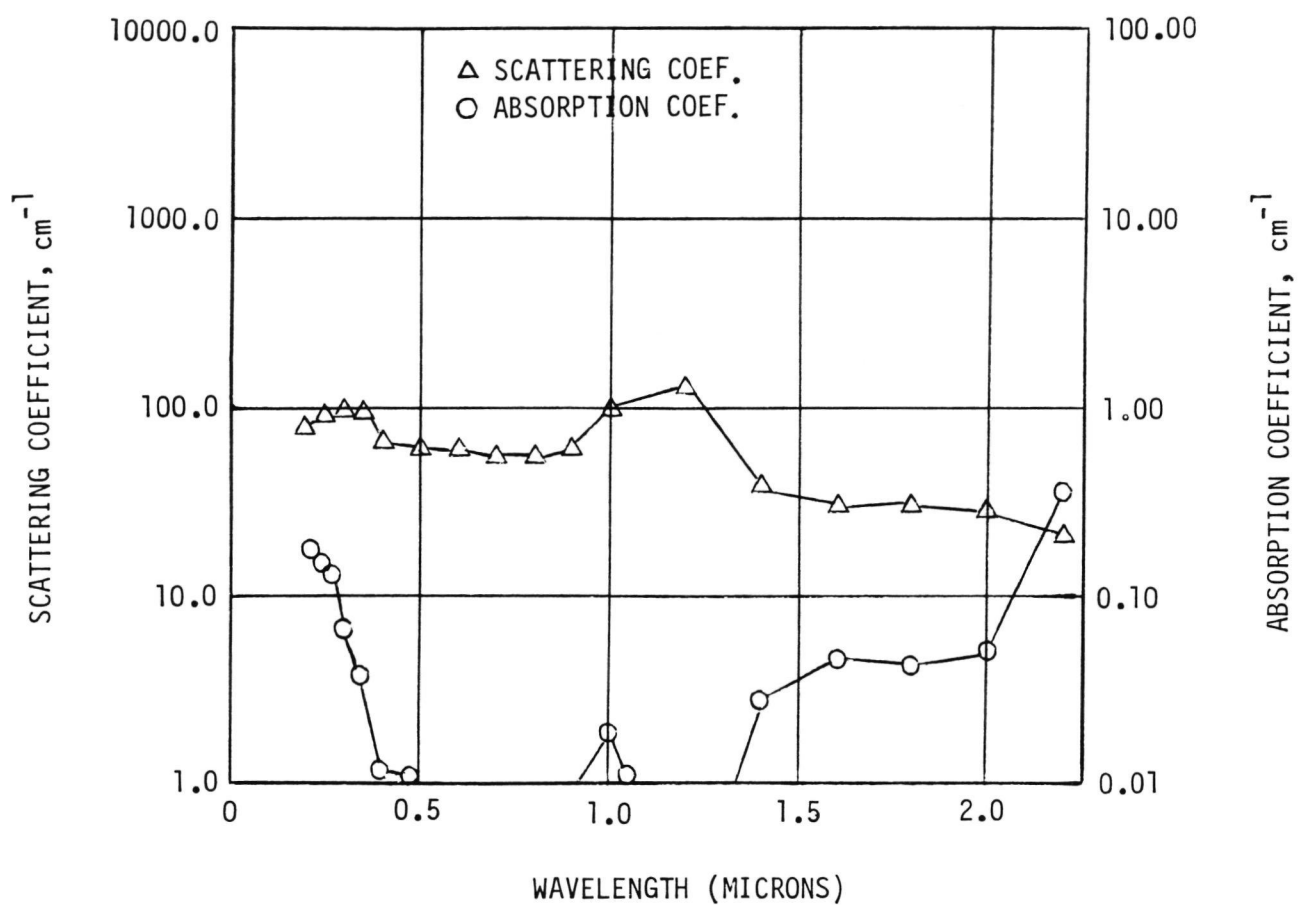


FIGURE 6-19 SCATTERING AND ABSORPTION COEFFICIENTS FOR 0.50 cm (0.20 in) THICK 0.23 cm Y-YARN SPACING HYPERPURE (Y DIRECTION)

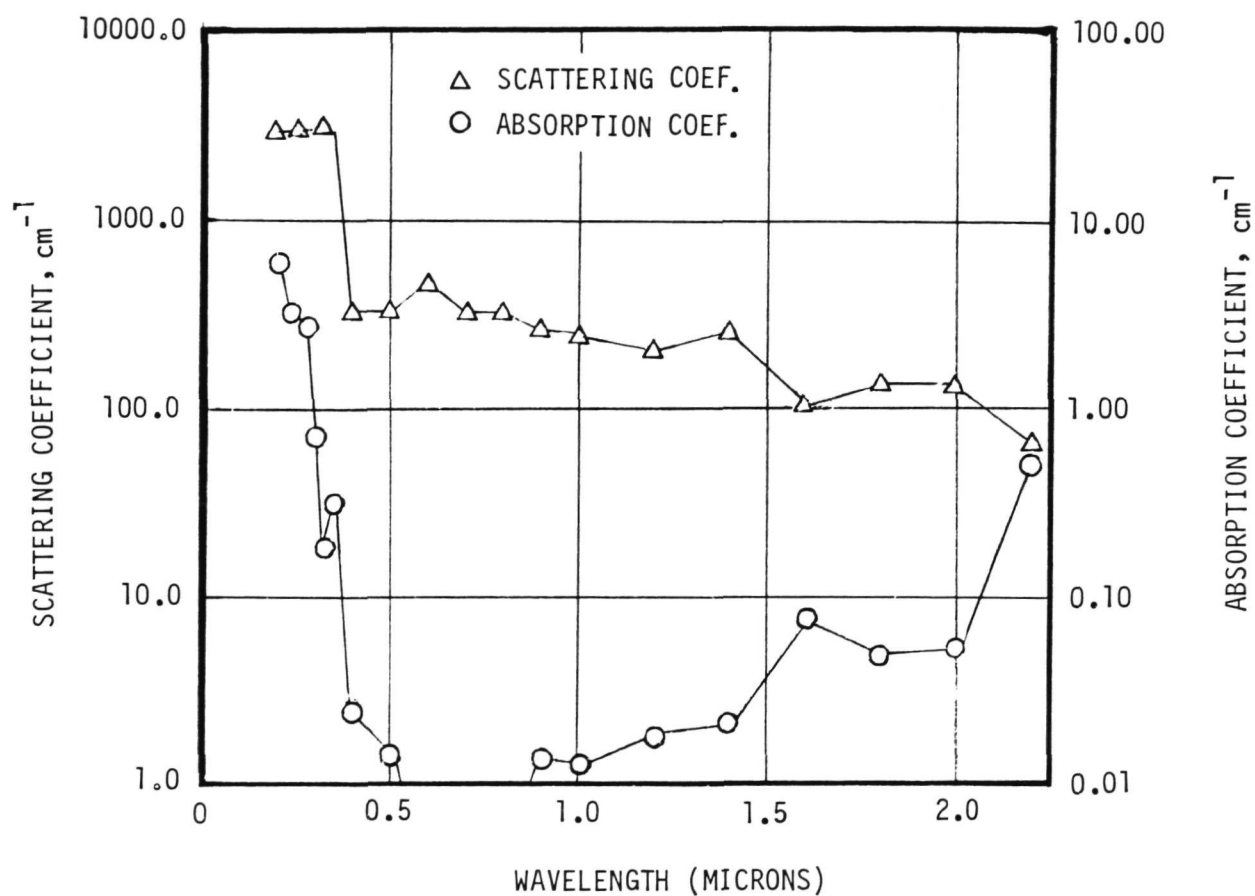


FIGURE 6-20 SCATTERING AND ABSORPTION COEFFICIENTS FOR 0.50 cm (0.20 in) THICK 0.23 cm Y-YARN SPACING HYPERPURE (Z DIRECTION)

7.0 MECHANICAL PROPERTY MEASUREMENTS

This section presents mechanical property test data obtained for 3D silica composite materials (Astroquartz and hyperpure silica preforms) impregnated with hyperpure silica grain. Previous mechanical property testing and analysis of aggregate-cast and fiber-reinforced hyperpure slip-cast fused silica indicated a low margin of safety when used for the forebody heat shield of a Jupiter Entry Probe (References 3 and 4). The slip-cast fused silica materials were marginal in strength and toughness necessary to meet the design goals for a Jovian type entry. It was expected that a densified 3D woven silica composite would provide a significant increase in strength and toughness to meet the heat shield structural design requirement and still maintain a high reflectance.

MDAC-St. Louis fabricated the mechanical property test specimens and IITRI performed the majority of the mechanical property tests under subcontract to MDAC-St. Louis.

7.1 TEST PLAN

The test plan for this study, shown in Figure 7-1, includes mechanical property testing at both room and elevated temperatures.

The number of specimens tested for a given test condition was limited to a maximum of three; therefore, the test data is useful only to indicate trends and is not sufficient to establish minimum design properties for structural analysis and design of a flightworthy 3D silica heat shield.

7.1.1 Test Specimen Definition

A total of 38 specimens were tested. Six of these specimens were utilized early in the program to establish an optimum firing temperature for the remainder of the specimens. Six specimens from each of the three densified Astroquartz preforms and from the densified hyperpure preform were tested in short beam flexure at 24°C (75°F) and 1066°C (1950°F) to obtain flexure strength and elastic modulus data. To evaluate effects of specimen geometry, two eight-inch-long beam flexure specimens were fabricated from the 0.23 cm (.090 in.) Y-yarn spacing hyperpure preform. Also, six specimens (three hyperpure and three Astroquartz) were tested for interlaminar shear capability by using the short beam shear test set-up shown in Figure 7-2.

The original test plan had established a number of tensile specimens having a "dog-bone" configuration. Unfortunately, it soon became apparent that machining the specimens to this configuration was difficult. Consequently, it was decided to machine the specimens to a constant cylindrical configuration and bond them to metallic gripping blocks. In preliminary tests, using excess hyperpure material, attempts to bond the specimens to the gripping blocks with an epoxy adhesive failed. Failure occurred at the bondline between the adhesive and the simulated test specimens. Changing

SPECIMEN CODE	MATERIAL DESIGNATION	SIZE OF MACHINED SPECIMENS	TEST SPECIMEN TYPE	NUMBER OF TEST SPECIMENS	SPECIMEN CONDITION Δ	TEST TEMPERATURE		SPECIMEN IDENTIFICATION	PROPERTIES MEASURED	COMMENTS
						$^{\circ}\text{C}$	$^{\circ}\text{F}$			
A	ASTROQUARTZ 0.15 CM (.060 IN.) Y-YARN SPACING	1.27 x 1.27 x 10.2 CM (0.50 x 0.50 x 4.0 IN.)	SHORT BEAM FLEXURE	1	UNFIRED	24	75	AF4	σ_f, E_s	TESTING OF THE UNFIRED SPECIMEN INDICATED A NEED FOR THE SUBSEQUENT FIRING
				2	FIRED	24	75	AF5, AF6		
				3	FIRED	1066	1950	AF1, AF2, AF3		
B	ASTROQUARTZ 0.23 CM (.090 IN.) Y-YARN SPACING	1.27 x 1.27 x 10.2 CM (0.50 x 0.50 x 4.0 IN.) 1.27 x 1.27 x 3.81 CM (0.50 x 0.50 x 1.5 IN.) (ITTRI'S TEST GEOMETRY)	SHORT BEAM FLEXURE	3	FIRED	24	75	BF1, BF4, BF5	σ_f, E_s	
				3	FIRED	1066	1950	BF2, BF3, BF6		
			SHORT BEAM SHEAR	3	FIRED	24	75	BF1, BF4, BF5	σ_s	SPECIMENS OBTAINED FROM BROKEN END OF ROOM TEMP. SHORT BEAM FLEXURE
C	ASTROQUARTZ 0.32 CM (.120 IN.) Y-YARN SPACING	1.27 x 1.27 x 10.2 CM (0.50 x 0.50 x 4.0 IN.)	SHORT BEAM FLEXURE	1	UNFIRED	24	75	CF1	σ_f, E_s	
				2	FIRED	24	75	CF2, CF3		
				3	FIRED	1066	1950	CF4, CF5, CF6		
D	HYPERPURE 0.23 CM (.090 IN.) Y-YARN SPACING	1.27 x 1.27 x 10.2 CM (0.50 x 0.50 x 4.0 IN.) 1.27 x 1.27 x 20.3 CM (0.50 x 0.50 x 8.0 IN.) 1.27 x 1.27 x 3.8 CM (0.50 x 0.50 x 1.5 IN.) (ITTRI'S TEST GEOMETRY)	SHORT BEAM FLEXURE	3	FIRED	24	75	DF2, DF3, DF7	σ_f, E_s	
				3	FIRED	1066	1950	DF1, DF4, DF8		
			LONG BEAM FLEXURE	2	FIRED	24	75	DF5, DF6	σ_f, E_s	
		1.3 CM DIA. x 4.5 CM LONG (0.50 IN. DIA. x 1.77 IN. LONG) (MDAC'S TEST GEOMETRY)	SHORT BEAM SHEAR	3	FIRED	24	75	DF5, DF6, DF7	σ_f, E_s	SPECIMENS OBTAINED FROM BROKEN END OF ROOM TEMP. LONG BEAM FLEXURE
				6	FIRED	24	75	DT1, DT2, DT3 DT4, DT5, DT6	σ_f	USED TO OPTIMIZE FIRING TEMPERATURE

NOTES 1 ALL SPECIMENS HELD AT TEST TEMPERATURE FOR APPROXIMATELY 20 MINUTES PRIOR TO TESTING

2 FIRED SPECIMENS WERE FIRED AT 1088°C (1990°F) FOR 5 HOURS

3 ALL STRAIN MEASUREMENTS DETERMINED BY DEFLECTOMETER

4 ALL SPECIMENS WERE LOADED WITH THE DIRECTION OF LOADING NORMAL TO THE 'Y' FIBERS

FIGURE 7-1 MECHANICAL PROPERTIES TEST MATRIX

to a different epoxy adhesive did not resolve the problem. Consequently, as the specimens could not be configured for tensile testing, they were subsequently used in a firing temperature study to determine firing cycle temperatures that might increase the material strength or stiffness.

7.1.2

Specimen Testing

Initial room temperature tests performed at IITRI on two short beam flexure specimens indicated lower-than-expected strength and modulus (stiffness). In an attempt to improve strength, the effects of firing temperature were evaluated using the six 3D hyperpure tensile specimens (DT1-DT6) as specimens for short beam shear tests. Individual specimens were fired for five hours at various temperatures increasing from 932°C (1800°F) to 1177°C (2150°F). One unfired specimen was used as a control. Short beam shear tests were performed at MDAC-St. Louis. Testing was performed in series to obtain the optimum firing temperature. The tests were conducted in an 890 newton (200 pound) capacity Instron Universal test machine, using the three point shear test setup shown in Figure 7-2. The load rate for these tests was 0.05 cm (0.02 in.) head travel per minute. Ultimate flexure stress was determined as a function of temperature. From developed data (discussed further in Paragraph 7.2.1), it was decided to fire the remaining specimens for five hours at 1038°C (1900°F).

Beam flexure tests were conducted at IITRI in an 89,000 newton (20,000 pound) capacity Instron Universal test machine. The four-point flexure test setup is shown schematically in Figure 7-3. Figure 7-4 is a photograph of a typical long beam flexure test in progress. A three-point deflectometer was used to measure beam deflection as a function of applied load. Load rate was 0.05 cm (.02 in) head travel per minute. Ultimate stress and elastic moduli were determined from data obtained.

Short beam shear tests conducted at IITRI also utilized the 89,000 newton (20,000 pound) Instron Universal test machine. The specimens were machined from the ends of 0.23 cm (0.090 in) spacing densified Astroquartz specimens that failed at room-temperature and from densified hyperpure specimens. The three-point shear test setup is shown in Figure 7-2. Figure 7-5 is a photograph of IITRI's short beam shear test setup.

Elevated temperature flexure tests were run in a resistance heated furnace, utilizing silicon carbide test fixtures. The specimens were held at the test temperatures for approximately twenty minutes prior to applying load.

Because of the sensitivity of high purity silica strength to low levels of contamination, care was required not to introduce impurities to the material during handling and testing. All samples were handled with plastic or cotton gloves or plastic-coated metal tongs. When possible, the materials were placed in contact only with other high purity silica specimens or clean plastic film.

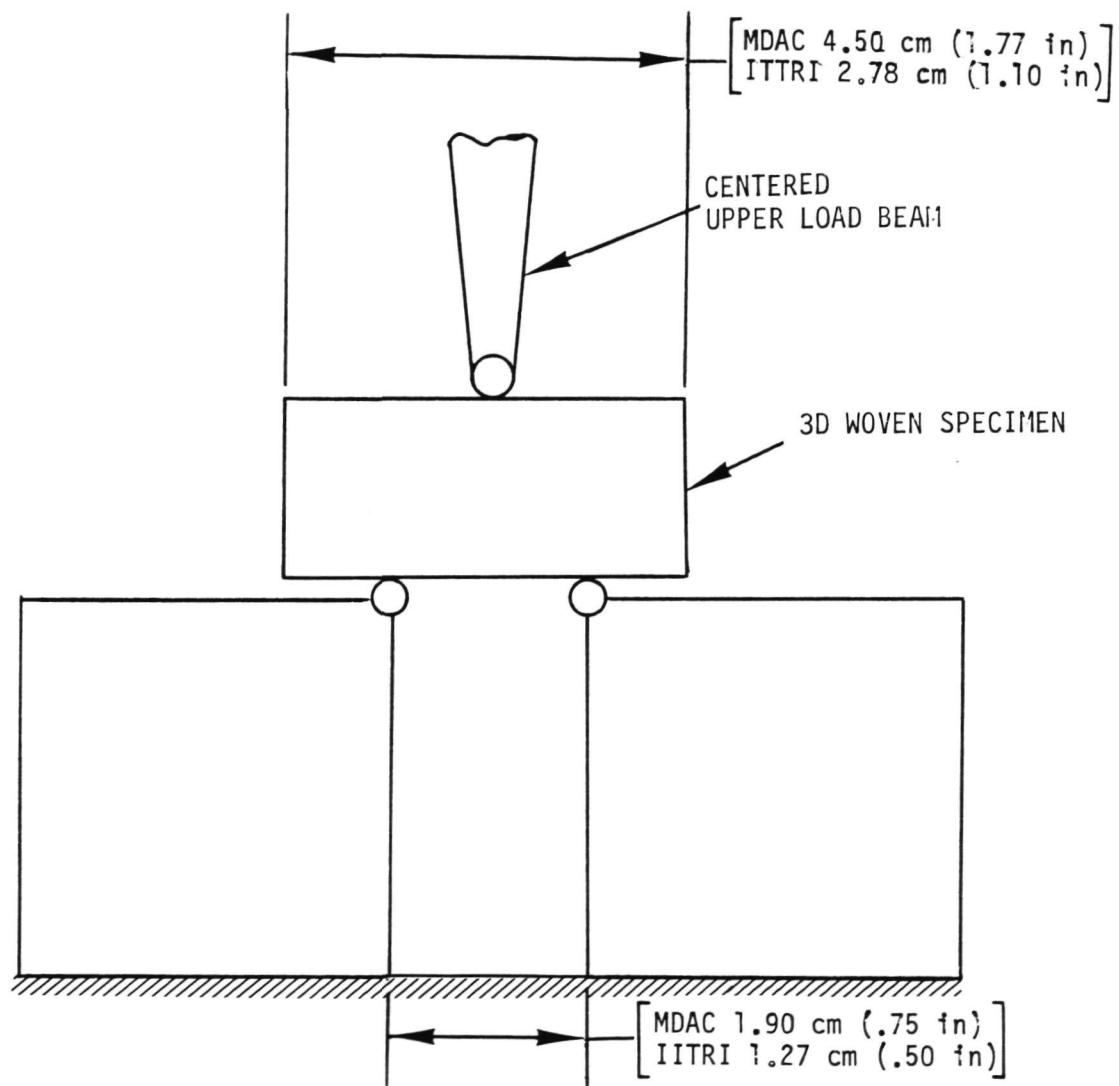


FIGURE 7-2 SCHEMATIC OF SHORT BEAM SHEAR TEST SETUP

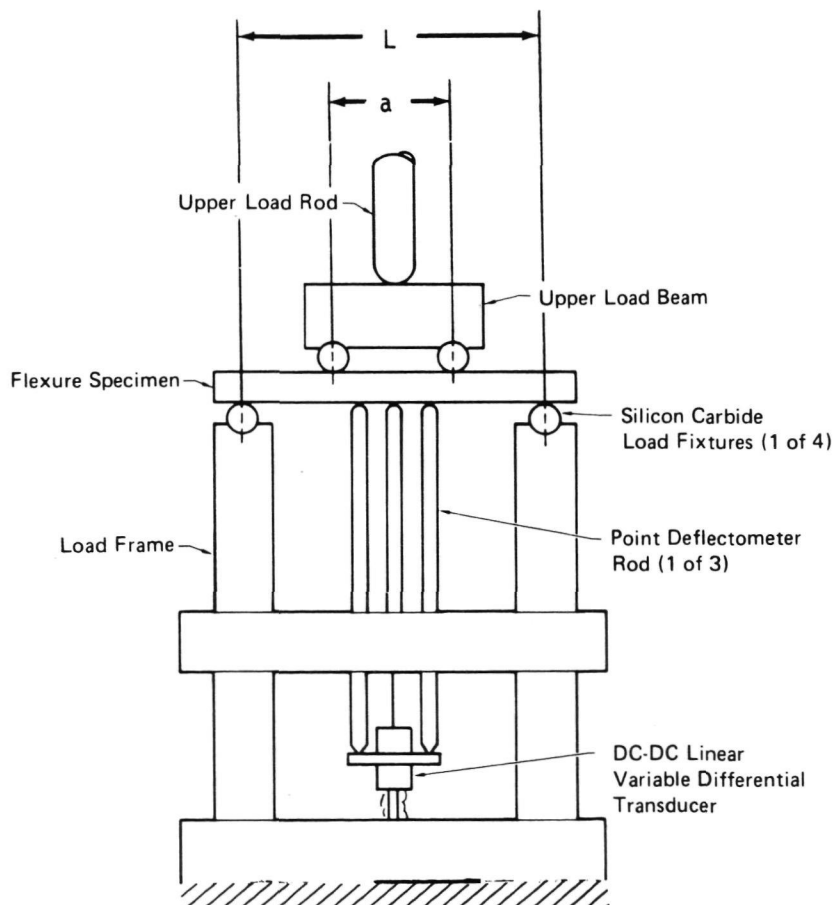
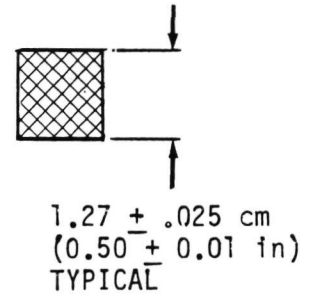
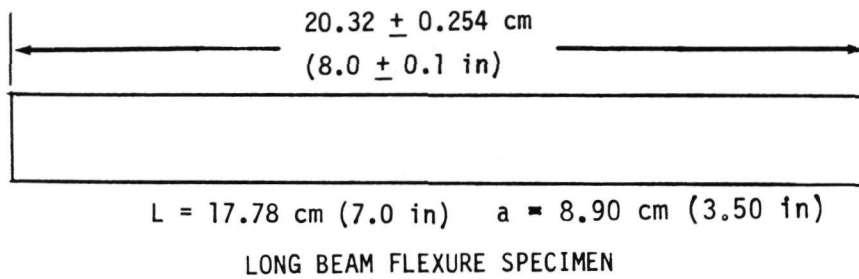
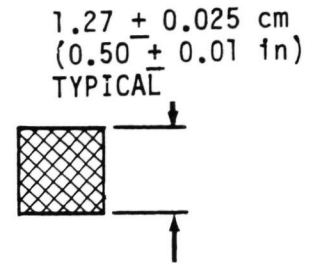
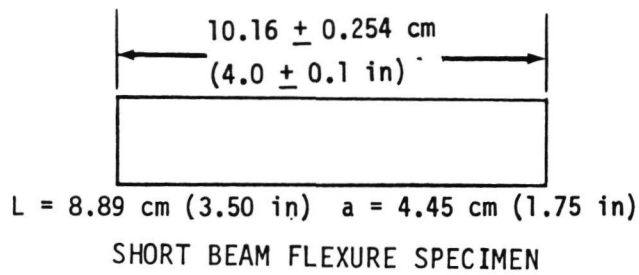


FIGURE 7-3 SCHEMATIC OF BEAM FLEXURE TEST SET-UP

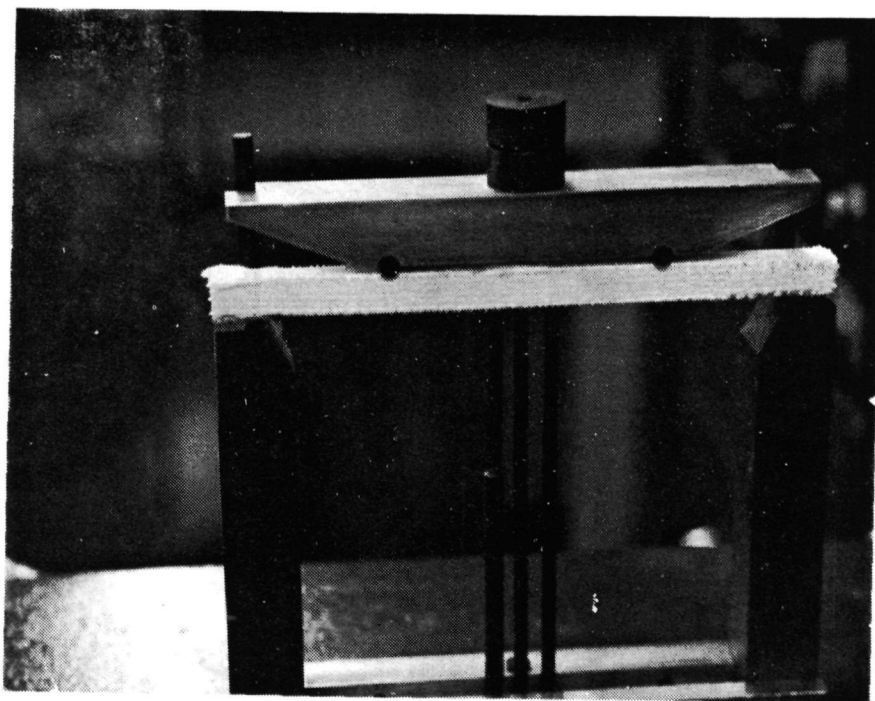


FIGURE 7-4 PHOTOGRAPH OF LONG BEAM FLEXURE TEST SETUP

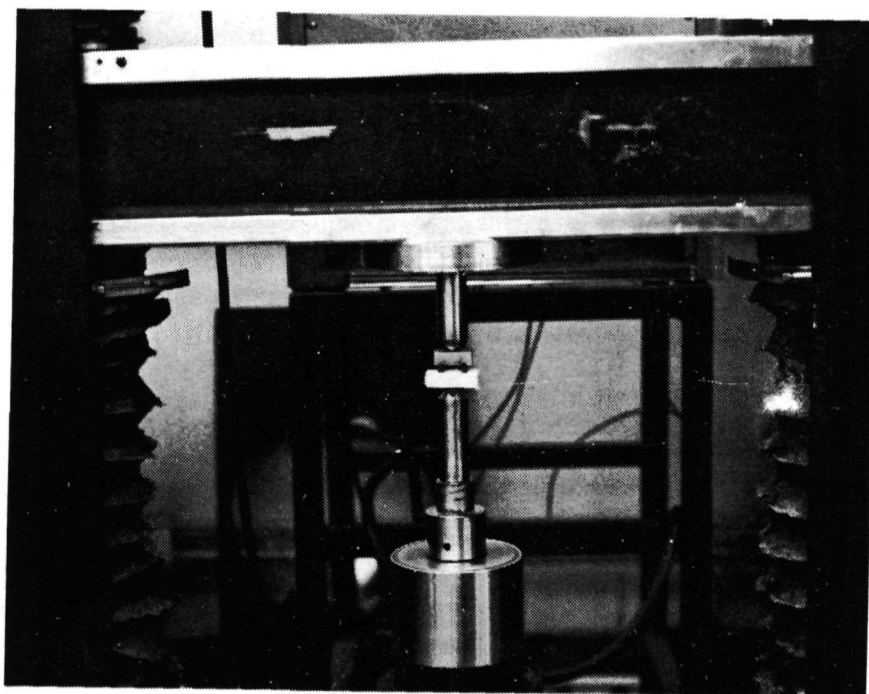


FIGURE 7-5 PHOTOGRAPH OF IITRI SHORT BEAM SHEAR TEST

ORIGINAL PAGE IS
OF POOR QUALITY

In general, very large deformations were displayed by the samples during testing. Most of this deformation was recovered after load removal. Because of the 3D weave, the specimens possessed the capability of redistributing the load to the internal fibers after the outer tension fibers failed. This redistribution of internal stresses was evident in analysis of the load/deflection curves. As the outer fibers failed, the load would drop somewhat and then start increasing again as the redistribution occurred. As very large deformations were required to fail the specimen completely, most of them were not entirely fractured. For purposes of analysis and comparison with other various silica materials, failure was considered to occur when the load receded (first set of outer fibers breaking).

7.2.1

Firing Temperature Study

The results of the firing study to determine the optimum firing temperature for improved strength and modulus are presented in Figure 7-6. The data indicates that an increase in strength occurred as a result of the firing, with the optimum firing temperature occurring at approximately 1037°C (1900°F). Specimen DT1 had a strength considerably lower than any of the other specimens tested, indicating that the higher firing temperature of 1177°C (2150°F) for Specimen DT1 had a detrimental effect on strength. All flexure specimens, (except AF4 and CF1 which had already been tested) were then fired at 1038°F for five (5) hours.

The physical properties of the flexure specimens before and after firing are presented in Figures 7-7 and 7-8, respectively. There was no measured shrinkage, visible warpage, or significant decrease in density in any of the specimens as a result of the firing cycle.

7.2.2

Room Temperature Flexure Tests

Considerable scatter occurred in the room temperature flexure strength of the Astroquartz specimens tested (Figure 7-9). The individual specimens varied from 5.17 MPa (750 psi) to 13.17 MPa (1910 psi). Likewise the same scatter was evident in the average flexure strength values (varying from 5.17 MPa [750 psi] to 11.10 MPa [1610 psi] [Figure 7-10]). The room temperature hyperpure specimens had considerably less scatter, varying from 8.27 MPa (1200 psi) to 9.10 MPa (1320 psi), with an average of 8.76 MPa (1270 psi).

The long beam flexure test results were compared to results of the short beam tests. Examining flexure values indicates that there is no significant difference in flexure strengths, although there is a considerable difference in calculated secant modulus. Although the correlation of the strength was expected, the large difference in modulus was not. Additional testing would be required before conclusions could be made for this difference.

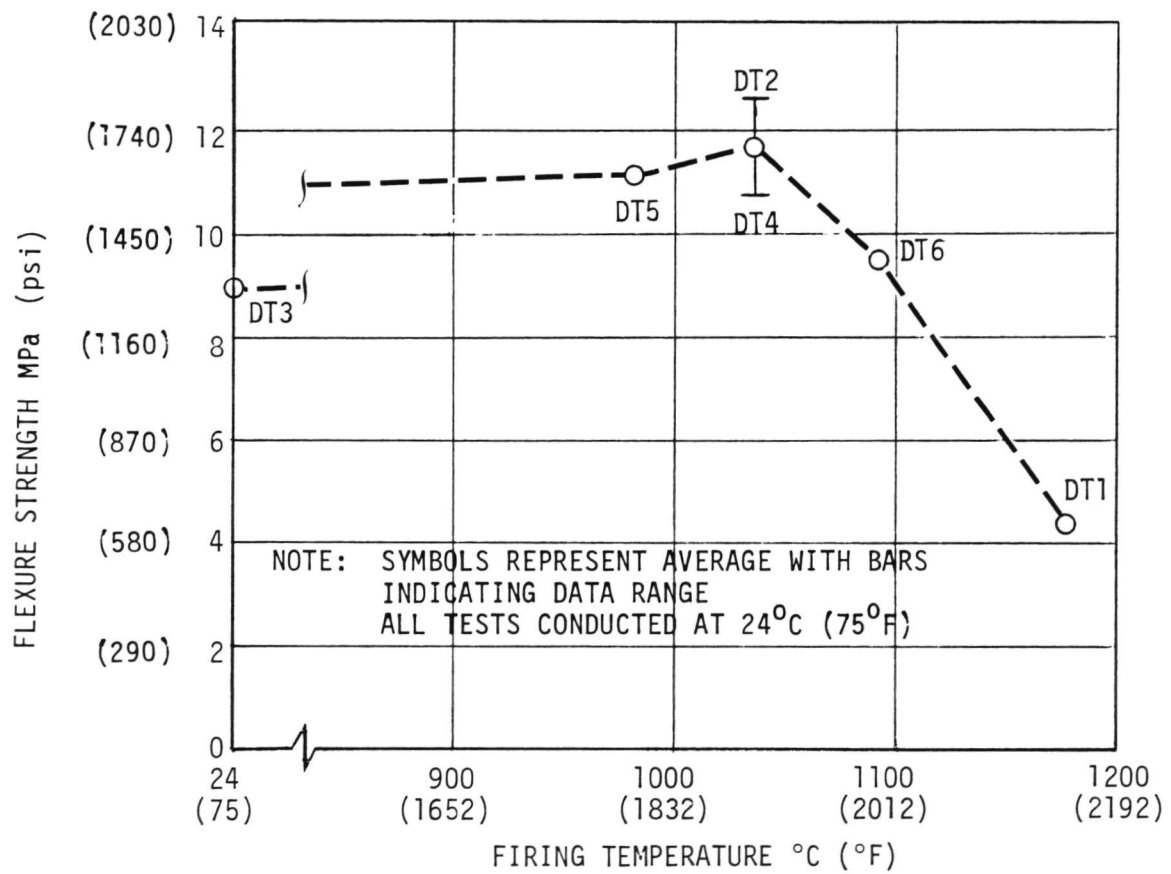



FIGURE 7-6 EFFECT OF FIRING TEMPERATURE ON FLEXURE STRENGTH

TEST SPECIMEN CONFIGURATION	LENGTH		WIDTH		DEPTH		NET WT	DENSITY	
	CM	INCH	CM	INCH	CM	INCH	GM	GM/CM ³	pcf
SMALL BEAM									
AF 1	10.21	4.02	1.27	0.50	1.27	0.50	21.72	1.32	82.40
AF 2	10.21	4.02	1.24	0.49	1.29	0.51	20.76	1.27	79.28
AF 3	10.21	4.02	1.24	0.49	1.27	0.50	21.34	1.33	83.03
AF 4	10.49	4.13	1.27	0.50	1.27	0.50	21.29	1.25	78.57
AF 5	10.49	4.13	1.27	0.50	1.27	0.50	20.74	1.23	76.79
AF 6	10.34	4.07	1.24	0.49	1.27	0.50	20.55	1.26	78.66
SMALL BEAM									
BF 1	10.21	4.02	1.27	0.50	1.27	0.50	21.58	1.31	81.78
BF 2	10.18	4.01	1.37	0.54	1.22	0.48	21.35	1.25	78.33
BF 3	10.18	4.01	1.27	0.50	1.24	0.49	21.67	1.35	84.28
BF 4	10.36	4.08	1.29	0.51	1.27	0.50	21.84	1.29	80.53
BF 5	10.34	4.07	1.27	0.50	1.27	0.50	21.03	1.26	78.66
BF 6	10.34	4.07	1.27	0.50	1.27	0.50	21.07	1.26	78.66
SMALL BEAM									
CF 1	10.21	4.02	1.27	0.50	1.27	0.50	20.41	1.24	77.37
CF 2	10.18	4.01	1.27	0.50	1.27	0.50	20.33	1.23	76.79
CF 3	10.16	4.00	1.27	0.50	1.27	0.50	21.20	1.29	80.53
CF 4	10.24	4.03	1.27	0.50	1.27	0.50	21.01	1.27	79.28
CF 5	10.21	4.02	1.27	0.50	1.27	0.50	20.94	1.27	79.28
CF 6	10.18	4.01	1.27	0.50	1.24	0.49	20.43	1.27	79.28
SMALL BEAM									
DF 1	10.21	4.02	1.29	0.51	1.24	0.49	19.86	1.22	76.16
DF 2	10.18	4.01	1.27	0.50	1.24	0.49	19.87	1.24	77.41
DF 3	10.21	4.02	1.24	0.49	1.19	0.47	18.37	1.22	76.16
DF 4	10.21	4.02	1.14	0.45	1.27	0.50	17.68	1.20	74.91
DF 7	11.30	4.45	1.29	0.51	1.24	0.49	23.24	1.28	79.91
DF 8	11.28	4.44	1.27	0.50	1.29	0.51	23.82	1.29	80.53
LONG BEAM									
DF 5	20.52	8.08	1.27	0.50	1.27	0.50	40.64	1.23	76.79
DF 6	20.47	8.06	1.24	0.49	1.24	0.49	38.25	1.22	76.16

FIGURE 7-7 BEAM FLEXURE SPECIMEN PHYSICAL PROPERTY DATA (PRIOR TO FIRING)

TEST SPECIMEN CONFIGURATION	LENGTH		WIDTH		DEPTH		NET WT	DENSITY	
	CM	INCH	CM	INCH	CM	INCH	GM	GM/CM ³	pcf
SMALL BEAM									
AF 1	10.21	4.02	1.27	0.50	1.27	0.50	21.63	1.31	81.99
AF 2	10.24	4.03	1.27	0.50	1.27	0.50	20.69	1.25	78.23
AF 3	10.21	4.02	1.27	0.50	1.27	0.50	21.35	1.30	80.93
AF 4	---	---	---	---	---	---	---	---	---
AF 5	10.54	4.15	1.27	0.50	1.27	0.50	20.71	1.22	76.04
AF 6	10.34	4.07	1.27	0.50	1.27	0.50	20.51	1.23	76.79
SMALL BEAM									
BF 1	10.24	4.03	1.27	0.50	1.27	0.50	21.52	1.30	81.37
BF 2	10.18	4.01	1.37	0.54	1.22	0.48	21.30	1.25	78.07
BF 3	10.18	4.01	1.27	0.50	1.24	0.49	21.59	1.34	83.72
BF 4	10.36	4.08	1.27	0.50	1.27	0.50	21.76	1.30	81.27
BF 5	10.36	4.08	1.27	0.50	1.27	0.50	20.99	1.26	78.39
BF 6	10.34	4.07	1.27	0.50	1.27	0.50	21.00	1.26	78.62
SMALL BEAM									
CF 1	---	---	---	---	---	---	---	---	---
CF 2	10.18	4.01	1.27	0.50	1.27	0.50	20.18	1.23	76.68
CF 3	10.16	4.00	1.27	0.50	1.29	0.51	21.09	1.26	78.77
CF 4	10.24	4.03	1.27	0.50	1.27	0.50	20.93	1.27	79.14
CF 5	10.21	4.02	1.27	0.50	1.27	0.50	20.86	1.27	79.07
CF 6	10.18	4.01	1.27	0.50	1.27	0.50	20.34	1.24	77.24
SMALL BEAM									
DF 1	10.21	4.02	1.27	0.50	1.24	0.49	19.88	1.23	76.89
DF 2	10.21	4.02	1.27	0.50	1.24	0.49	19.80	1.23	76.59
DF 3	10.21	4.02	1.24	0.49	1.19	0.47	18.29	1.21	75.26
DF 4	10.21	4.02	1.14	0.45	1.27	0.50	17.57	1.18	74.00
DF 7	11.30	4.45	1.27	0.50	1.29	0.51	23.08	1.24	77.48
DF 8	11.28	4.44	1.27	0.50	1.29	0.51	23.74	1.28	79.88
LONG BEAM									
DF 5	20.52	8.08	1.27	0.50	1.27	0.50	40.44	1.22	76.27
DF 6	20.47	8.06	1.27	0.50	1.24	0.49	38.11	1.18	73.52

FIGURE 7-8 BEAM FLEXURE SPECIMEN PHYSICAL PROPERTY DATA (AFTER FIRING)

MATERIAL	TEST SPECIMEN 	TEST TEMPERATURE		FLEXURE STRENGTH (σ_f)		STRAIN %	SECANT MODULUS (E_s)		MATERIAL TOUGHNESS	
		°C	°F	MPa	psi		GPa	Msi	$10^3 \frac{m \cdot n}{3}$	$\frac{in \cdot lb}{3}$
Astroquartz 0.15 cm (.060 in) Y-Yarn Spacing	Short Beam AF4 AF5 AF6 AF1 AF2 AF3	24	75	14.41	2090	.311	4.63	.672	22.41	3.25
		25	75	6.14	890	.249	2.46	.357	7.65	1.11
		24	75	9.79	1420	.249	3.93	.570	12.20	1.77
		1066	1950	19.51	2830	.043	45.38	6.581	4.21	.61
		1066	1950	15.24	2210	.061	24.98	3.623	4.62	.67
		1066	1950	16.00	2320	--	--	--	--	--
Astroquartz 0.23 cm (.090 in) Y-Yarn Spacing	Short Beam BF1 BF4 BF5 BF2 BF3 BF6	24	75	13.17	1910	.284	4.64	.673	18.69	2.71
		24	75	12.00	1740	.142	8.45	1.225	8.55	1.24
		24	75	8.21	1190	.081	10.13	1.469	3.31	.48
		1066	1950	19.93	2890	--	--	--	--	--
		1066	1950	25.86	3750	.196	13.19	1.913	25.37	3.68
		1066	1950	23.31	3380	.516	4.52	.655	60.12	8.72
Astroquartz 0.32 cm (.125 in) Y-Yarn Spacing	Short Beam CF1 CF2 CF3 CF4 CF5 CF6	24	75	3.93	570	.082	4.79	.695	1.59	.23
		24	75	--	--	--	--	--	--	--
		24	75	5.17	750	.110	4.70	.682	2.83	.41
		1066	1950	18.34	2660	.057	32.18	4.667	5.24	.76
		1066	1950	17.44	2530	.267	6.54	.948	23.31	3.38
		1066	1950	18.13	2630	--	--	--	--	--
Hyperpure 0.23 cm (.090 in) Y-Yarn Spacing	Short Beam DF2 DF3 DF7 DF1 DF4 DF8	24	75	8.89	1290	.023	38.67	5.609	1.03	.15
		24	75	9.10	1320	--	--	--	--	--
		24	75	8.27	1200	.381	2.17	.315	15.79	2.29
		1066	1950	24.96	3620	2.614	.95	.138	326.20	47.31
		1066	1950	22.82	3310	2.738	.83	.121	312.41	45.31
		1066	1950	23.51	3410	1.938	1.21	.176	227.81	33.04
	Long Beam DF5 DF6	24	75	8.69	1260	1.790	.48	.070	77.78	11.28
		24	75	10.62	1540	.090	11.80	1.711	4.76	.69

Notes:



Specimen was not fired

Indicates value not obtainable from test data

FIGURE 7-9 INDIVIDUAL SPECIMEN BEAM FLEXURE RESULTS

MATERIAL	SPECIMEN	TEMPERATURE		AVERAGE FLEXURE STRENGTH (σ_f)		AVERAGE STRAIN %	AVERAGE SECANT MODULUS (E _c)		AVERAGE MATERIAL TOUGHNESS	
		°C	°F	MPa	psi		GPa	Msi	$10^3 \frac{\text{in-lb}}{\text{in}^3}$	$\frac{\text{in-lb}}{\text{in}^3}$
Astroquartz 0.15 cm (.060 in) Y-Yarn Spacing	Short Beam	24	75	8.00	1160	.249	3.17	.46	9.93	1.44
		1066	1950	16.89	2450	.052	35.16	5.10	4.41	.64
Astroquartz 0.23 cm (.090 in) Y-Yarn Spacing	Short Beam	24	75	11.10	1610	.169	7.72	1.12	10.20	1.48
		1066	1950	23.03	3340	.356	8.83	1.28	42.75	6.20
Astroquartz 0.32 cm (.125 in) Y-Yarn Spacing	Short Beam	24	75	5.17	750	.110	4.69	.68	2.83	.41
		1066	1950	18.00	2610	.162	19.37	2.81	14.27	2.07
Hyperpure 0.23 cm (.090 in) Y-Yarn Spacing	Short Beam	24	75	8.76	1270	.202	20.41	2.96	8.41	1.22
		1066	1950	23.79	3450	2.430	1.03	.15	288.83	41.89
	Long Beam	24	75	9.66	1400	.94	6.14	.89	41.27	5.99

Notes: Averages are based on fired specimens only (firing cycle 5 hours at 1900°F)

FIGURE 7-10 SUMMARY OF BEAM FLEXURE RESULTS

As the range of densities was rather small, a significant pattern between density and strength could not be detected. All room temperature flexure specimens had lower strength than the previously tested slip cast fused silica (Reference 4). This is primarily due to lower densities (1.18 to 1.34 gm/cc) for the 3D silica composites versus a density of 1.65 gm/cc for the slip-cast fused silica. Specimens fired at 1038°C (1900°F) were compared to those that were unfired. When specimens AF5 and AF6 are compared to AF4 and when CF3 is compared to CF1, it is not obvious that the firing temperature did improve the strength, as the original firing temperature study (Figure 7-6) indicated. This is not to say that the 1038°C (1900°F) firing does not improve strength or modulus, but does show that other variables, such as density and the limited number of specimens, have a masking effect. Additional testing of specimens at the same densities would be required to clarify the inference.

Toughness (area under stress-strain curve) of the various densified materials was also determined. The room temperature toughness was considerably higher than slip-cast fused silica (Reference 4). The average room temperature toughness varied from $2.83 \times 10^3 \text{ m-n/m}^3$ (.41 in-lb/in³) to $41.27 \times 10^3 \text{ m-n/m}^3$ (5.99 in-lb/in³). This compares with a toughness of 0.91 m-n/m^3 (.13 in-lb/in³) for the slip-cast fused silica. Figure 7-9 indicates the individual specimen toughness values, while 7-10 shows the averages. Figure 7-11 provides a visual representation of the relative toughness. It is felt that a portion of the large scatter present is due to the deflectometer's inability to accurately monitor the deflections on this type of a specimen. The deflectometer points were rounded off after it was determined that they were protruding into the specimens. After rounding the points, the deflectometers continued to locally surface-penetrate the specimens. In addition, the deflectometers would occasionally slide off the fibers and into a local cavity. These conditions made it difficult to interpret the deflections and the resulting toughness.

7.2.3

Elevated Temperature Flexure Tests

The elevated-temperature (1066°C) flexure strength was considerably higher than the room-temperature strength, as shown in Figure 7-12. The increase in strength varied from 107% for the 0.23 cm spacing Astroquartz to 248% for the 0.32 cm spacing Astroquartz. Strength of the hyperpure material increased by 172%. This compares with an increase of 62% for the slip-cast fused silica (Reference 4).

This increase in strength is possibly due, in part, to the removal of hydroxyl ions. It has been reported in Reference 13 by Kingery that the strength of glass is reduced in the presence of water vapor. This would account in part for strength increases noted at elevated temperatures. It was also noted in Reference 13 that abrasion of the surface of glass will reduce its strength. It would be reasonable to assume that some of the fibers were abraded during handling, weaving, and machining of the yarns and that elevated temperature could cause some viscous flow to mend some of the abrasion, thus reducing crack propagation tendencies and increasing the

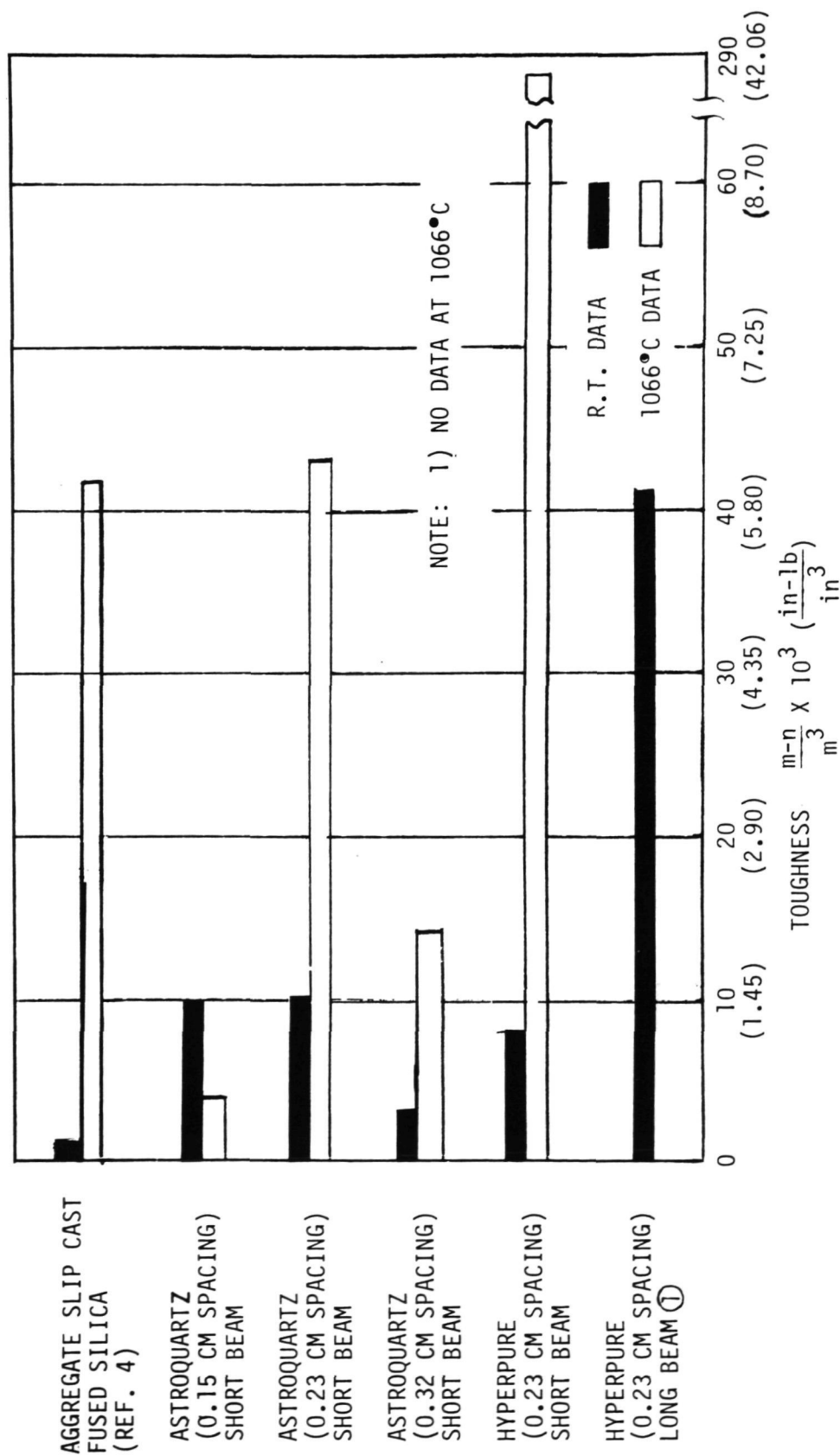


FIGURE 7-11 AVERAGE TOUGHNESS COMPARISON OF THE VARIOUS DENSIFIED MATERIALS

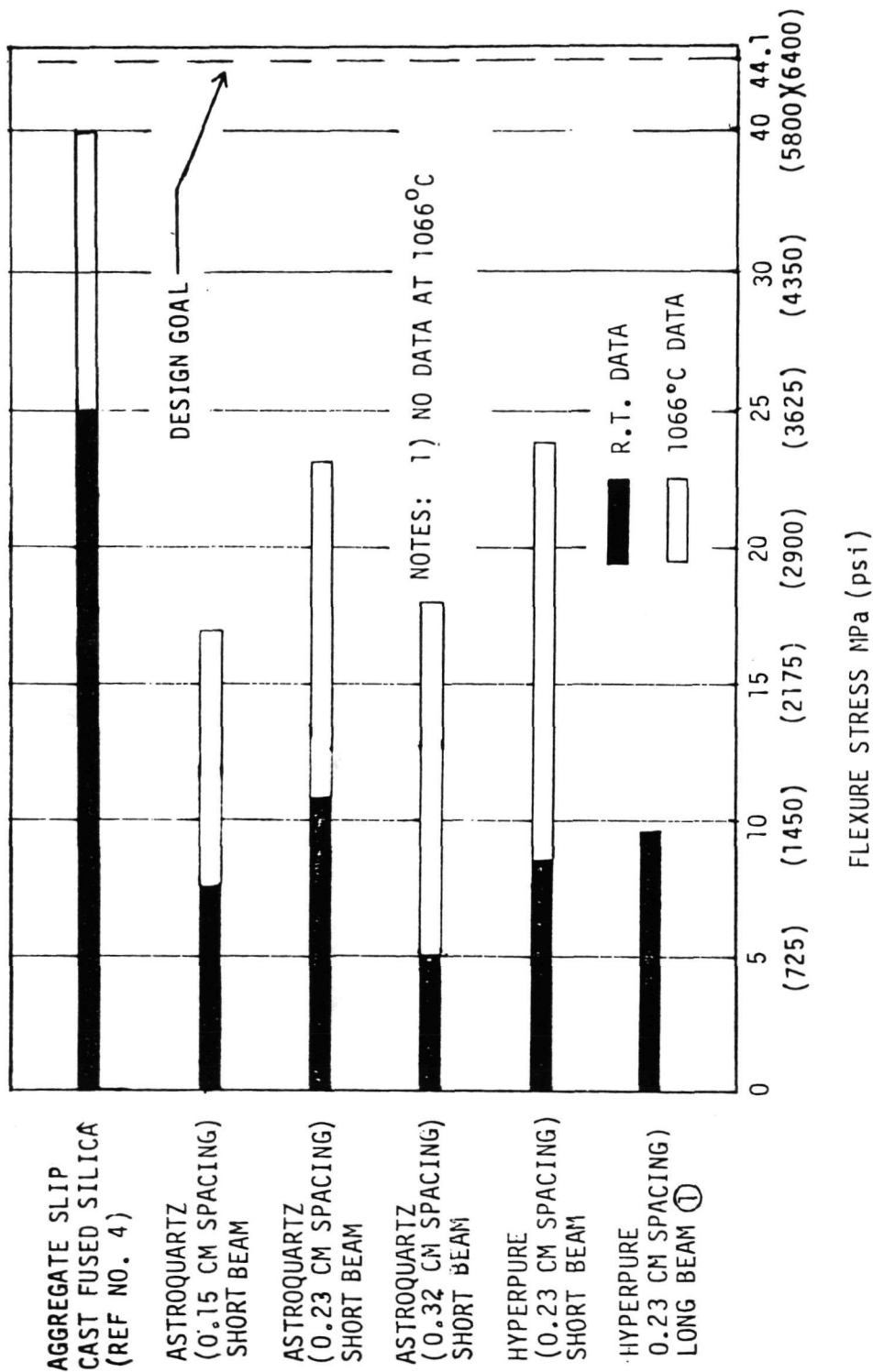


FIGURE 7-12 AVERAGE FLEXURE STRENGTH VALUE COMPARISON OF THE VARIOUS DENSIFIED MATERIALS

strength at elevated temperatures. Also, some sintering could have taken place as the test specimens were tested at 1066°C (1950°F), which is above the original firing temperature of 1038°C (1900°F).

Even with this increase in strength, the strength is still far below that of the slip-cast fused silica (Reference 4) and the design goal. The highest strength material tested was the hyperpure material, with a flexure strength of 23.8 MPa (3450 psi). This compares with a value of 40.4 MPa (5860 psi) for the slip-cast fused silica and a design goal of 44.1 MPa (6400 psi). The strength of the 3D silica composite is compared to the slip-cast fused silica in Figure 7-13. As expected, the figure indicates that the strength of the 3D silica composite increases at approximately the same rate, relative to the increase in test temperature, as the slip-cast fused silica.

In general the toughness of the material increased with an increase in temperature, as shown clearly in Figure 7-11. The only exception to this is the 0.15 cm Astroquartz, which showed a 56% decrease in toughness. The largest increase in toughness was on the 3D hyperpure specimens where the toughness increased by 3300 percent. This compares with the aggregate slip-cast fused silica of Reference 4 where the toughness increased by 4600 percent. The only material that possesses sufficient toughness to satisfy the design goal of $69.0 \times 10^3 \text{ m-n/m}^3$ (10.0 in-lb/in³) is the hyperpure material, at $289 \times 10^3 \text{ m-n/m}^3$ (41.9 in-lb/in³). Although the data for this material may be somewhat suspect at first glance, since it varies appreciably from the Astroquartz data, it did have a low scatter range, varying from $227.8 \times 10^3 \text{ m-n/m}^3$ (33.0 in-lb/in³) to 326.2 m-n/m^3 (47.3 in-lb/in³) (see Figure 7-9). The increased toughness is conjectured to be due to the purity of this material, allowing for both a higher flexure stress and a larger strain before failure. Additional testing and analysis would be required to verify this conjecture.

7.2.4

Short Beam Shear Tests

The results of the short beam shear tests produced the same trends observed for the room-temperature flexure tests. The Astroquartz specimens had a larger average interlaminar shear stress [4.69 MPa (680 psi)] than the hyperpure specimens [2.55 MPa (370 psi)], as shown in Figure 7-14. For the test specimen configuration and geometry employed, the resulting tensile/compression stresses are three times as high as the interlaminar shear stresses. In addition, the tension stresses are approximately equal to the failure stresses determined in the flexure tests. Consequently, the failure was a result of the combined interlaminar shear stresses and tension stress. This combined stress failure condition was evident upon examination of the failed test specimens. All the specimen failures had occurred on a diagonal, whereas on a perfect interlaminar shear failure, the failure mode would be a horizontal fracture. Since the failures were a result of combined stresses,

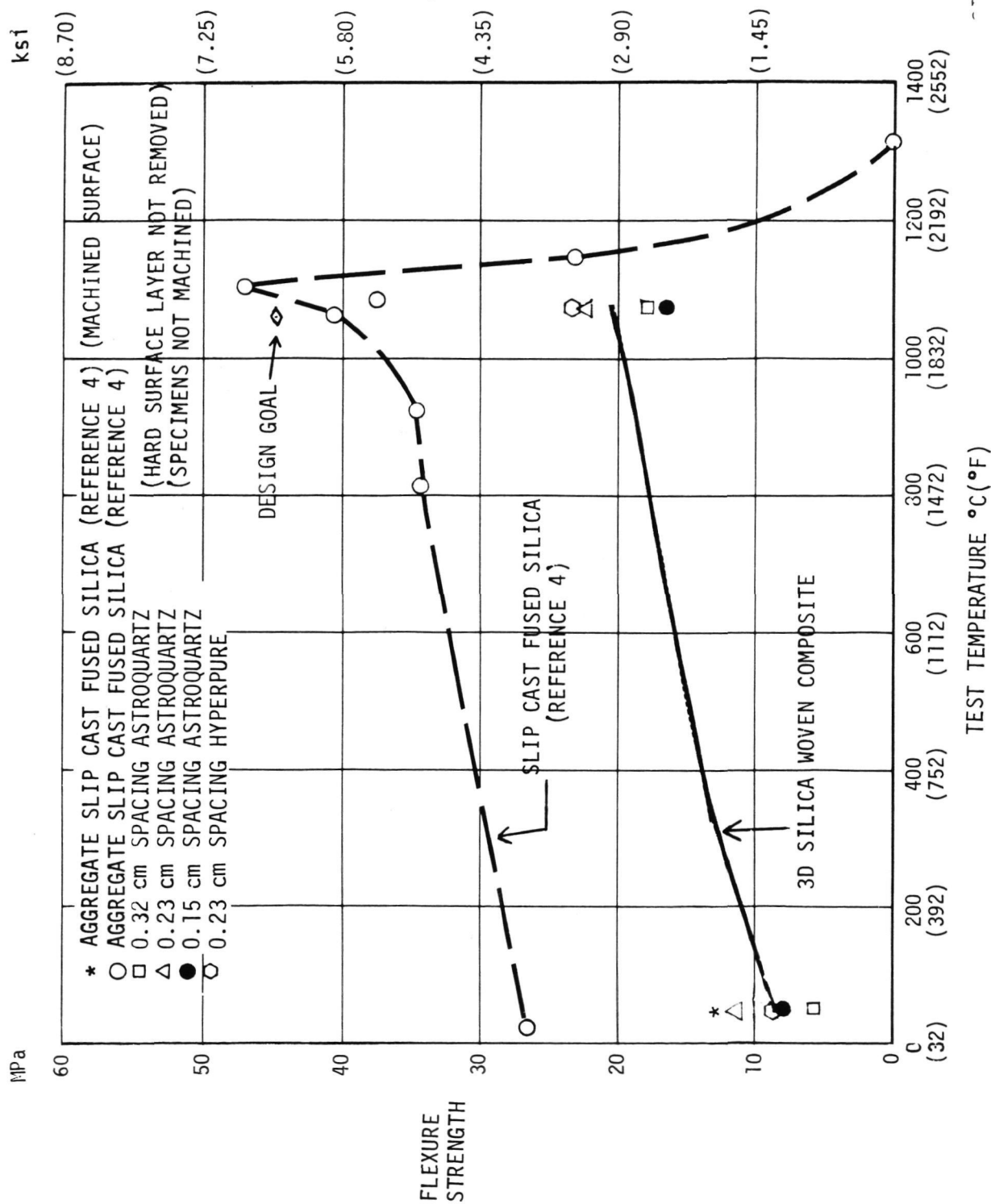


FIGURE 7-13 FLEXURAL STRENGTH COMPARISON OF HYPERPURE SLIP-CAST FUSED SILICA WITH 3D SILICA WOVEN COMPOSITE

Material	Test Specimen	Interlaminar Failure Stress (σ_s)		Average Interlaminar Failure Stress		Failure Tension Stress (σ_t)		Average Tension Stress (σ_a)	
		MPa	psf	MPa	psf	MPa	psf	MPa	psf
Astronquartz 0.23 CM Spacing	B1F1	4.24	615	4.69	680	13.03	1890	14.17	2055
	B1F4	4.83	700			14.45	2095		
	B1F5	5.03	730			15.07	2185		
Hyperpure 0.23 CM Spacing	D1F5	2.24	325	2.55	370	6.69	970	7.65	1110
	D1F6	2.31	335			6.96	1010		
	D1F7	3.10	450			9.31	1350		

NOTES:

1. All specimens tested at room temperature.
2. Specimens were taken from broken ends of previously tested beam flexure specimens.

FIGURE 7-14 SUMMARY OF SHORT BEAM TEST RESULTS

the interlaminar stresses enumerated in Figure 7-14 cannot be considered the maximum obtainable values, but only an indication of the interlaminar stress capability.

7.3 DISCUSSION OF MECHANICAL PROPERTY TEST RESULTS

It must be emphasized that, because of the relatively few samples tested under each test condition, the mechanical property test data should only be considered as indicating general trends.

7.3.1 Physical Properties

Test specimen densities ranged between 1.1 g/cm³ (74.0 psi) and 1.34 g/cm³ (80.93 psi), as previously shown in Figures 7-8. Test specimens subjected to the added firing during elevated temperature testing did not exhibit weight or density changes. No significant change in test specimen physical appearance was observed at either room or elevated temperature.

7.3.2 Mechanical Properties

7.3.2.1 Room-Temperature Flexure Data

The summary of flexure test results is shown in Figure 7-10. These results indicate the average failure stress varied from 5.17 MPa (750 psi) to 11.10 MPa (1610 psi) and exhibited considerable data spread. The low flexure strength is considerably less than for the slip-cast fused silica tested in Reference 4 [25.0 MPa (3620 psi)]. The variation in flexure test results are typical and not totally unexpected in a porous ceramic material. All of the room-temperature toughness values shown in Figure 7-10 exceeded the previously tested aggregate slip-cast fused silica (Reference 4).

7.3.2.2 Elevated Temperature Flexure Data

The summary of elevated temperature results is also shown in Figure 7-10. These results indicate that considerable strength was gained at the elevated temperature. The average failure stress varied from 16.89 MPa (2450 psi) to 23.79 MPa (3450 psi). The elevated temperature strength was still considerably below the strength developed in the aggregate slip-cast fused silica tested in Reference 4 [40.4 MPa (5860 psi)].

In general, the toughness of the materials increased with an increase in temperature. Only the hyperpure material had sufficient toughness to exceed the aggregate slip-cast fused silica (Reference 4) and satisfy the design goals. (Figure 7-11.)

7.3.2.3

Short Beam Shear Data

The summary of the short beam shear data is presented in Figure 7-14. As shear properties of the aggregate slip-cast fused silica were not determined (Reference 4), there are no data available for quantitative evaluation.

7.3.2.4

Mechanical Property Summary Data

A complete summary of mechanical property data is presented in Figure 7-15.

7.4

CONCLUSIONS

Conclusions based upon analysis of the mechanical property testing performed during this program are as follows:

- o Silica strength increases with an increase in test temperature within the range of temperatures tested.
- o Toughness increases with an increase in test temperature within the range of temperatures tested.
- o Hyperpure silica has less strength than Astroquartz at room temperature but more strength at elevated temperatures.
- o The room-temperature toughness of both Astroquartz and hyperpure silica is better than slip-cast fused silica.
- o The elevated-temperature toughness of Astroquartz is less than the aggregate slip-cast fused silica and significantly less than the design goal.
- o The elevated temperature toughness of the hyperpure is considerably better than the aggregate slip-cast fused silica and far exceeds the design goal.
- o All flexure strengths measured were less than the slip cast fused silica or design goal.

Material	Flexure Strength (σ_f)		Material Toughness		Interlaminar Shear Strength (σ_s)		Secant Modulus (E_c)		Strain at Failure
	MPa	psf	10^3 n-m/m ³	in-lb/in ³	MPa	psf	GPa	Msi	
Design Goal	44.1	6400	69.0	10.0	-	-	14.1	2.05	0.313
Slip Cast Fused Silica	40.4	5860	42.6	6.2	-	-	19.2	2.78	0.211
Astroquartz	16.9-23.0	2450-3340	4.4-42.8	0.6-6.2	4.69	680	8.8-35.2	1.28-5.10	.052-.356
Hyperpure	23.8	3450	288.9	41.9	2.55	370	1.03	.15	2.430

NOTES:

1. All of the above values (except for the interlaminar shear strength) are based on 1066°C (1950°F) temperatures.
2. Interlaminar shear strengths are room temperature data.

FIGURE 7-15 MECHANICAL PROPERTY SUMMARY

8.0 FULL SCALE PROTOTYPE 3D SILICA HEAT SHIELD COST ANALYSIS

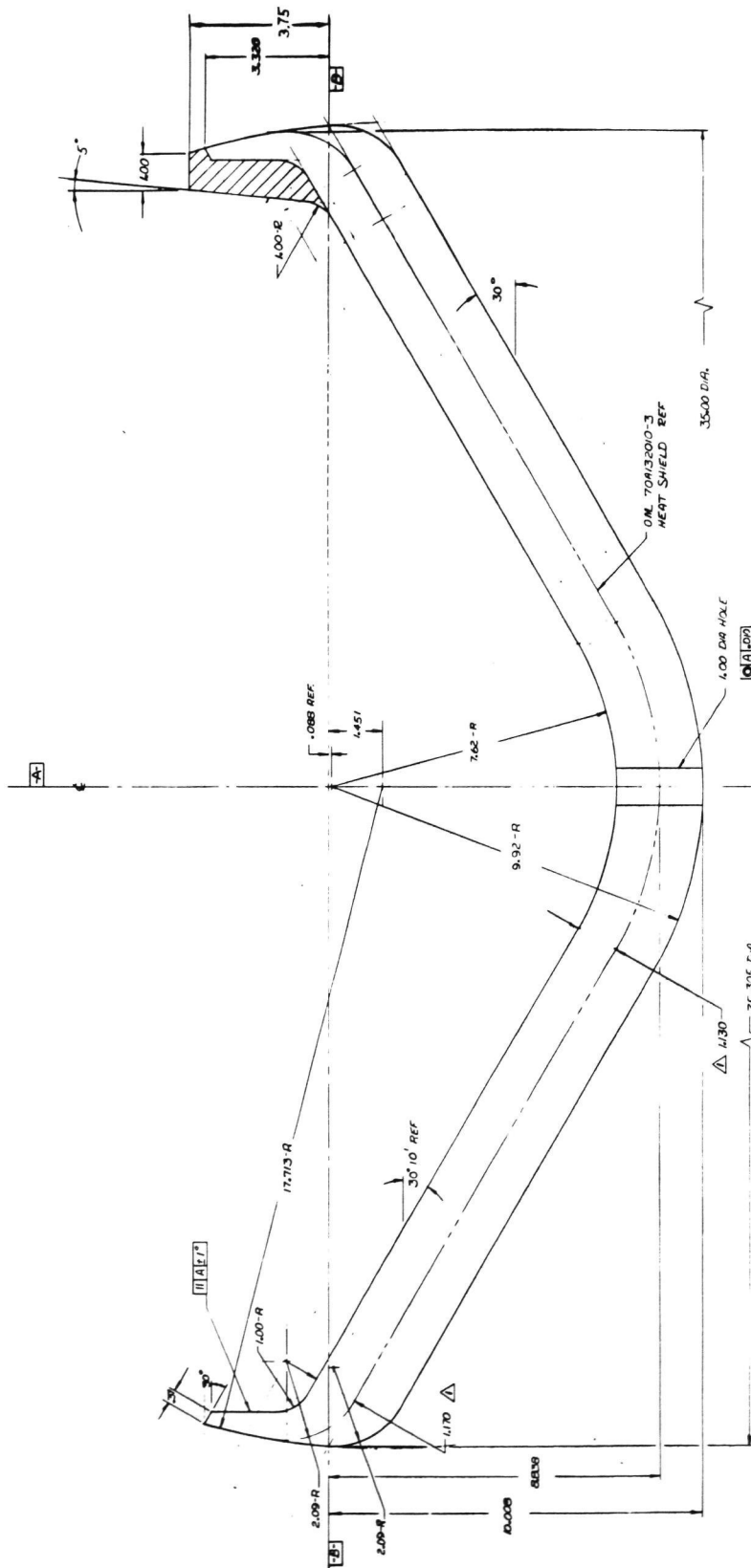
This section contains a rough order of magnitude (ROM) cost estimate for fabrication of a full scale prototype 3D woven silica planetary heat shield. The estimate presented is based on the experience gained and data collected during this contract. Processing techniques used in this study would have to be improved to produce a 3D woven silica reflective heat shield that would meet the strength and toughness requirements for a Jupiter entry probe, while maintaining a high reflectance. The improved processing costs and/or added tooling necessary to produce a viable heat shield are not included in this estimate, because their characteristics have yet to be defined.

There were several assumptions made in arriving at the cost presented in Figure 8-1. The major ones are as follows:

- o Two different silica yarns are considered. They are:
 - Hyperpure silica at 10 ppm ion impurities
 - Astroquartz silica at 500 ppm ion impurities
- o Both of these materials are available from J. P. Stevens and are identical to those used in this program. The hyperpure silica yarn is not yet a production material, so it would be produced as a special order; therefore, a higher cost and longer delivery time must be expected. The hyperpure silica yarn for this program cost approximately \$2300/lb versus \$140/lb for the more standard Astroquartz. Hyperpure silica yarn would probably require a lead time of about seven months after issuance a purchase order before material would be available for weaving.
- o FMI has determined that the weave pattern selected for this program can be used to weave a full scale heat shield. The dimensions of the as-woven heat shield were selected to be approximately the same as those proposed by MDAC-St. Louis for the Galileo probe. Figure 8-2 is a sketch showing approximate external dimensions. It should be realized that a hardware shield would have to be analytically sized based upon the final material characteristics. The MDAC-St. Louis Galileo Probe employed carbon/phenolic as the baseline heat shield, and Figure 8-2 is based on that selection.
- o The high purity silica grains used as densifier would be the same as those evaluated in this study. Dynasil is readily available, and no problems are envisioned in scaling up the processes to make an impregnation slip of high purity and acceptable average particle size.
- o Scale-up of the 3D weaving process has been assumed to be within the state-of-the-art. Even though nothing this size has ever been 3D woven before, it is the belief of FMI that it can readily be accomplished.

MATERIALS/PROCESSING	SOURCE	3D WOVEN SILICA HEAT SHIELD ROM COST	
		ASTROQUARTZ	HYPERPURE
SILICA YARN			
600 LBS	J. P. STEVENS		\$1,540,000
600 LBS	J. P. STEVENS	\$92,400	
IMPREGNANT (SILICA)	DYNASIL	5,000	5,000
PREFORM FABRICATION			
TOOLING	FMI	16,500	16,500
WEAVING	FMI	82,500	82,500
DENSIFICATION			
TOOLING	MDAC-ST. LOUIS	60,000	60,000
PROCESSING			
PREFORM CLEANING	MDAC-ST. LOUIS	17,554	17,554
BINDER PREPARATION	MDAC-ST. LOUIS	40,911	40,911
IMPREGNATION	MDAC-ST. LOUIS	131,584	131,584
DRYING & FIRING	MDAC-ST. LOUIS	23,357	23,357
MACHINING	MDAC-ST. LOUIS	48,745	48,745
TOTAL ROM COST		\$518,552	\$1,966,152

FIGURE 8-1 SUMMARY ROM COST FOR FULL SCALE PROTOTYPE 3D WOVEN
SILICA REFLECTIVE HEAT SHIELD



- NOTES: 1 TAPER IS TO BE UNIFORM BETWEEN POINTS OF TANGENCY
 2 ALL DIMENSIONS SHOWN ARE IN INCHES

FIGURE 8-2 TYPICAL GALILEO PROBE HEAT SHIELD

- o Scale-up of the impregnation and densification process, although it may require more than one attempt to arrive at correct tooling, is also considered within the state-of-the-art. It was assumed that high pressure impregnation processes would not be required, so that special requirements would not cause estimated tooling costs to grow.
- o Firing of the densified woven heat shield preform would not exceed temperatures of 1093°C (2000°F), thereby minimizing the need or cost for special, clean furnace facilities.
- o Machining of the densified preform to final dimensions, although requiring diamond tooling, is well within MDAC-St. Louis capabilities. Prime examples are the Gemini heat shield, for which special techniques were developed and employed (and which was much larger than the proposed prototype), and the prototype carbon/phenolic heat shield made for ARC under technology studies related to the Galileo Probe.
- o Engineering costs associated with detail design, analysis, or further development to realize a flight worthy material are not included.
- o The estimate is for the fabrication of a prototype heat shield to verify that the materials/construction employed are adequate for full size heat shield fabrication.
- o The estimate includes only nominal Quality Assurance provisions. A heat shield having uniform properties should be expected. Engineering assessment of such processing details as broken fibers, voids, starved areas, drying distortion, etc., would not be resolved during the prototype heat shield fabrication.
- o The estimate covers fabrication only with no provisions for evaluating either process efficiency or final product quality.

As can be seen from the summary cost data presented in Figure 8-1, the raw material costs for a hyperpure heat shield make up approximately 75% of the total fabricated cost. For that reason, a cost comparison on an Astroquartz heat shield was included. By so doing, the practicality of fabricating a densified full-scale woven 3D structure could be provided for one third the cost. It is believed that very little fidelity would be lost by such a decision, and the gain in lead time would be a definite advantage.

9.0 CONCLUSIONS AND RECOMMENDATIONS FOR FUTURE WORK

This section contains the major conclusions derived from the program and offers suggestions for future work in the continuing development of a higher strength 3D woven silica material for use as a tough reflective heat shield for planetary entry applications.

9.1

CONCLUSIONS

The conclusions below are based on the experimental work performed during this program:

- o The A1100 surface finish (sizing) used on the Astroquartz fibers discolored during cleaning attempts of the preforms prior to densification and was difficult to remove. Removal was finally accomplished by heating at 540°C (1004°F) for three hours. The PVA finish used on hyperpure fibers was easily removed without residual discoloration.
- o Contamination from machining (matrix material that retains the diamond grit) was effectively removed by surface grinding with large size diamond particle (38-44 grit) end mills, without water coolant, and by heat treatment.
- o Analysis of the various cleaning steps indicated that heat treatment at 540°C (1004°F), which removed the A1100 finish, also reduced the strength of individual Astroquartz yarns.
- o Densification of 3D silica preforms with 0.7 μm hyperpure silica grains achieved densities in the range 1.3-1.45 gm/cc (81.0 pcf to 90.0 pcf). This was lower than expected and is attributed to filtration resistance of the binder material, preform weave patterns, and densification procedures.
- o Machining between impregnation cycles to remove buildup at densified preform surfaces did not result in increased impregnation efficiency.
- o Density variations were present in all preforms except for the 0.23 cm Y-yarn spacing Astroquartz material. Density gradient specimens indicated a higher density at the surface of the densified preforms, which is as one would expect. Radiographic analysis did not clearly depict density gradients.
- o The thermal conductivity of 3D woven hyperpure material was considerably lower than fused silica. This was attributed mainly to its lower density.

- o Reflectance was greatly improved as a result of densification. The hyperpure material had the highest reflectance, approaching 99 percent. The Astroquartz materials was also fairly high at ~96 percent. However, fiber-reinforced slip-cast hyperpure fused silica material maintained a higher overall reflectance at all wavelengths than did the 3D woven composites.
- o The strength of 3D woven densified materials was lower than expected. They did not achieve strength values equivalent to those of the slip-cast high purity material developed in Reference 3.
- o Both 3D woven silica materials (Astroquartz and hyperpure) increased in strength with increasing test temperature.

9.2

RECOMMENDATIONS FOR FUTURE WORK

At higher densities the 3D woven hyperpure silica material would probably have adequate strength and toughness to meet and exceed requirements for a Jupiter probe. It is recommended that work be continued to increase the densification efficiency of 0.23 cm Y-yarn spacing preforms by reducing the particle size of the binder material--i.e., smaller than 0.7 μm . A finer binder material can be obtained while maintaining high purity levels by employing a hyperpure ball mill. Materials for fabricating such a ball mill are available. An all ceramic mill has the additional advantage of higher efficiency in particle size reduction over the plastic ball mill used during this program.

It is also recommended that the following activities be investigated to develop an optimized material:

- o Determine the effects of firing temperature on composite (impregnated 3D preform) strength and toughness.
- o Increase specimen density by evaluating pressure impregnation techniques.
- o Measure the thermal performance of woven densified hyperpure silica materials to compare this type material with slip-cast fused silica.
- o Locate and evaluate colloidal silica materials that have high purity and can be used to impregnate preforms to higher densities. A trade study to be considered is the increased density obtained versus the potential loss of reflective characteristics because of the lower purity levels.

REFERENCES

1. Nachtsheim, P. R., Peterson, D. L., and Howe, J. T., "Reflecting Ablative Heat Shields for Radiative Environments," American Astronautical Society, the 17th Annual Meeting, 28-30 June 1971.
2. Blome, J. C., Drennan, D. N., Schmitt, R. J., "High Purity Silica Reflective Heat Shield Development," NASA CR-137617, MDC E1139, October 1974.
3. Rusert, E. L., Drennan, D. N., and Biggs, M. S., "Development, Fabrication and Test of a High Purity Silica Heat Shield," NASA CR-152117, April 1978.
4. Rusert, E. L., Biggs, M. S. and Dillow, C. F., "High Purity Silica Reflective Heat Shield Development," NASA CR-152118, May 1978.
5. Rusert, E. L., "Ablation Materials and Missile Insulation," MDC 90849-2, Vol. 1, 12 January 1978. Project No. 82100.
6. Hackett, T. L., Private Communication with J. Brooks, J. P. Stevens, MDAC-St. Louis Telecon, August 9, 1978.
7. G. H. Gessner, "The Condensed Chemical Dictionary," Eighth Edition, Van Nost and Reinhold Company, 1971, p. 714.
8. ASTM 2256, "Breaking Load (Strength) and Elongation of Yarn by the Single Strand Method," American Society for Testing and Materials, 1975.
9. ASTM 422, "Particle-Size Analysis of Soils," American Society for Testing and Materials, 1972.
10. Harris, J. N., and Welsh, E. A., "Fused Silica Design Manual," Volume 1, May 1973, Engineering Experimental Station, Georgia Institute of Technology.
11. Reichman, J., "Determination of Absorption and Scattering Coefficients for Nonhomogeneous Media 1; Theory," Applied Optics, 8 (1973).
12. Hackett, T. L. Private Communications with T. Place, Philco Ford, Inc., MDAC-St. Louis Telecon, May 1979
13. Kingery, W. D., Bowen H. K., and Uhlmann D. R., "Introduction to Ceramics," 2nd Edition, John Wiley and Sons, Inc. (1976).